TROLL 4.0: representing water and carbon fluxes, leaf phenology, and intraspecific trait variation in a mixed-species individual-based forest dynamics model – Part 2: Model evaluation for two Amazonian sites

Sylvain Schmitt[1,2,3], Fabian J. Fischer[4], James G. C. Ball[5], Nicolas Barbier[3], Marion Boisseaux[6], Damien Bonal[7], Benoit Burban[8], Xiuzhi Chen[9], Géraldine Derroire[1,2,10], Jeremy W. Lichstein[11], Daniela Nemetschek[4], Natalia Restrepo-Coupe[12], Scott Saleska[12], Giacomo Sellan[10], Philippe Verley[3], Grégoire Vincent[3], Camille Ziegler[6], Jérôme Chave[13], Isabelle Maréchaux[3]

[1]CIRAD, UPR Forêts et Sociétés, F-34398, Montpellier, France
[2]Forêts et Sociétés, Univ Montpellier, CIRAD, Montpellier, France
[3]AMAP, Univ Montpellier, INRAE, IRD, CIRAD, CNRS, F-34000 Montpellier, France
[4]School of Biological Sciences, University of Bristol, 24 Tyndall Avenue, Bristol, BS8 1TQ, UK
[5]Department of Plant Sciences, University of Cambridge, Downing Street, Cambridge, CB2 3EA, UK
[6]Univ. Bordeaux, INRAE, BIOGECO, 33612 Pessac, France
[7]Université de Lorraine, AgroParisTech, INRAE, UMR Silva, 54000 Nancy, France
[8]INRAE, UMR EcoFoG (Agroparistech, Cirad, CNRS, Université des Antilles, Université de la Guyane), Campus Agronomique, 97310 Kourou, French Guiana
[9]School of Atmospheric Sciences, Sun Yat-sen University, Guangzhou 510275, China
[10]Cirad, UMR EcoFoG (Agroparistech, CNRS, INRAE, Université des Antilles, Université de la Guyane), Campus Agronomique, 97310 Kourou, French Guiana
[11]Department of Biology, University of Florida, Gainesville, Florida 32611, USA
[12]University of Arizona, Ecology & Evolutionary Biology, Tucson, Arizona, United States of America
[13]Centre de Recherche Biodiversité et Environnement, UMR5300, CNRS, Université Paul Sabatier, IRD, INPT, Toulouse Cedex 9, France

Correspondence to: Sylvain Schmitt (sylvain.schmitt@cirad.fr)

Summary. We evaluate the capability of TROLL 4.0, a simulator of forest dynamics, to represent tropical forest structure, diversity, dynamics and functioning in two Amazonian forests. Evaluation data include forest inventories, carbon and water fluxes between the forest and the atmosphere, and leaf area and canopy height from remote-sensing products. The model realistically predicts the structure and composition, and the seasonality of carbon and water fluxes at both sites.

Abstract. TROLL 4.0 is an individual-based forest dynamics model that jointly simulates the structure, diversity and functioning of tropical forests, including their water balance, carbon fluxes and leaf phenology, while accounting for intraspecific trait variation for a large number of species. In a companion paper, we describe how the model represents the physiological and demographic processes that control the tree life cycle in a one-metre-resolution spatially-explicit scene and uses plant functional traits measurable in the field to parameterize such processes across species and individuals (Maréchaux et al., submitted companion paper). Here we evaluate the performance of TROLL 4.0 for two Amazonian sites with contrasting soil and climate properties. We assessed the model's ability to represent forest structure, composition, and dynamics using lidar-derived spatial distribution of top canopy height and forest inventories combined with information on plant functional traits. We also evaluated the model's ability to represent carbon and water fluxes, as well as leaf area variation, at daily and fortnightly resolution over a decade, using detailed information from on-site eddy covariance towers, satellite data and ground-based or air-borne lidar data. We finally compared the responses of carbon and water fluxes to environmental drivers between simulated and observed data. Overall, TROLL 4.0 provided a realistic representation of forests at both sites. The simulated canopy height distribution showed a high correlation coefficient (CC) with observed aerial and satellite data (CC>0.92), while the species and functional composition were well represented (CC>0.75). TROLL 4.0 also realistically simulated the seasonal variability of carbon and water fluxes (CC>0.46) and their responses to environmental drivers, while capturing temporal variations in leaf area (CC>0.76) and its partitioning in leaf age cohorts. However, TROLL 4.0 overestimated annual gross primary productivity at both sites (mean RMSEP=0.94 ± 0.67 kgC m^{-2} yr^{-1}) and evapotranspiration at one site (mean RMSEP=0.75 ± 0.63 mm day^{-1}), likely due to an underestimation of the soil water depletion and stomatal control during the dry season. This evaluation highlights the potential of TROLL 4.0 to represent ecosystem fluxes and the structure, diversity, and dynamics of plant communities at a fine resolution, paving the way for model predictions of the effects of climate change, fragmentation and forest management on forest structure and dynamics.

1 Introduction

Tropical forests cover just 7% of the Earth's land surface, yet they play a disproportionately large role in the biosphere, store around 25% of terrestrial carbon and contribute to more than a third of global terrestrial productivity (Bonan 2008). Regionally, tropical forests recycle around a third of precipitation through evapotranspiration, contributing to the generation and maintenance of a humid climate (Harper et al., 2013), effects that extend well beyond the tropics (Lawrence & Vandecar 2015). However, tropical forests remain a major source of uncertainty in simulations of global biogeochemical cycles (Fisher et al., 2014; Koch et al., 2020).

As an illustration, for light-limited tropical forests, dynamic global vegetation models (DGVMs, Prentice et al., 2007) typically simulate a decrease in productivity with a seasonal decline in precipitation (Restrepo-Coupe et al., 2017, Chen et al., 2020), while observations from eddy covariance data point to an increase in gross primary productivity during the dry season (Guan et al., 2015; Aguilos et al., 2018). Similarly, simulated forest responses to experimental and natural droughts have highlighted large model-data discrepancies and variation across models (Powell et al., 2013; Joetzjer et al., 2014; Yao et al., 2023; Paschalis et al., 2022). Improving the representation of tropical forest functioning in models is needed to enhance our understanding and ability to predict biogeochemical cycles.

One challenge is to better integrate the structure, diversity and functioning of forests into vegetation models (Purves and Pacala, 2008; McMahon et al., 2011; Evans, 2012; Mokany et al., 2016). In spite of progress (Fisher et al., 2018), most models still adopt a coarse grained representation of vegetation, which makes it difficult to use field data to parameterize and evaluate the models. Also, several processes driving the variation of tropical forest productivity and water fluxes remain incompletely represented in vegetation models. These include water uptake by the root system and seasonal variation of leaf quantity and quality at the ecosystem-level, which are driven by leaf phenology and allocation processes at the individual-level (Chen et al., 2020; Wu et al., 2021; Restrepo-Coupe et al., 2017, Cusak et al., 2024).

In a companion paper, we described the individual-based forest dynamics model TROLL 4.0 (Maréchaux et al., submitted companion paper). This model jointly simulates tropical forest structure, diversity and functioning, including forest water balance, carbon fluxes and leaf phenology, and accounts for intraspecific trait variation for a large number of species. TROLL 4.0 represents the processes underlying ecosystem fluxes, such as leaf gas exchanges and their responses to environmental variation, and is thus similar to DVGMs in that respect, with its outputs comparable with data from eddy covariance towers. However, unlike DGVMs that are designed for global applications and typically represent plant diversity with a few functional types, TROLL 4.0 represents diversity at the species level (e.g., 10s to 100s of tropical tree species). TROLL 4.0 is spatially-explicit and represents plant community structure and diversity at a spatial resolution of one metre, which is consistent with that used by field ecologists. Physiological and demographic processes are integrated using a parameterisation based on plant traits measurable in the field, relying on recent knowledge in plant physiology and functional ecology. The individual-based,

species-specific and spatially explicit representation of forest structure and composition enables TROLL 4.0 outputs to be directly compared with spatially explicit forest inventories, trait distributions or fine-scale remote sensing products.

In this paper, we evaluate TROLL 4.0 for two Amazonian sites with contrasting soil and climate properties. We parameterized the model using functional trait and soil data at both sites. We first calibrated three major forest structure parameters using inventory data, and then the three parameters of the phenological module that control leaf shedding as a function of soil water availability using litterfall data. We then ran simulations and evaluated the model's representation of forest structure, composition, and dynamics against independent data, including lidar-derived canopy height distribution, understory inventories and functional trait distribution. We also assessed the model ability to represent carbon and water fluxes at daily resolution, as well as leaf area variation at fortnightly resolution, against eddy covariance, satellite and terrestrial or drone lidar data. We finally compared the response of simulated and observed fluxes to incoming radiation, vapour pressure deficit, temperature, and wind speed. Finally, we discuss the potential model-data discrepancies and identify priorities for future developments.

2 Methods

TROLL represents individual trees explicitly in an aboveground voxelized space (1 m^3), in which light diffusion is modelled, and in a belowground space, which consists of several layers with user-defined thickness and horizontal resolution (here 25 m^2). Belowground water flow is simulated using a bucket model. We assign a species label to each simulated tree and provide as input species-specific mean plant trait values and intraspecific trait variances and covariances. New trees appear in the community through the process of tree recruitment, which is only possible in empty cells and with favourable light and water availability. Trees of a given species are recruited if there is at least one seed of that species in the local seed bank. Individual trait values of each recruited tree are randomly drawn from the intraspecific trait distribution. These traits parameterize the physiological and demographic processes that govern the life cycle of trees, from recruitment to growth, seed dispersal, and finally death. Carbon assimilation by trees is computed using the photosynthesis model of Farquhar, von Caemmerer and Berry (1980), coupled to the stomatal conductance model of Medlyn et al. (2011), as a function of leaf micro-environmental conditions, tree access to water, and leaf photosynthetic capacity and leaf respiration rate. Sugars produced during photosynthesis are used for tree respiration and allocation to plant tissues, including foliar production, carbon storage and woody growth.

We conducted model calibration and evaluation at two lowland Amazon forest sites: the Paracou research station in French Guiana (5°28'N, 52°92'W), hereafter Paracou (Gourlet-Fleury et al., 2004; Bonal et al., 2008), and the Tapajos National Forest in Brazil in the K67 site also named BR-Sa1 (2°86'S, 54°96'W), hereafter Tapajos (Silver et al., 2000; Saleska et al., 2003). Both sites are covered by a high biomass and species rich lowland moist tropical forest, and they present contrasting soil characteristics and climate (Table 1), with a longer dry season in Tapajos than in Paracou resulting in 2,075 mm per year

against 3,041 in Paracou. They thus differ in water regimes and resulting plant water stress and phenology. In addition, the two sites have been intensively monitored for several decades, mainly through repeated forest inventories and eddy flux tower measurements, fulfilling the requirement for in-depth model evaluation as previously used for such applications (Longo et al., 2019b). Additionally, we assumed forest dynamics to be at equilibrium, as both sites are characterised by old-growth forests.

To provide a conservative assessment of the model's performance and its transferability to multiple sites, we restricted the number of site-specific calibrated parameters to the ones that are currently poorly informed by available data, or to which the model is known to be sensitive based on sensitivity analyses performed on previous versions of the model (Maréchaux & Chave 2017; Fischer et al. 2019). At each site, we calibrated six parameters. These include three parameters related to forest structure: the reference background mortality rate m, and the intercept a_{CR} and slope b_{CR} of the crown radius scaling relationship (Table A1; Maréchaux and Chave, 2017; Fischer et al., 2019). m can be site-specific as it is used to simulate tree mortality events that are triggered by processes not explicitly represented in the model, such as site-specific disturbance regimes (e.g. Rau et al. 2022). Novel developments in TROLL 4.0 were based on known or measurable ecological parameters and physical constants but the three parameters of the new leaf phenology module $a_{T,o}$, $b_{T,o}$ and δ_o (Table A1) are more empirical and not ecologically measurable. In TROLL 4.0, the shedding of old leaves is accelerated as soil water availability decreases (Maréchaux et al., submitted companion paper). When the leaf predawn water potential (ψ_{pd}, MPa) falls below a threshold $\psi_{T,o}$ (MPa), the residence time of old leaves is decreased using a multiplicative factor $f_0 < 1$. The parameter $\psi_{T,o}$ varies with the tree leaf drought tolerance and its size as follows:

$$\psi_{T,o} = min(a_{T,o} \times \pi_{tlp}, -0.01 \times h - b_{T,o})$$

where π_{tlp} is the leaf water potential at turgor loss point in MPa and h is the tree height in m. f_0 is decremented (resp. incremented) by δ_o when $\psi_{pd} < \psi_{T,o}$ (resp. $\psi_{pd} > \psi_{T,o}$). The first term accounts for a decline in leaf drought tolerance with age, i.e. a reduced ability of old leaves to maintain turgor when the soil dries, where $a_{T,o}$ controls the ratio of the turgor loss point of old to mature leaves. The second term accounts for the height dependence of this susceptibility to decreasing water availability: it makes large trees susceptible to a (small) decrease in soil water availability $b_{T,o}$, while preventing them from constantly shedding their old leaves at a fast rate. Finally, δ_o controls the rate of leaf shedding in old leaves as they begin to lose turgor, but in the absence of water depletion. Overall, the parameters $a_{T,o}$, $b_{T,o}$ and δ_o control the intensity and timing of the peak of litterfall under drying soil conditions. This scheme is consistent with field observations (Maréchaux et al. submitted companion paper), uncertainties remain on the values of $a_{T,o}$, $b_{T,o}$ and δ_o however, and they need to be calibrated. After calibration, we compared model outputs with site-specific data for evaluation at each site.

Table 1: Site overview with climate, vegetation and soil properties. Soil properties are those used as input of the pedotransfer functions implemented in TROLL 4.0.

Variables	Units	Paracou	Tapajos	References

Climate

Annual rainfall	mm	3,041	2,075	P: Aguilos et al., 2018; T: Silver et al., 2000
Average air temperature	°C	25.7	26.1	

Vegetation

Aboveground biomass ($DBH \geq 10$)	Mg ha^{-1}	419	287	P: Rutishauser et al., 2010; T: Rice et al., 2004
Number of stems ($DBH \geq 10$)	ha^{-1}	612	470	P: Derroire et al., 2023; T: Rice et al., 2004
Basal area ($DBH \geq 10$)	m^2 ha^{-1}	31	24	P: Derroire et al., 2023; T: Goncalves et al., 2018

Soil

Type	-	Sandy clay loam	Clay	-
Depth	m	2.50	16.10	P: Hiltner et al., 2021; T: Nepstad et al., 2002
Layer thickness (top to bottom)	m	0.10 / 0.23 / 0.40 / 0.80 / 0.97	0.10 / 0.40 / 1.00 / 2.50 / 12.10	-
Sand	%	65.25	37.27	P: Van Langenhove et al., 2021; T: Silver et al., 2000
Clay	%	21.50	60.09	
Silt	%	13.25	2.64	
Soil Organic Content	%	2.37	2.54	P: Van Langenhove et al., 2021; T:Quesada et al., 2010
Dry Bulk Density	g cm^{-3}	1.040	1.125	P: Van Langenhove et al., 2021; T: Silver et al., 2000
Cation Exchange Capacity	mEq 100g^{-1}	2.98	2.97	P: Sabatier et al., 1997; T:Quesada et al., 2010

pH		4.34	3.84	P: Sabatier et al., 1997; T:Quesada et al., 2010

2.1 Simulation inputs and climatic drivers

154 TROLL 4.0 uses 35 global parameters defined by the user and provided as inputs. These parameters relate to atmospheric

155 constants, light transmission, leaf carbon acquisition, leaf shedding, tree carbon allocation, tree shape, reproduction, and death,

156 and intraspecific trait variability (Table S1). Except for the three parameters of forest structure mentioned above and the three

157 parameters of the leaf shedding module that have been calibrated at each site, all values are assumed site independent.

158

159 TROLL 4.0 requires trait parameters for each species: values need to be provided as input for six functional traits and three

160 scaling parameters. The scaling parameters are species maximum diameter at breast height (dbh_{thres}, cm), and parameters

161 defining the relationship between height and diameter at breast height (dbh), which are the asymptotic height (h_{lim}, m) and the

162 parameter a_h (see Maréchaux et al. submitted companion paper, Eqs (16) and (62)). We used forest inventories from Paracou

163 (Derroire et al., 2023) and Tapajos (Goncalves et al., 2018) to create a species list for each site, and computed dbh_{thres} as the

164 95th quantile of species diameter at breast height for species including more than 10 individuals. We used the TALLO global

165 database of height and diameter measurements (Jucker et al., 2022) to infer species-specific values of h_{lim} and a_h for the 496

166 species of the database that are present in Amazonia (latitude between 10°N and 18°S and longitude between 39°W and 78°W;

167 n = 24,609 trees with a mean of 49.62 ±730 trees per species). Parameters a_h and h_{lim} were inferred using Bayesian inference

168 as follows:

169
$$log(h) \sim N[log(h_{lim} \times \frac{dbh}{a_h + dbh}), \sigma^2] \mid h_{lim} \sim N(h_{lim,0}, \sigma^2_h), a_h \sim N(a_{h,0}, \sigma^2_a)$$

170 with the logarithm of height (h, in m) following a normal distribution centred on the log of a Michaelis-Menten model with

171 asymptotic height h_{lim}, height-dbh scaling parameter a_h, and variance σ^2. We used a Michaelis-Menten model form for tree

172 height h, which grows with diameter dbh towards a plateau value h_{lim} at a rate a_h (Molto *et al.,* 2014). The two species-

173 specific parameters h_{lim} and a_h are random parameters following a normal distribution centred respectively on $h_{lim,0}$ and $a_{h,0}$

174 with variances σ^2_h and σ^2_a.

175

176 The functional traits used in the parameterization include leaf area (LA, in cm^2), leaf mass per area (LMA, g m^{-2}), leaf nitrogen

177 content per dry mass (N, mg g^{-1}), leaf phosphorus content per dry mass (P, mg g^{-1}), leaf water potential at turgor loss point

178 (π_{tlp}, MPa), and wood specific gravity (wsg, g cm^{-3}). We used several datasets to retrieve species-specific mean values for

179 these traits (Vleminckx et al. 2021, Boisseaux et al., submitted; Kattge, Bönisch, and al., 2020; Maréchaux et al., 2015;

180 Maréchaux et al., 2019; Nemetschek et al., 2024; Ziegler et al., 2019). Finally, we used predictive mean matching (Van Buuren

181 and Groothuis-Oudshoorn, 2011) to impute missing trait values for a_h, h_{lim}, dbh_{thres}, and π_{tlp}. Overall, this procedure leads to

182 a parameterization of 114 species for Paracou and 113 species for Tapajos, with imputed values for only 4 to 7 species for a_h,

183 h_{lim}, dbh$_{thres}$, and π_{tlp} (Fig. A1).

184

185 TROLL 4.0 requests nine soil parameters to describe the texture, depth and chemistry. These were gathered from the literature,

186 assuming a single soil type and depth per site for simplicity and setting the number of soil layers to five (Table 1). Testing the

187 influence of horizontal and vertical soil heterogeneity on model outputs is left for future work.

188

189 TROLL 4.0 simulations are forced with six climatic drivers. Two of them are daily: cumulative rainfall (mm), and average

190 nighttime temperature (°C). The remaining four drivers are provided every half hour during the daytime (defined below):

191 incoming shortwave radiation (SW, W m^{-2}), temperature (T, °C), vapour pressure deficit (VPD, kPa), and wind speed (WS, m

192 s^{-1}). Historical time series for these climatic variables have been retrieved from the FLUXNET 2015 dataset (Pastorello et al.,

193 2020), which provides standardised data from eddy flux towers located at each site (2004-2014 for Paracou, and 2002-2011

194 for Tapajos). However, at Tapajos, rainfall data from FLUXNET 2015 is not reliable due to issues with rain gauges (Restrepo-

195 Coupe et al., 2017). Instead, we used rainfall data from the ERA5-Land reanalysis dataset (Muñoz-Sabater et al., 2021)

196 available at hourly resolution between 2002 and 2011. For other climatic variables, data from ERA5-Land showed high

197 correlation with FLUXNET 2015 data and ERA5-Land showed a better agreement with on-site precipitation data from

198 FLUXNET 2015 at Paracou when compared to other products, like CHIRPS (Funk et al. 2015; Fig. A2). We used spline

199 interpolation to derive half-hourly time series from the hourly FLUXNET 2015 data in Tapajos. The half-hourly net radiation

200 time series was used to define daytime hours (i.e. with S$_{net}$ > 0) which were set from 6 a.m. to 6 p.m. in Paracou, and from 7

201 a.m. to 7 p.m. in Tapajos. The dry season was defined as a period with fortnightly rainfall below 50 mm on average across

202 years, consistent with the 100 mm per month used by Bonal et al. (2008). This leads to a 4-month dry season in Paracou

203 (August 1st to December 1st), and a 4.5-month dry season in Tapajos (June 15 to November 1st). Dry seasons were defined

204 for illustration purposes only and have no effect on the model behaviour, which is driven by the meteorological inputs described

205 above.

206 **2.2 Calibration and simulation set-up**

207 As opposed to fine-tuning the model, we opted for minimum calibration to assess the model's behaviour with a minimum of

208 information per site, and tuning to assess its transferability, at least across Amazonian sites. We calibrated the three forest

209 structure parameters (m, a_{CR} and b_{CR}) for each site. a_{CR} and b_{CR} are not independent, and we used the TALLO global database

210 of crown radius (*CR*) and diameter (*dbh*) measurements (Jucker et al., 2022) to infer their relationship. To do so, we restricted

211 the TALLO database to observations located within 10 km around sites from which we generated a thousand pairs of (a_{CR}, b_{CR})

212 values. Each pair of values was determined by randomly drawing 10 individuals per 10-cm diameter class to generate a size-

213 balanced dataset to which the following model was fitted: $log(CR) \sim N[a_{CR} + b_{CR} \times log(dbh), \sigma^2]$. This resulted in the

214 following linear relationship between the two parameters: $b_{CR} = -0.39 + 0.59 \times a_{CR} + \epsilon_{b_{CR}}$, with $\epsilon_{b_{CR}}$ the error around

the relation. This relationship constrained the exploration of the three-dimensional parameter space, so we only had to calibrate a_{CR}, $\epsilon_{b_{CR}}$, and m. Based on preliminary exploratory analyses with the previous version of TROLL, we defined the range of calibration for each parameter and site as follows: a_{CR} varied from 1.60 to 2.00 in Paracou and from 2.3 to 2.7 in Tapajos with a step of 0.05, $\epsilon_{b_{CR}}$ from -0.30 to 0.10 in both sites with a step of 0.05, and m from 0.030 to 0.050 in both sites with a step of 0.0025. This resulted in $9\ a_{CR} \times 5\ \epsilon_{b_{CR}} \times 9\ m \times 2\ site = 810$ triplets of parameter values.

For each set of three parameter values, we performed a 600-year simulation from bare ground over a 4-ha area. Simulations were run with an external seed rain uniformly distributed across species, so that the simulated community structure is an emergent property resulting from the community assembly mechanisms embedded in the model. As succession unfolds and the number of mature trees increases in the simulation, internal seed production increases according to the assumed relationships between individual size and fecundity. An alternative to uniform seed rain across species would be to prescribe non-uniform seed rain based on species' regional abundances. This approach would tend to make the simulated species abundances more closely resemble the observed regional abundances. In contrast, uniform seed rain as simulated here, biases the simulated abundances towards evenness across species, and differences in simulated abundances reflect differences in demographic performance controlled by the model trait-based parameterization rather than prescribed differences in the seed rain. Each simulation was forced each year by randomly drawing a year among the ten years of climatic data. In doing so, we avoided applying a periodic climatic forcing or any potential trend linked to global warming.

To evaluate the forest structure simulated with each triplet of parameter values, we compared simulated to observed total aboveground biomass (AGB^{tot}, Mg ha^{-1}), total number of stems (N^{tot}, ha^{-1}), and number of stems per 5-cm diameter class (N^i, ha^{-1} for dbh class i) at the end of the 600-year regeneration. The Paracou reference dataset was a 2015 inventory of trees with dbh >10 cm in six 6-ha plots (Derroire et al., 2023). The Tapajos reference dataset was a 1999 inventory of trees with dbh > 10 cm in 19.75 ha along four 1-km transects (Rice et al., 2004). At both sites, we calculated the relative root mean squared error defined as:

$$RRMSEP = \frac{AGB^{tot}_o - AGB^{tot}_s}{AGB^{tot}_o} + \frac{N^{tot}_o - N^{tot}_s}{N^{tot}_o} + \frac{\sqrt{\frac{1}{n} \times \sum_{i=1}^{n} (N^i_o - N^i_s)^2}}{|N^i_o|}$$

where AGB$^{tot}_o$, N$^{tot}_o$ and N^i_o are observed values, and AGB$^{tot}_s$, N$^{tot}_s$ and N^i_s are the simulated values. n is the number of dbh classes and $|N^i_o|$ is the mean number of stems among dbh classes. We extracted the simulation with the lowest *RRMSEP* at each site and used the corresponding values for m, a_{CR} and b_{CR} in all subsequent simulations.

After 600 simulated years of forest dynamics the system reached a mature forest stage with stable forest structure (Fig. A3), composition, and functioning at both sites. This is referred to as the 'spin-up phase'. We then used this mature forest stage to calibrate the three parameters of the phenological module. We performed an exhaustive search in the parameter space for

248 combinations of $a_{T,o}$ in [0.01, 0.025, 0.05, 0.075, 0.1, 0.2, 0.3, 0.4, 0.5], $b_{T,o}$ in [0.01, 0.015, 0.02, 0.05, 0.04, 0.06, 0.08, 0.10],

249 and δ_o in [0.1, 0.2, 0.3, 0.4, 0.5] resulting in $9\ a_{T,o}\ \times 8\ b_{T,o} \times 5\ \delta_o \times 2\ sites = 720$ simulations. For each triplet, we ran a

250 20-year simulation with historical weather repeating the 10 years of data twice with the mature forest as an initial condition.

251 Only the last 10 years were used for the calibration to allow the leaf dynamics to adjust to new parameter values.

252

253 To evaluate each simulation, we used leaf litter data from litter traps at both sites (unpublished data at Paracou, Rice et al.,

254 2008 at Tapajos). Litter traps were typically collected fortnightly (although time intervals between consecutive litter trap

255 collections were sometimes higher and up to 80 days in Paracou) between 2004 and 2023 in Paracou, and between 2000 and

256 2005 in Tapajos. The litter collected from the traps was oven-dried until the mass stabilised, partitioned between leaves, fruits

257 and woody debris, and then the fraction were weighed. We computed observed leaf litterfall flux in Mg ha^{-1} year^{-1} as the mean

258 across traps converted from trap surface to hectare and time interval in days to year. We also recorded the time interval between

259 consecutive trap collections to account for the smoothing effect of the longer time intervals in simulated data. Simulated leaf

260 litterfall fluxes over the last 10 years of simulation for each triplet of parameter values were compared to the observed fluxes

261 using the same observation dates and corresponding time intervals.

262

263 To compare simulations against observations, we defined two yearly indices that quantify the timing and intensity of the

264 litterfall peak. The two indices are (i) the day of the litterfall peak as the Julian day of the maximum annual litterfall flux value

265 (*day*), and (ii) the ratio between the maximum value (computed as the average of litterfall flux over the two consecutive time

266 intervals before and after the peak day) divided by the basal flux (computed as the yearly average between January and April)

267 (*ratio*). Both indices are key features of litterfall patterns in tropical rainforests (Chave et al., 2010; Yang et al., 2021). For

268 each simulation we calculated the root mean squared error defined as:

269
$$RMSEP = \sqrt{\frac{\sum_{y=y_0}^{y=y_{max}} (ratio_{y,o} - ratio_{y,s})^2}{N_{year}} + \frac{\sum_{y=y_0}^{y=y_{max}} (day_{y,o} - day_{y,s})^2}{N_{year}}}$$

270 where day$_{y,o}$ and ratio$_{y,o}$ are observed z-scores (i.e., standard deviations from the mean) for year y, and day$_{y,s}$ and ratio$_{y,s}$ are

271 simulated z-scores for year y. Thus a unit *RMSEP* corresponds to a ratio error of one standard deviation, *i.e.* 7.6 folds, or to a

272 day error of one standard deviation, *i.e.* 45.5 days. The best-fit parameters were those corresponding to the lowest *RMSEP* at

273 each site.

274

275 To assess the model sensitivity to the chosen parameters, we used the calibration parameter spaces and measured response

276 variable sensitivity to each parameter with partial correlation coefficients (PCC). Moreover, we used a sequential calibration

277 scheme to reduce computation load based on the hypothesis that the second calibration of litterfall parameters does not interfere

278 with the first of forest structure parameters. To assess this assumption, we explored the sensitivity of forest structure variables

279 to forest litterfall parameters.

280

281 Finally, to quantify the envelopes of stochastic simulation outputs, we ran ten replicates of 600-year simulations starting from
282 bare ground with the six calibrated parameter values.

2.3 Evaluation of forest structure, composition and dynamics

284 To assess the model's ability to simulate forest structure and dynamics, as well as species and functional composition, we used
285 airborne lidar scanning (ALS) and satellite data, as well as forest inventories combined with functional traits. Independently
286 from the calibration, we evaluated the diameter distribution of the forest understory at Paracou using an independent 9-ha
287 inventory of trees with dbh between 1 and 10 cm from 2020-2023 (unpublished data). We evaluated the structure of the
288 simulated forest at the end of the 600-year replicates against observed basal area (BA, $m^2 \, ha^{-1}$) and logarithm of number of
289 stems (ha^{-1}) per 1-cm diameter class below 10 cm. We evaluated tree height distributions using ALS data from 2015 at Paracou
290 (unpublished data) and from 2012 at Tapajos (dos-Santos et al., 2019), which were processed into canopy height models with
291 a standardised pipeline (Fischer et al., 2024). From both simulated and ALS-derived canopy height models, we derived the
292 distribution of top canopy height, expressed in proportion of 1-m^2 pixels per 1-m height class. We evaluated the species
293 composition after the 600-year replicates against the observed rank-abundance curve of the 114 most abundant species at both
294 sites, and the functional composition against the observed density distribution of each trait for each site and each plot. Due to
295 a lower taxonomic resolution of botanical identification at the Tapajos site, we used genus level functional trait data at Tapajos
296 and species level functional trait data at Paracou. Finally, we evaluated forest dynamics by retrieving the simulated individual-
297 tree growth rates (cm yr^{-1}) and death rates (% yr^{-1}) over 10 years per 5-cm diameter class and comparing them to the ones
298 estimated from field inventories of six 6.25-ha plots in Paracou from 2003 to 2013.

299

2.4 Evaluation of total leaf area dynamics

301 We assessed the model's ability to represent the dynamics of total leaf area and its partitioning into three leaf age cohorts
302 (Maréchaux et al., submitted companion paper). For evaluation, we gathered leaf area index (LAI) datasets as follows: LAI
303 from MODIS satellites at both sites, LAI from terrestrial lidar at Tapajos (Smith et al., 2019), and LAI from UAV-borne lidar
304 at Paracou (unpublished data; Vincent et al., 2017). The MODIS LAI product was at 8 day and 500 m resolution, and pre-
305 processed in PLUMBER2 (Ukkoloa et al., 2020). At Tapajos, plant area index (PAI) was derived from terrestrial lidar scanning
306 (TLS) performed every 1-2 months in 2010, 2012, 2015 and 2017 along four 1-km long transects representing 0.4 ha with a
307 spatial resolution of about 3 m to characterise canopy porosity (Smith et al., 2019). PAI was derived from lidar hits following
308 Stark et al. (2012) and based on the MacArthur–Horn transformation (MacArthur & Horn, 1969). This PAI was then converted
309 to LAI using an annual mean LAI of 5.7 (Stark et al., 2012). In Paracou, the PAI was derived from repeated UAV-borne lidar
310 surveys, resulting in PAI mapping at 21 day and 1 m resolution between 2020 and 2022 over a 2.5 ha forest area. This PAI
311 derived from UAV lidar was obtained by vertical integration of Plant Area Density (PAD) profiles previously recalibrated to
312 match a TLS-derived PAD profile of a common 1-ha plot scanned in October 2019. This was required because the limited

penetration of the UAV lidar yielded overestimation of raw PAD values (Vincent et al., 2023). This PAI was converted to LAI variation with a factor of 0.68, where the conversion factor is derived from other products.

Simulated LAI variation per leaf age cohort (Eqs 56-57, Maréchaux et al. submitted companion paper) were compared qualitatively against the one derived from phenological cameras by Wu et al., (2016) at Tapajos and from the reanalysis of Yang et al. (2023) at both sites. Wu et al. (2016) analysed 478 images collected over 24 months from 65 tree crowns and fitted the transition from young to mature and from mature to old leaf pools, assumed to occur at 1 and 3 months, respectively. Yang et al. (2023) used global satellite observations of the TROPOMI satellite Solar Induced Fluorescence (SIF) sensor as an indicator of leaf photosynthesis variation, validated by *in situ* measurements, and set the transition from young to mature and from mature to old leaf pools, occuring at 1.71 and 5.14 months, respectively. By comparison, simulated leaf age per cohort depends on the individual leaf lifespan in TROLL 4.0 (see Maréchaux et al. submitted companion paper).

2.5 Evaluation of carbon and water fluxes

To assess the model's ability to simulate carbon and water fluxes, we evaluated gross primary productivity (GPP, kgC m^{-2} year^{-1}) and evapotranspiration (ET, mm day^{-1}). We extracted GPP and latent heat flux (LE, W m^{-2} half-hour^{-1}) from the FLUXNET 2015 dataset (Pastorello et al., 2020). ET was derived from LE and temperature (T, in °C) using $ET = \frac{LE \times 60 \times 30 \times 10^{-6}}{\lambda(T)}$ $with$ $\lambda(T) = 2.501 - (2.361 \times 10^{-3}) \times T$ (Allen et al., 1998). GPP was obtained from net ecosystem exchange with the nighttime partitioning method (Reichstein et al., 2005). We summarised half-hourly GPP and ET into daily values by calculating the daily mean and sum. TROLL 4.0 carbon fluxes were also compared with a remotely sensed product of GPP derived from TROPOMI SIF using the formula $GPP = 15.343 \times SIF$ (Chen et al. 2022). We additionally computed the light use efficiency (LUE in mol$_C$ mol$_{photons}$$^{-1}$) normalizing GPP by photosynthetic photon flux density (PPFD) and the fraction of absorbed photosynthetically active radiation (fAPAR) derived from leaf area index (LAI) to explore carbon flux environmental drivers independently of the overriding effect of light as in Bloomfield et al. (2023). We compared how the fluxes depended on environmental drivers in both simulated and observed data. Using the FLUXNET 2015 dataset (Pastorello et al., 2020), daily values of cumulative photosynthetically active radiation (PAR, mol m^{-2}), maximum vapour pressure deficit (VPD, kPa), mean temperature (T, °C), and mean wind speed (WS, m s^{-1}) were calculated, and simulated and observed responses of GPP, LUE, and ET to PAR, VPD, T and WS were compared. TROLL 4.0 water fluxes were assessed using the relative variation of soil water content (RSWC, %) of the top horizon from the Paracou eddy flux tower (Bonal et al., 2008) and the relative variation of soil water content of the top horizon reanalysed against the climatic water deficit at Tapajos (Restrepo-Coupe et al., 2024). RSWC is defined as the daily mean of soil water content (m^3 m^{-3}) divided by the annual 95th quantile of the daily mean.

All simulations were run using TROLL 4.0 (Maréchaux et al., submitted companion paper) wrapped in the R package *rcontroll* (Schmitt et al., 2023) and encapsulated in a Singularity image (Kurtzer et al., 2017) leveraging a Python Snakemake workflow

346   (Köster et al., 2012) on a high performance computing platform using 100 cores. To compare simulations and observations,

347   we used the same metrics for all variables, regardless of their type, origin, spatial or temporal resolution: the goodness of fit

348   R^2 from linear regression with null intercept, the Pearson's correlation coefficient CC, the root mean square error of prediction

349   RMSEP, the standard deviation of the error of prediction SD.

350   **3 Results**

351   **3.1 Forest structure, composition and dynamics**

352   We calibrated background mortality rate (m) and crown radius scaling parameters (a_{CR} and b_{CR}) at Paracou and Tapajos against

353   observed aboveground biomass, total number of stems and number of stems per 5-cm dbh classes, and found m=0.035,

354   a_{CR}=1.80 and b_{CR}=0.3860 at Paracou, and m=0.040, a_{CR}=2.45 and b_{CR}=0.7565 at Tapajos. For tree with 10-cm dbh, the calibrated

355   crown radius - dbh allometry (equ. 17 in Maréchaux et al., submitted companion paper) predicts a crown radius of 2.49 m at

356   Paracou and 2.03 m at Tapajos a variation that falls well within the one reported globally (Jucker et al., 2024). The modelled

357   aboveground biomass, total number of stems and number of stems per 5-cm dbh classes were in good agreement with

358   observations (correlation coefficient, CC>0.99 at both sites, Fig. 1). The three parameter values were very similar across the

359   five best simulations, i.e. the ones minimising RRMSEP (m±0.0025, a_{CR}±0.1 and b_{CR}±0.057 at Paracou and m±0.01, a_{CR}±0.1

360   and b_{CR}±0.0285 at Tapajos, Table A3 & A4), and we used the values of the best simulation in all subsequent simulations.

361   Finally, in agreement with results on previous versions of the model, forest structure showed high sensitivity to the explored

362   parameters. Partial correlation coefficients (PCC) were around -0.4 for a_{CR} and around 0.4 for b_{CR} with number of stems,

363   aboveground biomass, and basal area. The background mortality rate m also had a strong effect on aboveground biomass and

364   basal area with a PCC around -0.2 but little to no effect on number of stems (Fig. A4).

365

366
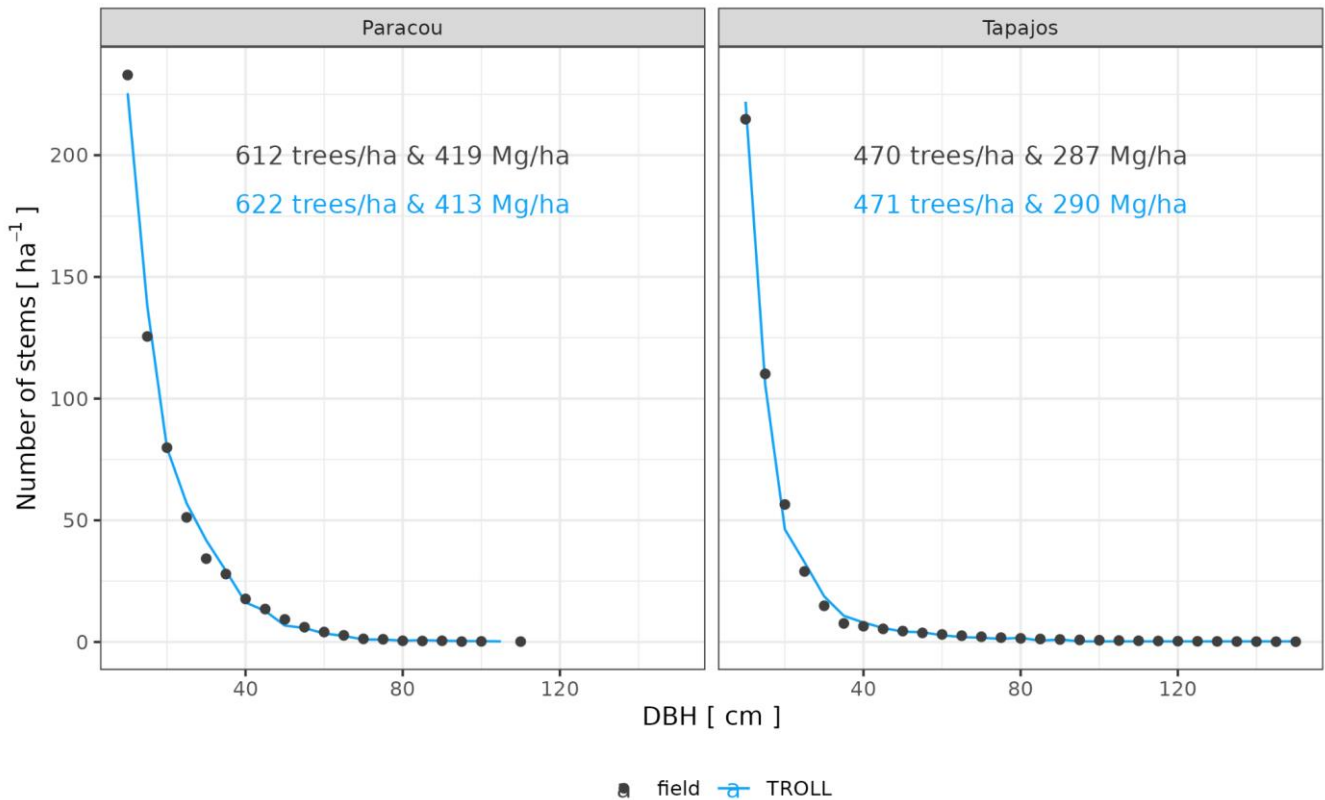
Figure 1: Tree size structure at Paracou and Tapajos, expressed in terms of number of stems per 5 cm-dbh classes. Comparison between distributions simulated by TROLL 4.0 after calibration of m, a_{CR} and b_{CR} in blue and the ones derived from field inventories of trees with dbh >10 cm in black, at Paracou (left) and Tapajos (right). Observed (black) and simulated (blue) densities of trees with dbh > 10 cm, and aboveground biomass are also provided. All simulated values correspond to the end-state of a 600-year regeneration from bare ground with calibrated values for m, a_{CR} and b_{CR} at each site.

After calibration, the top canopy height distribution simulated by TROLL 4.0 matched that measured by lidar aerial scanning (ALS), with a root mean square error of prediction (RMSEP) of the proportion of 1-m² pixels per 1-m height class below 0.8% and a correlation coefficient (CC) above 0.91, despite a slight overestimation of low canopy areas in Paracou, at heights below 20 m, and a slight underestimation of high canopy areas, above 40 m in Tapajos (Fig. 2). For example, in Paracou, 4% of the 1-m² pixels scanned by ALS had a canopy height around 25m. An RMSEP of 0.8% means that TROLL simulations could lead to 3.2 or 4.8% of pixels with a canopy height of 25m. TROLL 4.0 simulations also reproduced the forest understory structure characterised by basal area (BA) and number of stems distribution per 1-cm diameter classes for trees < 10 cm dbh at Paracou (Fig. 3). However, TROLL 4.0 underestimated the number of small trees (2,139 vs. 3,787 trees ha^{-1}), resulting in an underestimation of basal area (BA = 2.9 vs. 3.7 m² ha^{-1}).

382
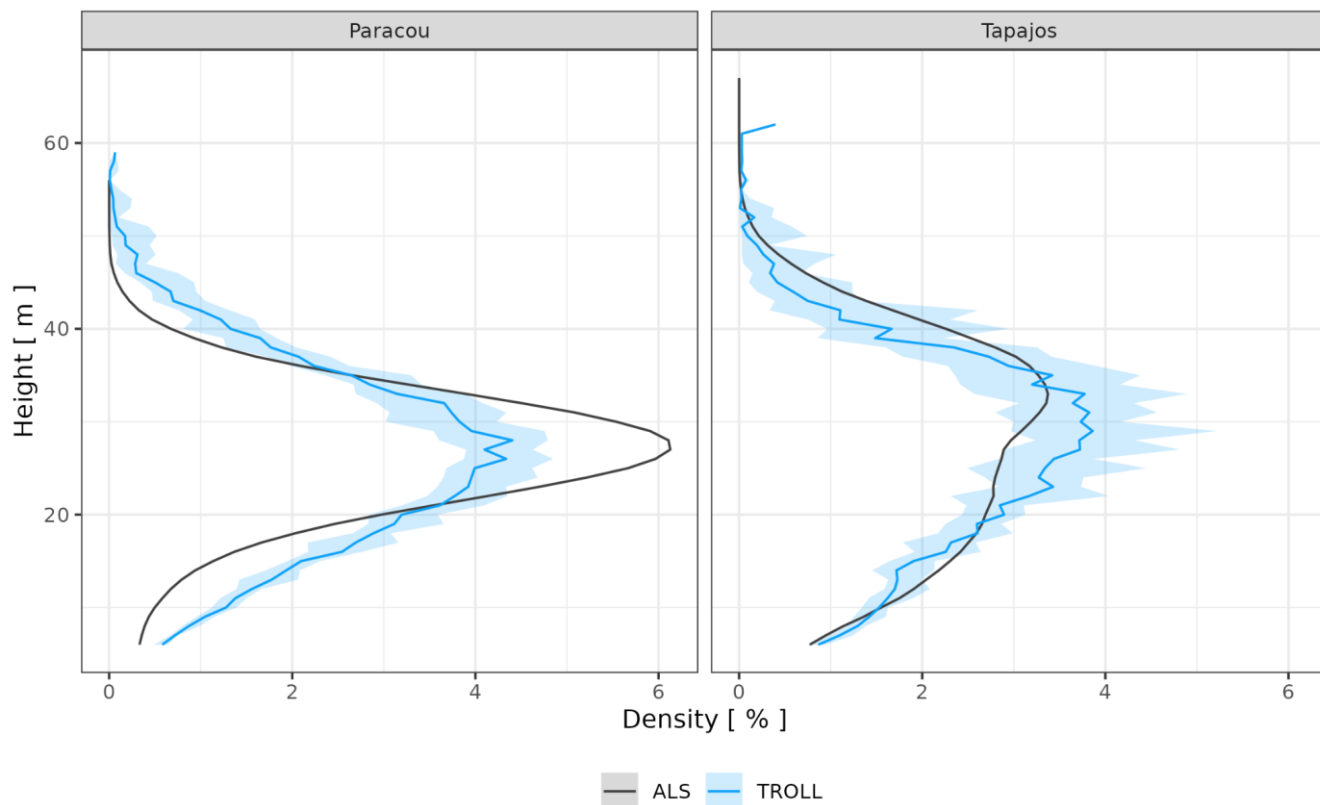
Figure 2: Canopy height distribution at Paracou and Tapajos. For each 1-m² pixel of the ground, the top canopy height in that pixel
(i.e. the height of the highest voxel with positive plant area density, or PAD, and located above this ground pixel) was determined,
and its distribution across 1-m² pixels plotted as the proportion of 1-m² ground pixels (%, x-axis) with a given canopy height (m, y-
axis, at 1-m resolution). The figure shows a comparison between distributions derived from PAD fields simulated by TROLL 4.0
(blue lines), and the ones derived from airborne laser scanning point clouds (black lines). Simulated values and their confidence
intervals correspond to the end-state of simulations of ten 4-ha 600-year regeneration from bare ground for each site.

389
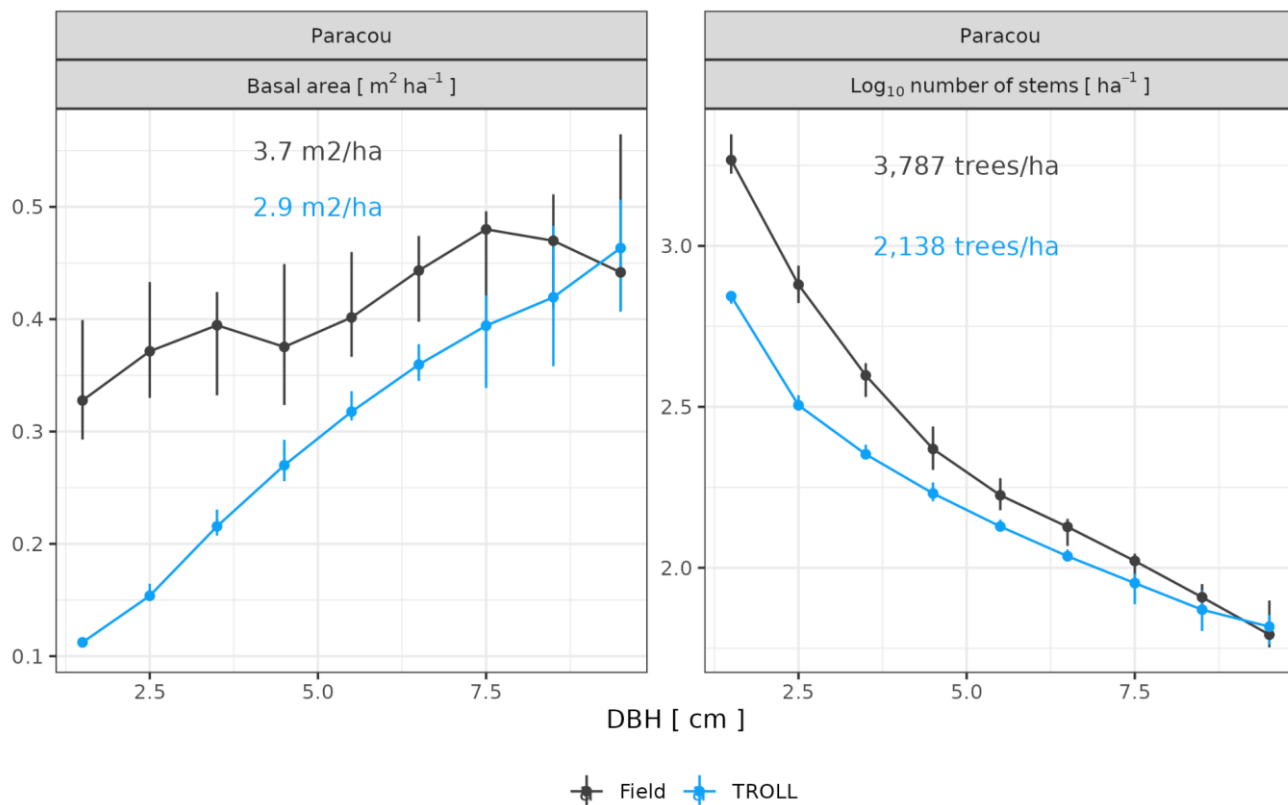
Figure 3: Understory tree size structure at Paracou, expressed in terms of basal area distributions (left) and number of stems (right) per 1 cm-dbh classes. The figures compare distributions simulated by TROLL 4.0 in blue and field inventory observations in black. Simulated values and their confidence intervals correspond to the end-state of simulations of ten 4-ha 600-year regeneration from bare ground. Confidence intervals at 95 % are shown with error bars and are based on variations among plots (9 plots of 1 ha) for the observations. Simulated (blue) and observed (black) total basal area (left) and densities (right) for trees with dbh >1 cm and < 10 cm are also provided. To the best of our knowledge, similar data was not available in Tapajos.

396   At Paracou, the simulated and observed species rank-abundance curves were similar (Fig. 4), with a RMSEP of 3.67 trees ha$^-$

397   ^{1} and a CC of 0.93, but with an underestimation in the abundance of dominant species and an overestimation in the

398   abundance of rare species resulting in a higher evenness overall. At Tapajos, the simulated and observed rank-abundance

399   curves displayed similar patterns as at Paracou (RMSEP=3.62 trees ha^{-1} and CC=0.94) but amplified , with a strong

400   underestimation of the abundance of dominant species and an overestimation of the abundance of rare species.

401
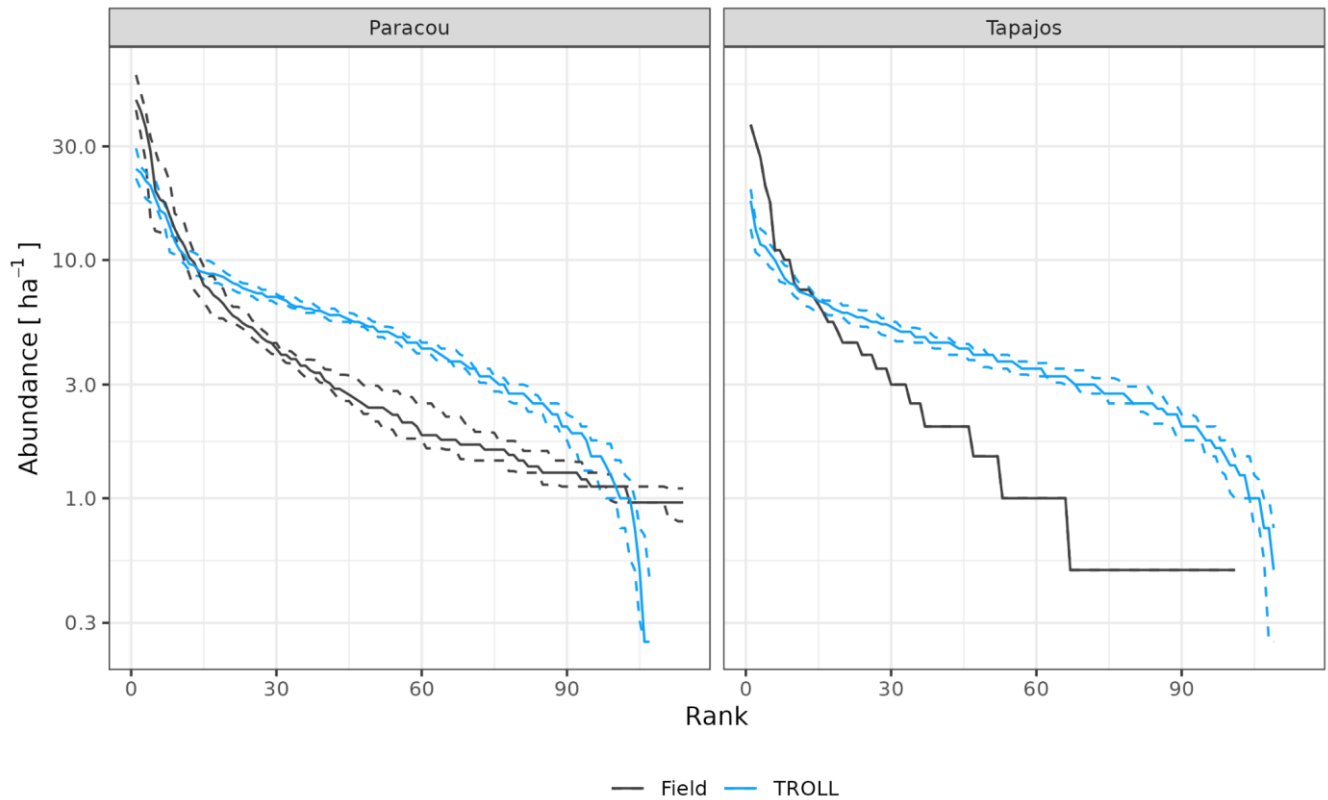
402 **Figure 4: Species-rank abundance curves at Paracou and Tapajos. Comparisons between curves simulated by TROLL 4.0 (blue)**
403 **and derived from field inventories at both sites. Simulations included 114 and 113 species at Paracou and Tapajos respectively.**
404 **Curves derived from inventories were cut at the 114th species. Simulated values and their confidence intervals correspond to the**
405 **end-state of ten 4-ha 600-year regeneration from bare ground. Confidence intervals at 95 % are shown with error bars and are**
406 **based on variations among plots for observations.**

407 Functional trait distributions simulated by TROLL 4.0 were consistent with empirical ones at Paracou and Tapajos (Fig. 5),

408 with a CC from 0.91 to 1.00 for all traits at both sites, except for leaf area at Paracou (CC=0.74) and Tapajos (CC=0.87).

409 However, abundances of low wood density trees, high LA trees, and high LMA trees were underestimated in simulations

410 when compared to observations at Paracou.

411
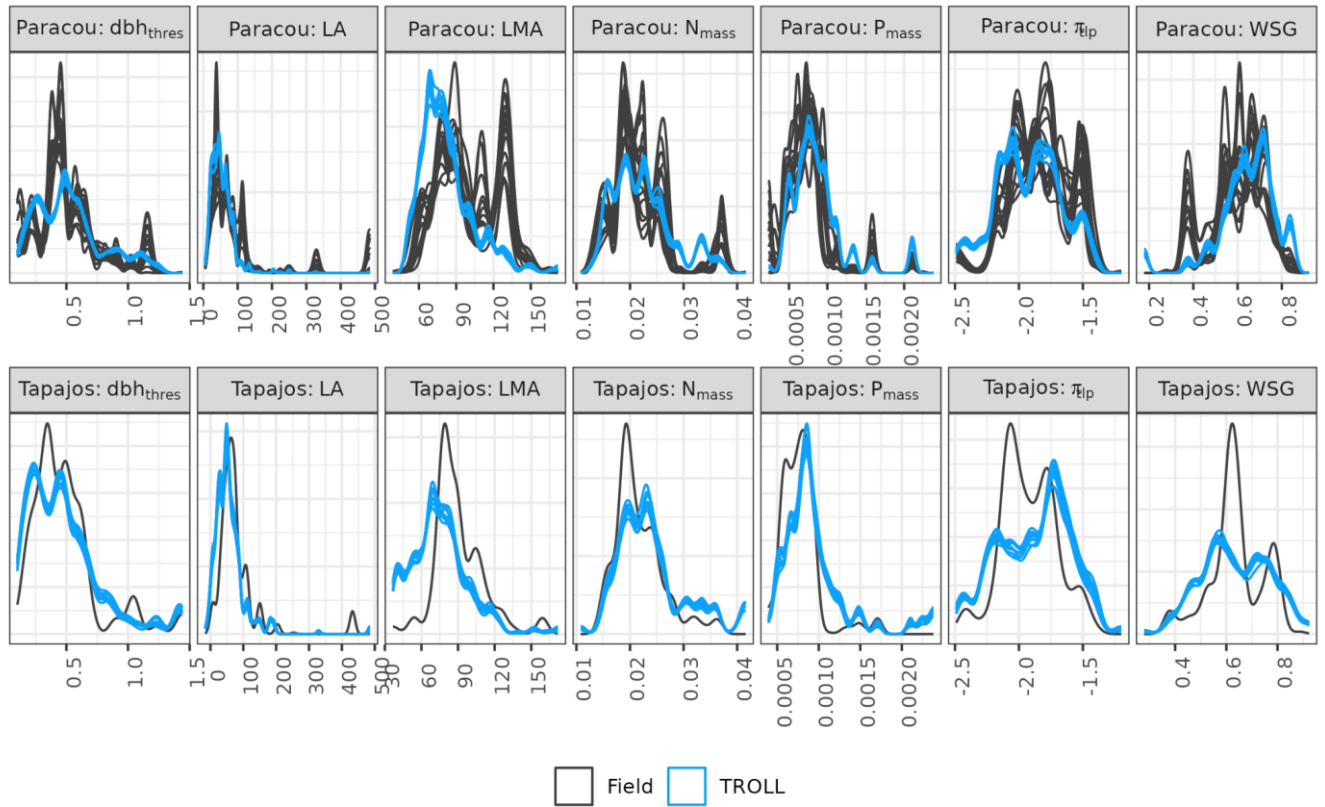
Figure 5: Functional trait distributions at Paracou and Tapajos. Distributions derived from field inventories (black) were based on botanical identification at the species level in Paracou and the genus level in Tapajos. Simulated distributions (blue) were based on the final stage of ten 4-ha 600-year regeneration from bare ground. Confidence intervals are shown with repeated lines and are based on variations among plots for observations and among repetitions for simulations. dbh_{thres}: maximum diameter in m, LA: leaf area in cm^2, LMA: leaf mass per area in g cm^{-3}, N_{mass}: leaf nitrogen content per dry mass in mg g^{-1}, P_{mass}: leaf phosphorus content per dry mass in mg g^{-1}, π_{tlp}: leaf water potential at turgor loss point in MPa, WSG: wood specific gravity in g cm^{-3}.

Forest dynamics simulated by TROLL 4.0 were consistent with the ones estimated from field inventories at Paracou (Fig. 6). Simulated individual-tree growth-size relationship were comparable to the ones retrieved from inventories (simulated mean of 0.18 cm yr^{-1} against 0.13 cm yr^{-1}) with an expected bell-shaped relationship (Hérault et al. 2011) and similar high variation (Schmitt, Hérault & Derroire 2023). Simulated death rates also showed magnitude and variation similar to observed ones (simulated mean of 1.73 % yr^{-1} against 2.60 % yr^{-1} observed at Paracou but with consistent and overlapping ranges).

423
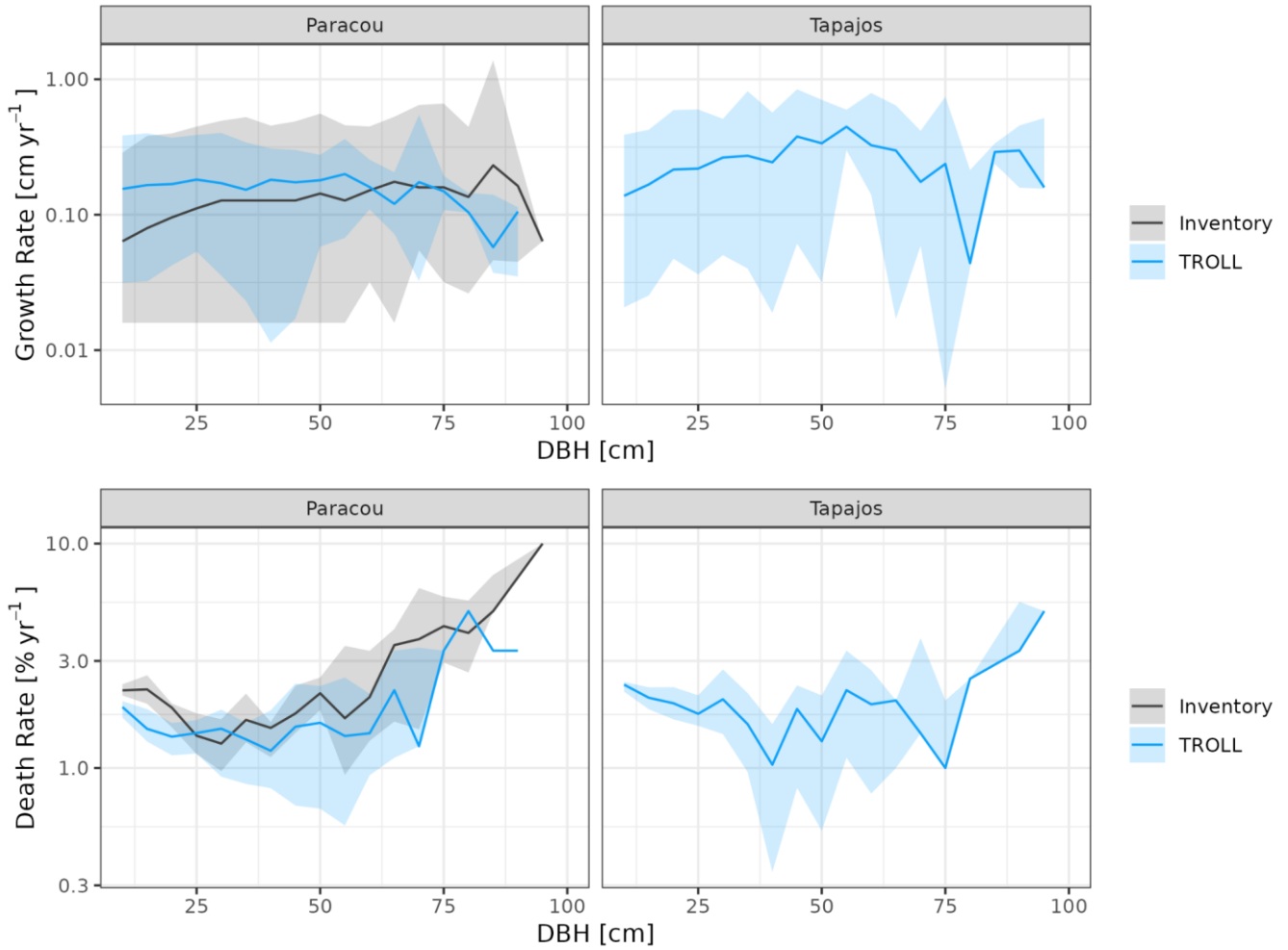
Figure 6: Forest dynamics at Paracou and Tapajos, expressed in terms of individual-tree growth rate (top) and death rate (bottom) both per 5 cm-dbh classes across 10 years. The figures compare distributions simulated by TROLL 4.0 in blue and multiple field inventory observations from six 6.25-ha plots in Paracou from 2003 to 2013 in black. Simulated values and their confidence intervals correspond to ten repetitions of 10-year simulations starting from the end-state of 600-year regeneration from bare ground with calibrated parameters at each site. Confidence intervals at 95 % are shown with shaded areas and are based on variations among plots (6 plots of 6.25 ha) for the observations.

3.2 Leaf phenology

The calibration of the three parameters of the leaf shedding module against observed litterfall illustrated how each parameter affects the simulated timing and intensity of the litterfall peak during the dry season, with no or little effect on the background litterfall rate (Fig. A5) but revealing a strong positive effect of $a_{T,o}$ and $b_{T,o}$ on the peak day of litterfall and negative effect on the ratio of the peak of litterfall, and a weak effect effect of δ_o on the peak of litterfall. As anticipated, litterfall calibration was independent of the forest structure calibration (Fig. A4). Calibration resulted in a best-fit $a_{T,o}$ value of 0.2, and a $b_{T,o}$ value of 0.015 at both sites. The calibrated δ_o differed across sites (δ_o=0.1 at Paracou and δ_o=0.2 at Tapajos). The simulated

437 seasonal variation of litterfall at Paracou and Tapajos shows qualitative agreement with the observed data (Fig. 7). Both
438 empirical and simulated data showed a marked peak in litterfall during the dry season, despite a clear under-estimation of
439 simulated litterfall flux during both wet and dry seasons, particularly at Tapajos, and a delayed peak during the dry season,
440 particularly at Paracou, in comparison to observations.
441
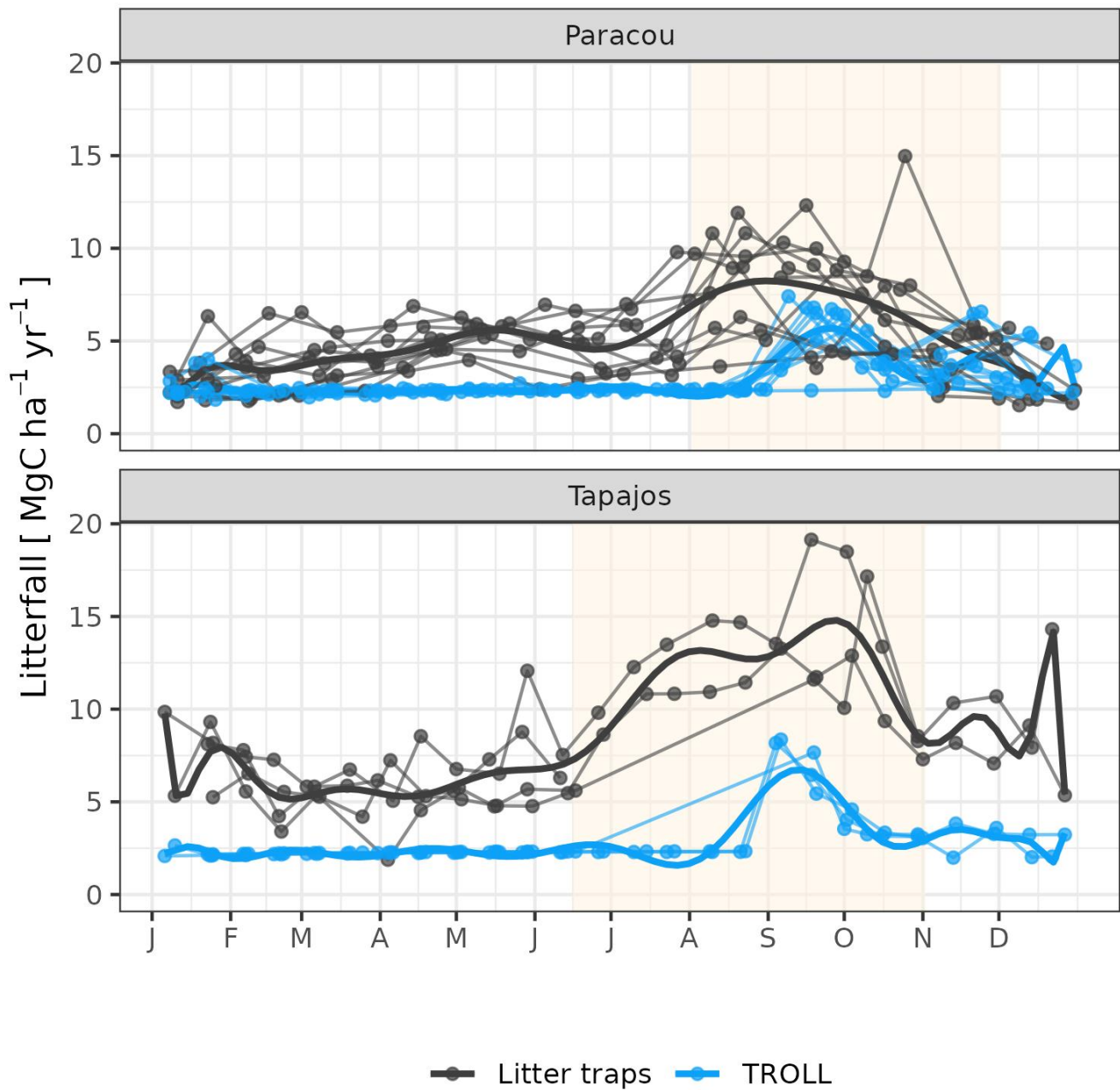
442

 Figure 7: Litterfall annual cycle from fortnightly litterfall fluxes at Paracou and Tapajos. Each thin line represents one year with
points showing values at sampling dates, the thick lines represent polynomial smoothing among years, and the vertical yellow bands
in the background correspond to the site's climatological dry season. Simulated values correspond to the last 10 years of 20-year
simulations starting from the end-state of 600-year regeneration from bare ground with calibrated parameters at each site.

The empirical LAI datasets displayed strikingly different results, illustrating the challenge of estimating LAI with confidence

in dense tropical forests (Fig. 8, Tab. S2). MODIS-derived LAI displayed almost no seasonality with mean LAI values

around 6.0 $m^2 m^{-2}$ at both sites. At Paracou, LAI derived from UAV-borne lidar showed a clear seasonality, with lowest

values around 5.5 $m^2 m^{-2}$ from April to June and highest values of almost 6.0 $m^2 m^{-2}$ in December, at the end of the dry

season. At Tapajos, LAI derived from terrestrial lidar showed no seasonality, around 5.8 $m^2 m^{-2}$ throughout the year, but LAI

derived from phenological cameras (PhenoCams) did display some seasonality, with lowest values at 5.5 $m^2 m^{-2}$ in June and

highest values above 6.0 $m^2 m^{-2}$ in December, at the end of the dry season. These observations were compared with

simulations. At Paracou, simulated LAI matched the one derived from UAV-borne lidar, both showing an increase during

the dry season (CC=0.84, RMSEP=0.11 $m^2 m^{-2}$). At Tapajos, simulated LAI matched the empirical LAI derived from

PhenoCams (CC=0.91, RMSEP=0.15 $m^2 m^{-2}$; Table S2).

The different datasets gathered to estimate LAI dynamics per cohorts also showed contrasted patterns (Fig. 9 and Fig. A6).

At Tapajos, PhenoCams indicate a maximum young leaf LAI reached during the dry season and a minimum during the wet

season, with inverse patterns for old leaf LAI. TROLL 4.0 simulations yielded patterns consistent with these observations

(Fig. 9). However, Yang et al.'s (2023) reanalysis predicts the exact opposite trends for young and old leaves, with a

maximum young leaf LAI during the wet season and a minimum during the dry season. At Paracou, we could only compare

simulated trends against Yang et al. (2023)'s reanalysis and the match was relatively poor (Fig 8).

464
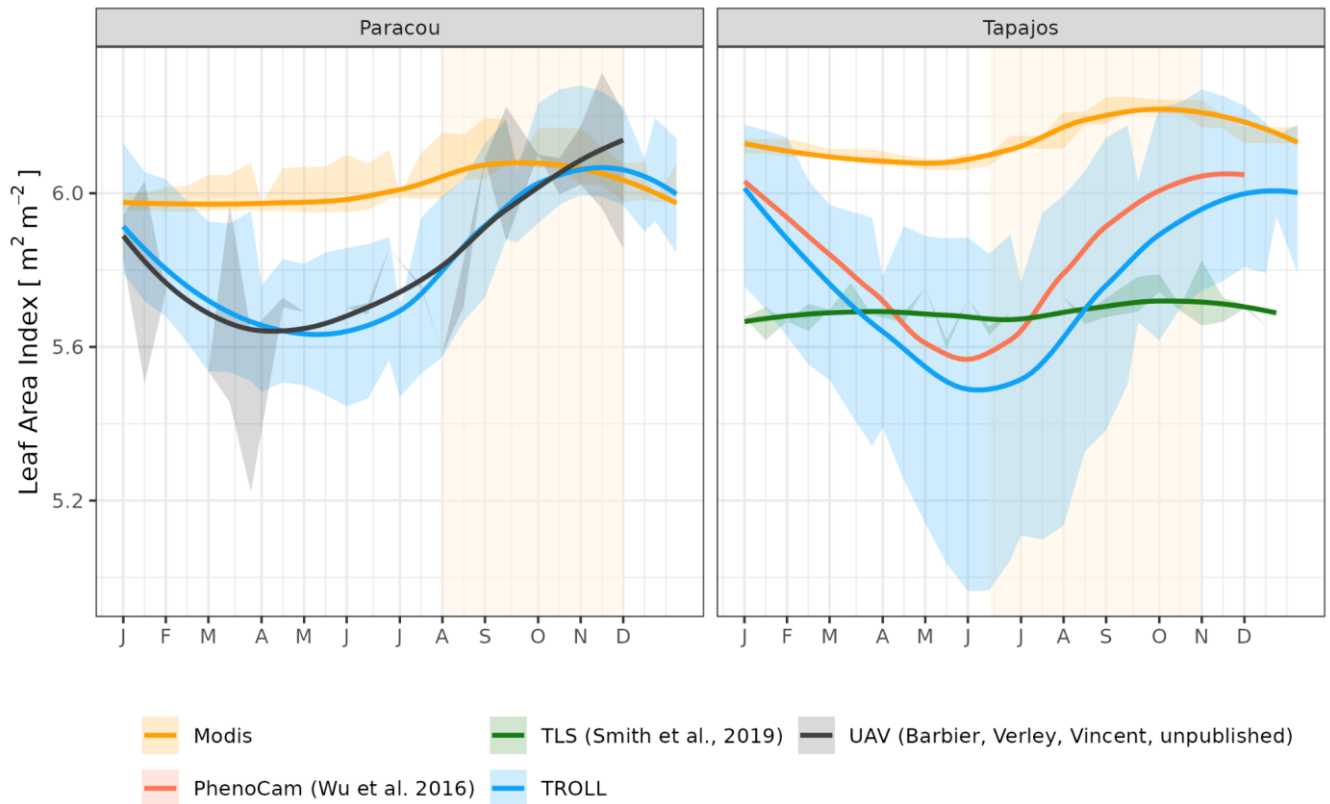
Figure 8: Mean annual cycle of leaf area index (LAI) at Paracou and Tapajos, derived from fortnightly means, from different sources (see methods). Bands are the intervals of means across years, and the vertical yellow bands in the background correspond to the site's climatological dry season. Simulated values correspond to 10 years of simulations starting from the end-state of 600-year regeneration from bare ground with calibrated parameters at each site.

469
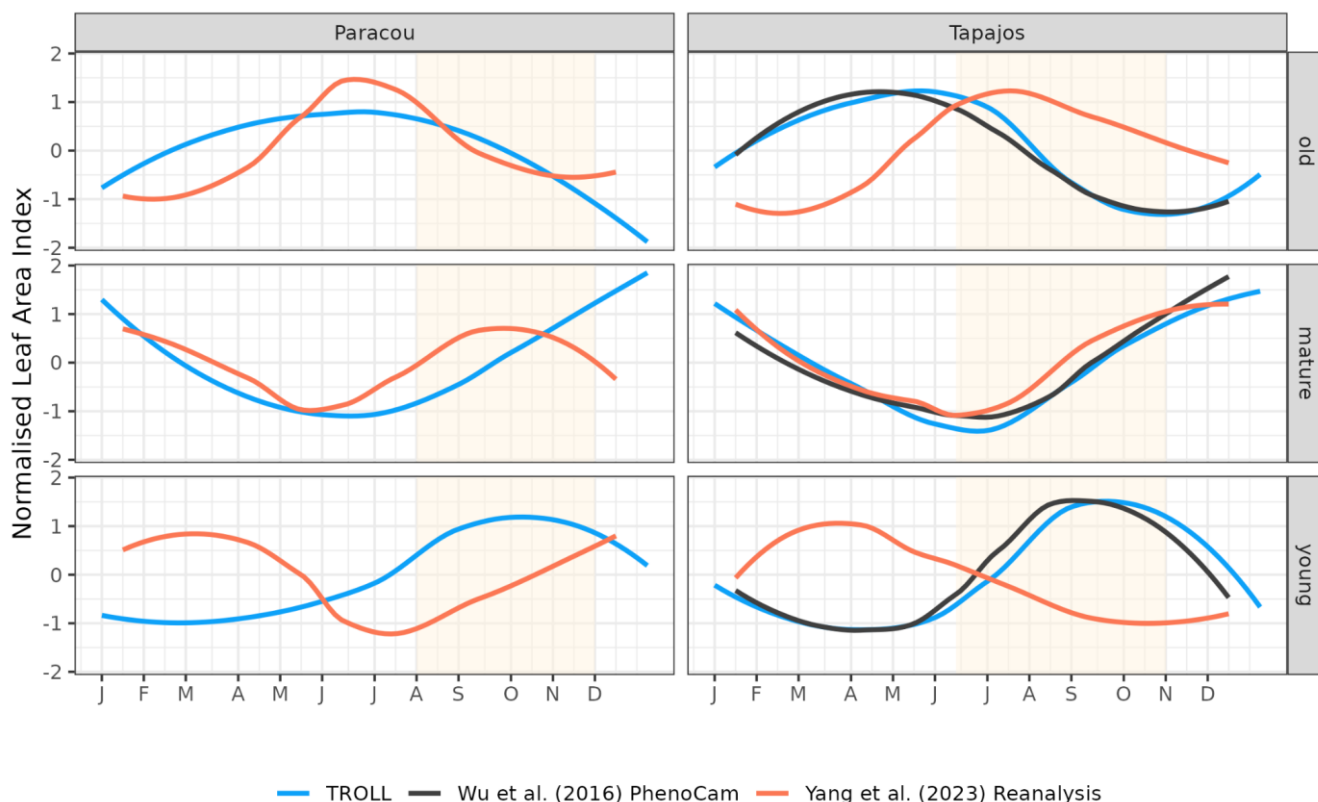
Figure 9: Mean annual cycle of normalised leaf area index per leaf age cohorts, derived from fortnightly means, at Paracou and Tapajos. Note that the three leaf age cohorts (young, mature and old leaves) are not defined the same way in the three independent sources. Leaf age per cohort depends on the individual leaf lifespan in TROLL 4.0 (see Maréchaux et al., submitted companion paper), while the transition from young to mature and mature to old are respectively fixed to 1.71 and 5.14 months in Yang et al. (2023) and fitted to 1 and 3 months in Wu et al. (2016). The vertical yellow bands in the background correspond to the site's climatological dry season. See figure A6 for absolute variation per cohort, site and dataset. Simulated values correspond to 10 years of simulations starting from the end-state of 600-year regeneration from bare ground with calibrated parameters at each site.

3.3 Water and carbon fluxes

TROLL 4.0 captured the seasonality of gross primary productivity (GPP) observed at the two sites, with an increase before the onset of the dry season, reaching its maximum during the dry season, and a decrease starting before or at the onset of the wet season (Fig. 10 and see Fig. A7 for interannual variations, Tab. S2). Comparison with eddy flux estimates with simulations were high both at Paracou (CC=0.60) and Tapajos (CC=0.46). TROLL 4.0 overestimated GPP at both sites, particularly during the dry season, with a RMSEP of 0.75 and 1.12 kgC m^{-2} year^{-1} when compared with both eddy flux and TROPOMI SIF estimates at Paracou and Tapajos, respectively.

484
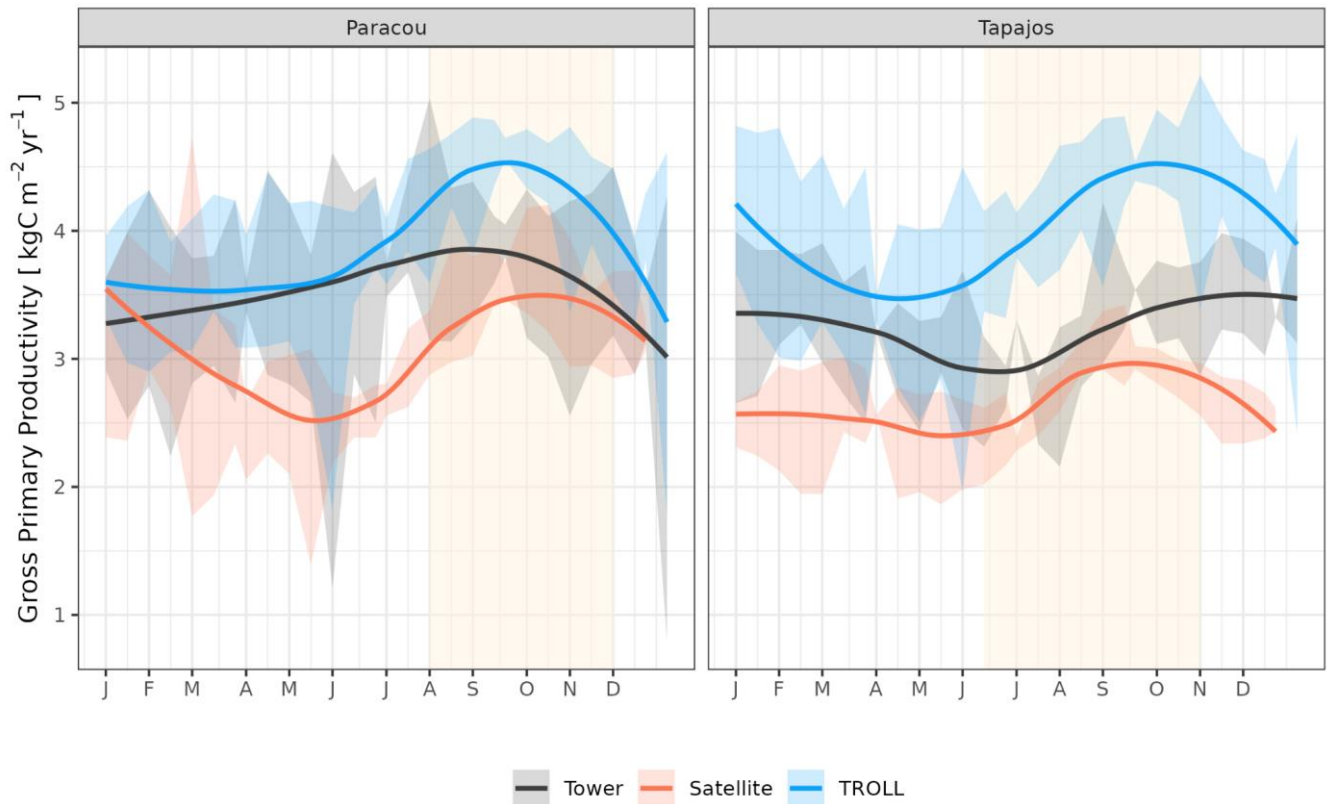
Figure 10: Mean annual cycle of gross primary productivity for Paracou and Tapajos, derived from fortnightly means. The red lines represent the gross primary productivity estimated from TROPOMI SIF while the black lines represent the one derived from eddy flux measurements, and the blue lines the simulated gross primary productivity with TROLL 4.0. Bands are the intervals of means across ten years, and the vertical yellow bands in the background correspond to the site's climatological dry season. Simulated values correspond to 10 years of simulations starting from the end-state of 600-year regeneration from bare ground with calibrated parameters at each site. Inter-annual variations are shown in Figure A7.

The seasonality of water flux was captured by TROLL 4.0 (Fig. 11 and see Fig. A8 for interannual variations, Tab. S2), with a pronounced increase in evapotranspiration (ET) during the dry season at both sites, and leading to CC of 0.66 and 0.70 when compared with eddy flux estimates at Tapajos and Paracou respectively. Although intra-annual variations of simulated and observed values overlapped, TROLL 4.0 tended to overestimate ET in Tapajos during the dry season, leading to RMSEP values of 0.60 and 0.75 mm day^{-1} when compared with eddy flux estimates at Paracou and Tapajos respectively. The partitioning of evapotranspiration between canopy evaporation, soil evaporation and tree transpiration (Fig. A9) showed that most of the evapotranspiration is due to tree transpiration in the dry season, while canopy evaporation is an important part of the total evapotranspiration in the wet season (Kunert et al., 2017). TROLL 4.0 also captured the seasonality in RSWC of the top soil layer at Paracou and Tapajos (Fig. A10, Table A2, see Fig. A11 for absolute variation with varying depth), with a high RSWC in the wet season close to 100% and a sharp decrease in RSWC in the dry season, although overall smoother in simulations than field estimates.

502

503
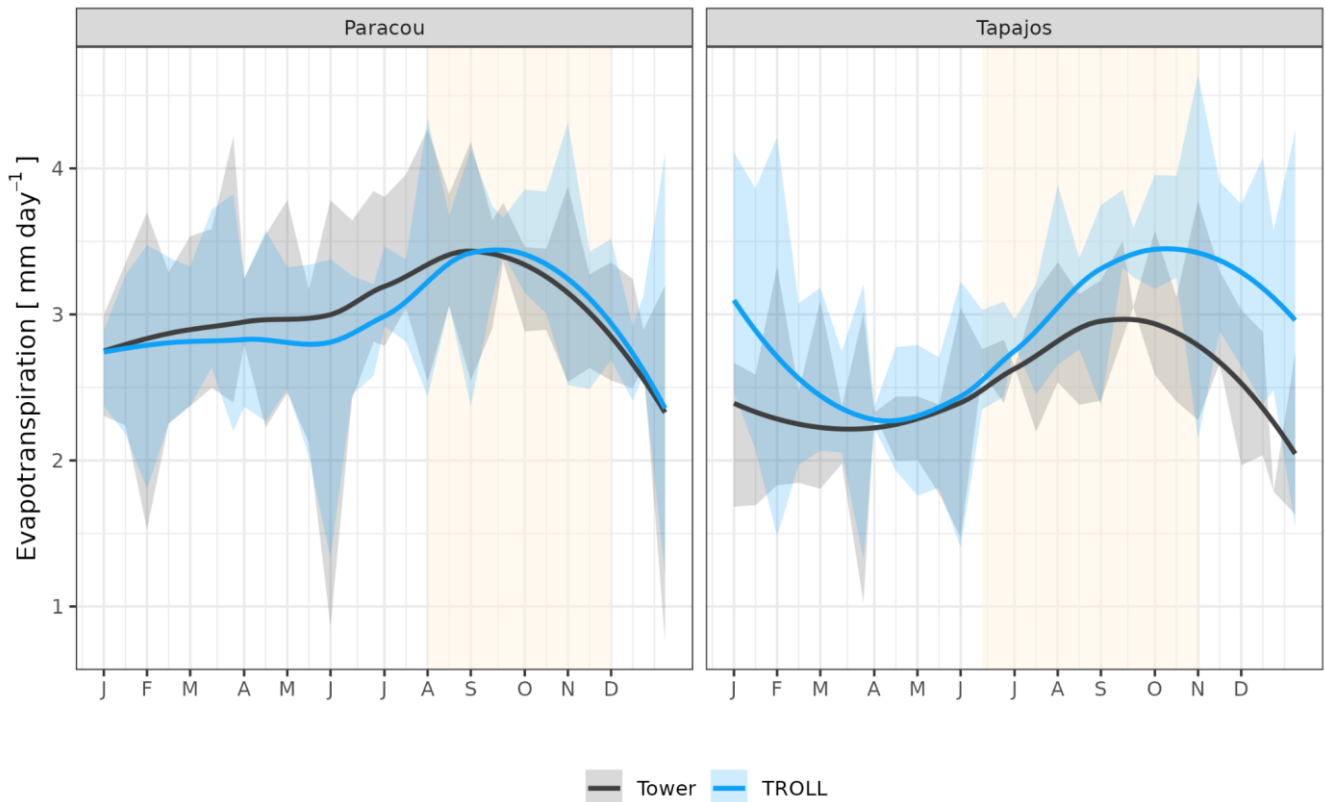
**Figure 11: Mean annual cycle of evapotranspiration for Paracou and Tapajos, derived from fortnightly means. The black lines
represent the evapotranspiration derived from eddy flux measurements and the blue lines the evapotranspiration simulated with
TROLL 4.0. Bands are the intervals of means across years, and the yellow vertical bands in the background correspond to the site's
climatological dry season. Simulated values correspond to 10 years of simulations starting from the end-state of 600-year
regeneration from bare ground with calibrated parameters at each site. Inter-annual variations are shown in Figure A8.**

Both eddy flux-derived and simulated GPP showed a positive logarithmic relationship with cumulative incoming PAR and

maximum VPD, and a positive linear relationship with mean temperature at daily scale (Fig. 12). Similarly, controlling for

absorbed light, both eddy flux-derived and simulated LUE showed a negative logarithmic relationship with maximum VPD

and a negative linear relationship with mean temperature at daily scale (Fig. A12). Limitations of LUE at high VPD and T

values were however lower in simulations than in eddy flux- or SIF-derived estimates. TROLL 4.0 predicted a higher PAR

conversion to carbon under high irradiance, high VPD and high temperature conditions when compared to eddy flux estimates,

consistent with the higher dry-season GPP in simulations (Fig. 10). Responses of SIF-derived GPP to climatic variables were

weak in comparison to simulated and eddy flux derived GPP. Simulated ET was positively correlated with maximum VPD,

cumulative PAR and mean temperature, similarly to eddy flux derived ET (Fig. 13). At Paracou, the relationships between

environmental drivers and simulated ET, closely aligned with the ones obtained from eddy flux estimates. However, at

Tapajos, simulated ET was overestimated under high irradiance, VPD, temperature and windy conditions in comparison to

520 eddy flux estimates. Simulated GPP and ET at both sites were more strongly controlled by environmental variables (higher R^2

521 in Figs. 12-13) than eddy flux derived GPP and ET.

522
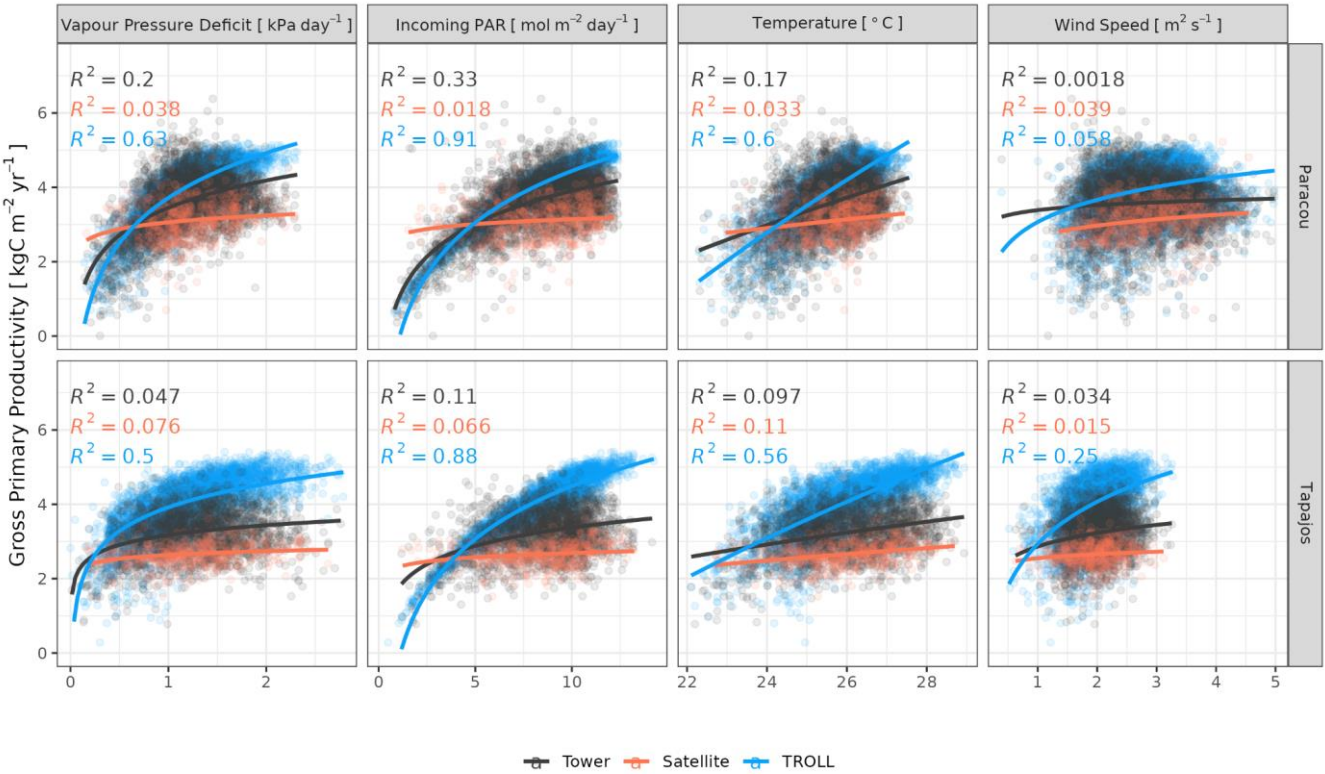
523 **Figure 12: Daily averages of gross primary productivity as a function of daily maximum vapour pressure deficit, total incoming**
524 **photosynthetically active radiation, average temperature, and average wind speed for model-, satellite- and eddy flux-based**
525 **estimates at Paracou (top) and Tapajos (bottom). Lines illustrate the linear regression of form y ~ log(x), and text the squared**
526 **Pearson's R correlation coefficient.**

527

Figure 13: Daily total evapotranspiration as a function of daily maximum vapour pressure deficit, total incoming photosynthetically active radiation, average temperature, and average wind speed for model- and eddy flux estimates at Paracou and Tapajos. Lines illustrate the linear regression of form y ~ log(x), and text the squared Pearson's R correlation coefficient.

4 Discussion

Here we tested the performance of TROLL 4.0 in reproducing observed forest structure and diversity, but also water and carbon fluxes, and leaf dynamics. We conducted a detailed model evaluation for two Amazonian rainforest sites, Paracou and Tapajos, presenting contrasting climate and soil properties. Both sites have been intensively monitored over the past decades, and we compared the model outputs with available data. We now discuss the consistencies and discrepancies between simulated and observed patterns, potential uncertainties in our results, and the advantages and possible improvements of TROLL 4.0.

4.1 Forest structure, composition and dynamics

TROLL 4.0 was found to jointly simulate realistic forest structure and species composition (Maréchaux et Chave, 2017). The calibration of three global parameters led to simulated number of stems across size classes and basal area or aboveground biomass in good agreement with observations from forest inventories above 10-cm dbh. Also, aerial lidar data allowed forest structure to be assessed independently of calibration data. This revealed a good ability of TROLL 4.0 to simulate the horizontal

and vertical structure of both forests, which is promising for various applications, including biomass estimation (Knapp et al., 2018). Similarly, the multiple inventories at Paracou from 2003 to 2013 revealed a good ability of TROLL 4.0 to simulate forest dynamics with both bell-shaped growth-size relationship and tree mortality. Understory inventories at Paracou also allowed us to independently evaluate TROLL 4.0's ability to simulate tree community structure in the 1 to 10-cm tree diameter range. TROLL 4.0 simulated the distribution of smaller trees reasonably well, although it underestimated individuals from the smallest cohorts. This underestimation of the density of small trees may be partly explained by the fact that the one-metre resolution of the voxel grid used in TROLL 4.0 only allows for one tree per square metre of ground, whereas smaller trees may be squeezed into certain areas of the understorey. However the number of simulated small stems remains lower than the maximal potential number in simulations. Another explanation could be a lack of light heterogeneity and associated trait variation in the understorey in simulations in comparison with observations (Montgomery and Chazdon, 2001), thus limiting the opportunities for recruitment and survival of small stems. Explorations of simulated micro-environmental variations within the canopy (de Frenne et al., 2019) and inclusion of trait ontogenetic shifts (Fortunel et al., 2019) and trait plasticity (Xu et al., 2017; Lamour et al., 2023) could further help understand and improve TROLL's ability to simulate forest structure and composition in the understory.

TROLL 4.0 attributes individual trees to botanical species and it permits tree functional traits to vary within species. It thus provides a finer-grained description of biodiversity compared to models based on plant functional types (e.g. Longo et al., 2018), and uses a description matching the one of ecologists, in contrast with taxonomy-free continuous trait spectrum approaches (e.g. Sakschewski et al., 2015). The simulated species composition presented classically observed L-shaped profile of species rank abundance distribution in the two sites, but with an over-estimated species evenness resulting in under-abundant dominant species and over-abundant rare species, as already observed in previous versions of the model (Maréchaux and Chave, 2017). Several simulation factors could have resulted in the overestimation of species evenness. The species trait values were extracted from global databases and partially imputed and may therefore not represent the true trait values for the region concerned, which could affect the behaviour of individual species in the model. However, as this noise is random, it seems unlikely that the global values and imputation have led to the skewed species abundance. More likely, the simulations used an external seed rain representing immigration from a continuous forest matrix. We here implemented a homogeneous seed rain, in which all species are equally-abundant, as a conservative test of the model's ability to represent community assembly. Here, the simulated composition after regeneration from bare ground is determined by species traits and their simulated effect on demographic processes and species fitness, rather than prescribed differences in seed rain. However, this homogeneous, and therefore unrealistic, seed rain maintains diversity in the simulated forest with a rescue effect, and can dampen species dominance by promoting less dominant species through a high immigration. The effects of the representation of seed production, dispersal and recruitment on simulated communities should be further explored in the future, especially for projections under disturbance scenarios where forest regeneration is key (Diaz-Yanez et al., 2024, Hanbury-Brown et al., 2022).

578 TROLL 4.0 also explicitly simulates forest functional diversity in the community. Simulated functional trait distributions
579 matched well the observed distributions at both sites, as already observed in previous versions of the model (Maréchaux and
580 Chave, 2017). In Paracou, the main discrepancies were the lack of individuals with high LMA (between 120 and 150 g m^{-2}),
581 low wood specific gravity (below 0.4 g cm^{-3}) and/or high leaf area (above 100 cm^2). In contrast, in Tapajos, the model tended
582 to simulate lower LMA and less negative turgor loss points on average. Since trait combinations are structured at the species
583 level, and trait integration is high dimensional in tropical forests, with decoupled leaf and wood economic spectra (Baraloto et
584 al., 2010) and weak associations between leaf turgor loss point and other leaf traits (Maréchaux et al., 2019), these
585 discrepancies can be more easily interpreted at Paracou where the trait distributions are built on species-level (and not genus-
586 level) information. Regarding the lack of high LMA individuals, TROLL 4.0 underestimated the abundance of common species
587 such as *Lecythis persistens* or *Licania alba*, which present high LMA. These species come from genera that are hyperdominant
588 across the Amazon basin (ter Steege et al., 2013) but may be underrepresented in the simulations due to the overestimation of
589 species evenness in TROLL 4.0 as discussed above. The lack of light wood and high leaf area individuals can be related to the
590 underestimated abundances of light demanding and pioneer species with fast growth (Chave et al., 2009), such as the ones of
591 the genus *Cecropia*. These species are known to quickly colonise forest gaps under high light conditions, thanks to fast carbon
592 assimilation and growth, and the dispersal of a high number of small, potentially dormant, seeds, leading to an omnipresence
593 of these species in the forest seed bank (Holthuijzen and Boerboom, 1982; Alvarez-Buylla and Martínez-Ramos, 1990). In
594 TROLL 4.0, the seed-size mediated tolerance-fecundity trade-off (Muller-Landau et al., 2010) is assumed to be perfectly
595 equalising, and all species present in the local seed bank and able to strive under the local light availability have the same
596 probability of being recruited per seed. However, this assumption likely disadvantages gap-affiliated species with a
597 colonisation strategy, and could easily be revisited in future model developments.

4.2 Leaf phenology

599 We calibrated and evaluated the new phenology module of TROLL 4.0. The calibration of the three module parameters ($a_{T,o}$,
600 $b_{T,o}$ and δ_o), which together control the variation of old leaf fall under drying conditions, was conducted using litterfall trap
601 data. This resulted in a realistic litterfall seasonality with a peak during the dry season as already documented (Manoli et al.,
602 2018, Chave et al., 2010, van Langenhove et al., 2020). Interestingly, the calibration resulted in the same values for two
603 parameters at the two sites ($a_{T,o}$, $b_{T,o}$) and close values for the third one (δ_o) to which the simulated litterfall pattern is less
604 sensitive (Fig. A5). At both sites, simulations with the mean value of the third parameter resulted in similar evaluations (not
605 shown). This suggests a good transferability of the phenology module across sites without the need for site-specific calibration,
606 although this remains to be further tested at additional sites and in contrasted conditions (e.g. Restrepo-Coupe et al., 2017). A
607 faster shedding of old leaves was assumed to depend on soil water potential in the root zone, rather than soil water content, on
608 individual leaf water potential at turgor loss point, and on tree size. These are biologically reasonable hypotheses and this
609 supports a good generality of the module. However, the current implementation of leaf dynamics in TROLL 4.0 leads to an
610 underestimation of the flux of litterfall in wet and dry seasons and, as a result, of total annual litterfall at both sites. In TROLL
611 4.0, leaf lifespan was parameterized based on an empirical relationship with leaf structure (leaf mass per area; Maréchaux et

al., companion paper). Previous relationships provided in the literature (Reich et al., 1991; Reich et al., 1997; Wright et al., 2004) provided contrasting leaf lifespan estimates, with the one implemented in TROLL 4.0 providing among the highest values, calling for a more in-depth exploration of the reliability and transferability of these empirical relationship. Alternative representations, such as the ones based on optimality principles (Kikuzawa 1991, Franklin et al., 2020, Manzoni et al., 2015), and their combination with the environmentally-driven old leaf shedding acceleration implemented in the new module could be explored in the future.

The evaluation of leaf area index (LAI) and its dynamics was difficult due to the number of products that yield inconsistent time series. Remotely sensed MODIS LAI showed a very small seasonal variation with a slight increase of LAI starting at the beginning of the dry season at both sites. However, MODIS LAI data products are known to be susceptible to the uncertainty affecting the bidirectional reflectance, and to saturate at high LAI values (Petri and Galvão, 2019). Local measurements of LAI through UAV-borne lidar in Paracou showed a stronger increase of total LAI of 0.5 m^2 m^{-2} starting at the beginning of the dry season, and leading to a maximum in the dry season. This pattern of variation was in strong agreement with that simulated for LAI by TROLL 4.0. Similarly, local measurements of top canopy LAI derived from phenological cameras in Tapajos (Wu et al., 2016) also showed a high increase of total LAI in the dry season, above 0.5 m^2 m^{-2}, also in good agreement with the seasonal LAI variation simulated by TROLL 4.0 at that site. By contrast, the LAI derived from terrestrial vertical lidar in Tapajos showed almost no variations (Smith et al., 2019), and such differences with both the patterns derived from phenological cameras and simulations need to be further scrutinised. Among potential explanations, LAI from TLS in Tapajos was adjusted to the annual mean of 5.7 (Stark et al., 2012), leading to lower absolute variations than what was obtained elsewhere, and used coarse spatial and temporal resolutions over small spatial and temporal extents (see material and methods). The discrepancy with simulated patterns could also be linked to uncertainties in LAI variations in the understory in our simulations. Recent studies have suggested opposite variations in LAI between the canopy and the understorey (Nunes et al., 2022), which should be further explored with TROLL 4.0. Overall, while obtaining a robust estimate of LAI temporal variation in tropical forests remains a challenge (Vincent et al., 2023; Bai et al., 2023), the relative variation of LAI simulated by TROLL 4.0 matched the most reliable products at each site, providing an encouraging assessment of this model's ability. Importantly, while total LAI variation remains limited on average within a year in tropical rainforests, this hides important turnover across leaf ages and species, and to ensure robust predictions models should endeavour to represent such turnover and its underlying processes (Wu et al., 2017).

The dry-season increase in total LAI simulated in TROLL 4.0 corresponds to a rejuvenation of the canopy leaf cover associated with a decrease in the LAI of old leaves at the beginning of the dry season, directly followed by an increase in the LAI of young leaves during the dry season. This turnover is in very good agreement with the one captured by phenological cameras at Tapajos (Wu et al., 2016) and documented in other studies (Yang et al., 2021; Doughty and Goulden, 2008), while the SIF-derived young LAI pattern (Yang et al., 2023) showed an opposite pattern at this site. The main difference in simulated cohorts between the two sites is the continuous dominance of old LAI in Tapajos while mature leaves dominated at the end of the dry

season in Paracou. This dominance of older (and less efficient) leaves in Tapajos simulations may be linked to the underestimated litterfall flux and soil water depletion during the dry season at this site. However, the relative proportion of leaf area across the different leaf age pools within and across datasets strongly depends on the definition of the leaf age pools themselves. These pools depend on the individual leaf lifespan in TROLL 4.0 (see section 2.6.2 in Maréchaux et al., submitted companion paper), while the transition from young to mature and mature to old are respectively fixed to 1.71 and 5.14 months in Yang et al. (2023) and fitted to 1 and 3 months in Wu et al. (2016). These contrasting approaches may explain the higher relative importance of old leaves in Wu et al. (2016) compared to Yang et al. (2023) and the intermediate values of TROLL 4.0 (Fig. 9). The seasonal dynamics of leaf cohorts remains poorly known in tropical forests and additional high-resolution optical imagery, *e.g.* by drones or phenological cameras, would be extremely useful to better document these patterns.

4.3 Water and carbon fluxes

At Tapajos, DGVMs simulated opposite seasonal trends in carbon and water fluxes compared to the observed ones (e.g. Fig. 1 in Chen et al., 2020; Fig. 5 in Longo et al., 2019b; Fig. 3 in Restrepo-Coupe et al., 2017). In contrast, TROLL 4.0 showed a good ability to represent the dynamics of both carbon and water fluxes estimated with eddy covariance data. In particular, TROLL 4.0 captures the dry season increase in gross primary productivity (GPP) and evapotranspiration (ET) documented for light-limited forests (Guan et al. 2017, Wagner et al. 2016, Aguilos et al. 2018). Simulated GPP and ET also presented realistic daily responses to environmental drivers, namely vapour pressure deficit (VPD), temperature, incident radiation and wind speed, both in direction and relative magnitude.

However, at Tapajos, we found that TROLL 4.0 overestimated ET during the dry season in comparison to eddy flux-derived ET values, under high irradiance, high VPD and high temperature. Simulated ET consists in tree transpiration summed over simulated individuals, water evaporation from the topsoil layer, and the direct evaporation of the rainfall intercepted by the canopy (Kunert et al., 2017). TROLL 4.0 may underestimate the stomatal control of transpiration during the dry season at Tapajos. Accordingly, the control of ET by atmospheric conditions in Tapajos was overestimated in simulated data in comparison to observations, suggesting a stronger coupling of vegetation and atmosphere at that site than simulated (de Kauwe et al., 2017). Underestimation of stomatal control can result from the representation of stomatal conductance and its responses to atmospheric dryness and soil water availability. In particular, the use of daily leaf predawn water potential to control leaf-level gas exchange, and not hourly variation of leaf water water potential (see equ. 39 and 40 in Maréchaux et al. submitted companion paper) can explain the overestimated ecosystem-level fluxes during the dry season. More generally, the understanding of leaf- to ecosystem-level fluxes are active areas of research and alternative representations could be considered in the future as availability of data increases (Wolf et al. 2016; Anderegg et al. 2018; Sabot et al., 2022, Lamour et al., 2022; see sections 2.5.2 and 2.5.3 and 4.1, and Appendix B in Maréchaux et al. submitted companion paper). Alternatively and/or concurrently, during the dry season, a lack of stomatal control can be due to an overestimation of soil water availability in the model. Soil water content dynamics depend on both the soil depth (Fig. A11) and on the soil hydraulic properties. The two sites are known to present heterogeneity in soil properties but we here performed simulations with homogenous soil properties,

both horizontally and vertically. For instance in Paracou, the topsoil layer is sandier than the 15-30 cm layer (Van Langenhove et al., 2021). Although TROLL 4.0 quantitatively captures the soil water depletion observed during the dry season, it appears to underestimate this depletion compared to empirical estimates at both sites (Fig. A10). This underestimation occurs in spite of the agreement between simulated and eddy covariance-derived ET during the dry season in Paracou, and of the higher simulated than eddy-covariance-derived ET during the dry season at Tapajos. Testing the model's sensitivity to soil layer thickness and properties will be important to perform prior to forest projections under drier future conditions and model spatial up-scaling (Meunier et al., 2022). For example, simulations with the ED2 model suggested that forest responses to drier conditions at Tapajos strongly depended on soil texture (Longo et al., 2018). Overall, it would be valuable to evaluate the model under drier conditions than the natural climate variation at the two sites we focused on in this study, such as under throughfall exclusion experiment (Powell et al. 2013; Yao et al. 2022). This would allow us to tease out potential model limitations and further test its forecasting capacity, and we hope to address this in a future contribution. Finally, the greater disagreement between simulated and eddy-covariance-derived ET at Tapajos than Paracou also calls for an in-depth evaluation of the global reanalysis precipitation data at this site. More generally, climate of the Amazon is notoriously challenging for models and it is important to further explore climate forcings in vegetation models.

TROLL 4.0 tended to overestimate empirical GPP estimates, particularly during the dry season, in comparison to both eddy covariance- and SIF-derived GPP. GPP is driven by the photosynthetic activity of the canopy, which depends on multiple processes (Diao et al., 2023; Slot et al., 2024) and further work would be needed to discriminate among them, while accounting for eddy covariance uncertainties (Cui and Chui, 2019). Absorbed light typically has an overriding effect on the variation of GPP across seasons in these light-limited rainforests (Yang et al. 2022, Guan et al. 2015), and simulated GPP is sensitive to the parameters that control light transmission and absorbance (light extinction coefficient, apparent quantum yield; Maréchaux & Chave, 2017). Both are assumed fixed and constant in simulations, but are known to vary with leaf angle distribution and leaf optical properties, depending on micro-environmental conditions and species (Long et al., 1993; Poorter et al., 1995; Meir et al., 2000; Kitajima et al., 2005). In addition, after removing the effect of absorbed light, simulated GPP showed less limitation to high values of VPD and temperature compared to eddy flux- or SIF-derived estimates. The response of leaf-level gas exchanges to the joint effect of atmospheric dryness and soil water availability shows no clear consensus across models (Powell et al, 2013; Trugman et al., 2018), and could be underestimated during the dry season in TROLL 4.0 simulations as discussed above for transpiration. Simulated GPP was higher than inferred from eddy covariance data, which was itself higher than GPP inferred from SIF satellite data (Chen et al., 2022). The eddy covariance-derived GPP were obtained from the net ecosystem exchanges using the nighttime partitioning method (Reichstein et al., 2005). This method was developed for temperate forests with greater temperature variations than tropical forests, which could therefore bias the empirical estimates. In addition, the eddy flux method has long been reported to underestimate CO_2 fluxes (Baldocchi, 2003; Gao et al., 2019). Similarly, even though solar induced fluorescence offers a great potential for the evaluation or the calibration of seasonal carbon fluxes in vegetation models, especially as the tropics are underrepresented by eddy flux tower networks (Villarreal et Vargas, 2021), current SIF products should be used with care (Marrs et al., 2020).

5 Conclusions

Here we evaluated the TROLL 4.0 individual-based forest dynamics model, which is capable of jointly simulating forest structure, diversity, dynamics and functioning. To this end, we assembled data from forest inventories, eddy flux towers, litterfall traps, UAV-borne and terrestrial lidar, phenological cameras, and satellite products at two Amazonian forest sites and found that TROLL 4.0 was able to realistically simulate the forest structure, composition, and dynamics, water and carbon fluxes, and leaf area dynamics. In using data of different nature and under the control of different processes, we limited the emergence of equi-finality issues (Medlyn et al., 2005), suggesting a good transferability and robustness of TROLL 4.0.

Comparison with field inventories, aerial and satellite data confirm TROLL 4.0's ability to realistically simulate the structure, composition, and dynamics of tropical forests, without imposing constraints beyond the species pool and calibrating more than three parameters. Discrepancies between observed and simulated number of stems in small size classes and abundance of trait values specific to colonising species suggest further developments of regeneration processes are needed, a worthy endeavour in the context of increased disturbance regimes. TROLL 4.0 was further able to simultaneously simulate the seasonality of productivity, evapotranspiration and leaf area in these two light-limited forests, as opposed to many current DGVMs (Chen et al., 2020; Restrepo-Coupe et al., 2017; Longo et al., 2019). The model's ability to simulate ecosystem fluxes is further shown by the responses of carbon and water fluxes to environmental drivers, whose direction and relative importance were well aligned with observations at both sites despite contrasting climate and soil properties. Additionally, the dynamics of total leaf area appeared realistically partitioned into different leaf pools, as shown by the leaf rejuvenation during the dry season in these systems (Wu et al., 2016; Yang et al., 2021). However, further inspection of the leaf area dynamics across the canopy vertical profile would be useful. Also, the model overestimation of productivity and evapotranspiration during the dry season calls for a more in-depth exploration of the model representation of respiration, plant hydraulics (e.g., stomatal control), and soil hydrology.

Overall, our analyses establish the suitability of TROLL 4.0 for simulating forest structure, diversity, dynamics and ecosystem functioning in short- and long-term studies of tropical forest dynamics, paving the way for multiple applications (Maréchaux et al., 2021). TROLL 4.0 could thus be used for projections of the effects of climate change on tropical forests, and exploration of the effect of biodiversity on forest resilience to these changes (Sakschewski et al., 2016). Similarly, as TROLL 4.0 retains the species-level taxonomic description, it can also help explore the effects of management practices such as timber production, for which half of tropical forests are designated (Blaser et al., 2011). While the development of TROLL 4.0 will continue, in light of knowledge improvement, novel data collection and identification of uncertainties and discrepancies, we believe it represents a valuable tool for addressing the major challenges tropical forests are currently facing.

Code and data availability

The TROLL version 4.0 and further developments are publicly available on GitHub as a C++ standalone at https://github.com/TROLL-code/TROLL (Maréchaux et al., 2024) or wrapped into an R package at https://github.com/sylvainschmitt/rcontroll/ (Schmitt et al., 2024). All the code associated with the analyses described in this paper are available at https://github.com/sylvainschmitt/troll_eval (Schmitt, 2024) with corresponding analyses notebook at https://sylvainschmitt.github.io/troll_eval/. Inventories data for Paracou trees over 10 cm are available through request on the CIRAD dataverse: https://dataverse.cirad.fr/dataverse/paracou. Paracou trees understory trees are available through request, PI: GS, GD, JC. Aerial Lidar Scanning from Paracou are available through request (PI: GV) and from dos-Santos et al. (2019) for Tapajos. Species data are available from Jucker et al., (2022), Maréchaux et al., (2015), Guillemot et al., (2022), Vleminckx et al., (2021), Maréchaux et al., (2019), Nemetschek et al., (2024), Schmitt and Boisseaux (2023), Boisseaux et al., (submitted), Ziegler et al., (2019), Baraloto et al., (2010), and from TRY (Kattge, Bönisch, et al., 2020). Soil data have been collected from Van Langenhove et al., (2021), Silver et al., (2000), Quesada et al., (2010), Sabatier et al., (1997), and Nepstad et al., (2002). Eddy covariance data from Paracou and Tapajos sites are available on FLUXNET at https://fluxnet.fluxdata.org (last access: 6 September 2023). ERA5-Land data are available on the Climate Data Store: https://cds.climate.copernicus.eu/cdsapp#!/dataset/reanalysis-era5-land?tab=overview. TROPOMI SIF satellite data are available in Chen et al., (2022). Litterfall data at Tapajos are available online through the Oak Ridge National Laboratory (ORNL) Distributed Active Archive Center (DAAC): https://daac.ornl.gov/LBA/guides/CD10_Litter_Tapajos.html and upon-request at Paracou, PI: DB. MODIS LAI data are available online and were extracted from PLUMBER2 on Research Data Australia: https://researchdata.edu.au/plumber2-forcing-evaluation-surface-models/1656048. Terrestrial LAD data from Tapajos are available in Smith et al., (2019). Lidar PAD data from Paracou are available upon-request, PIs: NB and GV. LAI variations among young, mature and leaf cohorts are available from the reanalysis of Yang et al. (2023) at: https://figshare.com/articles/dataset/Leaf_age-dependent_LAI_seasonality_product_Lad-LAI_over_tropical_and_subtropical_evergreen_broadleaved_forests/21700955/4 and from the phenological camera of Wu et al., (2016) at: https://datadryad.org/stash/dataset/doi:10.5061/dryad.8fb47. Tapajos soil moisture data from Restrepo-Coupe et al. (2024) are available at: https://datadryad.org/stash/dataset/doi:10.5061/dryad.d51c5b08g.

Supplement

The supplement related to this article is available below.

Author contributions

SS and IM designed the model assessment and carried out the TROLL 4.0 simulations. SS, FJF, JC and IM developed TROLL 4.0. SS, FJF, NB, MB, DB, BB, XC, GD, JL, DN, NRC, ScS, GS, PV, GV, CZ, JC, IM contributed to the data collection and compilation. SS and IM wrote the paper.

Competing interests

The authors declare that they have no conflict of interest.

Acknowledgements

We are particularly grateful to all the ground workers and data collectors (forest inventories, eddy flux measurements, litter traps, lidar acquisition, sampling and measurement of functional traits, and more) who are not named here but who contributed to the vast knowledge base without which the evaluation of TROLL 4.0 would have been impossible. We are grateful to the GenoToul bioinformatics facility (Castanet-Tolosan, Toulouse, Occitanie, France, doi:10.15454/1.5572369328961167E12) for providing computing resources.

Financial support

This research has been supported by fundings from ANR (the French National Research Agency) under the "Investissements d'avenir" program with the references ANR-16-IDEX-0006, ANR-10-LABX-25-01, ANR-10-LABX-0041, the Amazonian Landscapes in Transition ANR project (ALT), CNES Biomass-Valo project, and ESA CCI-BIOMASS.

References

Aguilos, M., Hérault, B., Burban, B., Wagner, F., and Bonal, D.: What drives long-term variations in carbon flux and balance in a tropical rainforest in French Guiana?, Agricultural and Forest Meteorology, 253-254, 114–123, https://doi.org/10.1016/j.agrformet.2018.02.009, 2018.

Allen, R. G., Pereira, L. S., Raes, D., & Smith, M. (1998). Crop evapotranspiration-Guidelines for computing crop water requirements-FAO Irrigation and drainage paper 56. *Fao, Rome*, *300*(9), D05109.

Alvarez-Buylla, E. R. and Martinez-Ramos, M.: Demography and allometry of cecropia obtusifolia, a neotropical pioneer tree - an evaluation of the climax-pioneer paradigm for tropical rain forests, The Journal of Ecology, 80, 275, https://doi.org/10.2307/2261011, 1992.

Aragão, L. E. O. C., Malhi, Y., Metcalfe, D. B., Silva-Espejo, J. E., Jiménez, E., Navarrete, D., Almeida, S., Costa, A. C. L., Salinas, N., Phillips, O. L., Anderson, L. O., Alvarez, E., Baker, T. R., Goncalvez, P. H., Huamán-Ovalle, J., Mamani-Solórzano, M., Meir, P., Monteagudo, A., Patiño, S., Peñuela, M. C., Prieto, A., Quesada, C. A., Rozas-Dávila, A., Rudas, A., Silva Jr., J. A., and Vásquez, R.: Above- and below-ground net primary productivity across ten Amazonian forests on contrasting soils, Biogeosciences, 6, 2759–2778, https://doi.org/10.5194/bg-6-2759-2009, 2009.

BALDOCCHI, D. D.: Assessing the eddy covariance technique for evaluating carbon dioxide exchange rates of ecosystems: past, present and future, Global Change Biology, 9, 479–492, https://doi.org/10.1046/j.1365-2486.2003.00629.x, 2003.

Baraloto, C., Timothy Paine, C. E., Poorter, L., Beauchene, J., Bonal, D., Domenach, A.-M., Hérault, B., Patiño, S., Roggy, J.-C., and Chave, J.: Decoupled leaf and stem economics in rain forest trees, Ecology Letters, 13, 1338–1347, https://doi.org/10.1111/j.1461-0248.2010.01517.x, 2010a.

Baraloto, C., Timothy Paine, C. E., Patiño, S., Bonal, D., Hérault, B., and Chave, J.: Functional trait variation and sampling strategies in species-rich plant communities, Functional Ecology, 24, 208–216, https://doi.org/10.1111/j.1365-2435.2009.01600.x, 2010b.

Berzaghi, F., Wright, I. J., Kramer, K., Oddou-Muratorio, S., Bohn, F. J., Reyer, C. P. O., Sabaté, S., Sanders, T. G. M., and Hartig, F.: Towards a New Generation of Trait-Flexible Vegetation Models, Trends in Ecology & Evolution, 35, 191–205, https://doi.org/10.1016/j.tree.2019.11.006, 2020.

Bloomfield, K. J., Van Hoolst, R., Balzarolo, M., Janssens, I. A., Vicca, S., Ghent, D., & Prentice, I. C. (2023). Towards a general monitoring system for terrestrial primary production: A test spanning the european drought of 2018. *Remote Sensing*, *15*(6), 1693. https://doi.org/10.3390/rs15061693

Bodegom, P. M. van, Douma, J. C., and Verheijen, L. M.: A fully traits-based approach to modeling global vegetation distribution, Proceedings of the National Academy of Sciences, 111, 13733–13738, https://doi.org/10.1073/pnas.1304551110, 2014.

Boisseaux et al. submitted

BONAL, D., BOSC, A., PONTON, S., GORET, J.-Y., BURBAN, B., GROSS, P., BONNEFOND, J.-M., ELBERS, J., LONGDOZ, B., EPRON, D., GUEHL, J.-M., and GRANIER, A.: Impact of severe dry season on net ecosystem exchange in the Neotropical rainforest of French Guiana, Global Change Biology, 14, 1917–1933, https://doi.org/10.1111/j.1365-2486.2008.01610.x, 2008.

Bonan, G. B.: Forests and Climate Change: Forcings, Feedbacks, and the Climate Benefits of Forests, Science, 320, 1444–1449, https://doi.org/10.1126/science.1155121, 2008.

Bugmann, H.: Climatic Change, 51, 259–305, https://doi.org/10.1023/a:1012525626267, 2001.

Buuren, S. van and Groothuis-Oudshoorn, K.: mice: Multivariate Imputation by Chained Equations inR, Journal of Statistical Software, 45, https://doi.org/10.18637/jss.v045.i03, 2011.

Chave, J., Andalo, C., Brown, S., Cairns, M. A., Chambers, J. Q., Eamus, D., Fölster, H., Fromard, F., Higuchi, N., Kira, T., Lescure, J.-P., Nelson, B. W., Ogawa, H., Puig, H., Riéra, B., and Yamakura, T.: Tree allometry and improved estimation of carbon stocks and balance in tropical forests, Oecologia, 145, 87–99, https://doi.org/10.1007/s00442-005-0100-x, 2005.

Chave, J., Navarrete, D., Almeida, S., Álvarez, E., Aragão, L. E. O. C., Bonal, D., Châtelet, P., Silva-Espejo, J. E., Goret, J.-Y., Hildebrand, P. von, Jiménez, E., Patiño, S., Peñuela, M. C., Phillips, O. L., Stevenson, P., and Malhi, Y.: Regional and seasonal patterns of litterfall in tropical South America, Biogeosciences, 7, 43–55, https://doi.org/10.5194/bg-7-43-2010, 2010.

Chen, X., Maignan, F., Viovy, N., Bastos, A., Goll, D., Wu, J., Liu, L., Yue, C., Peng, S., Yuan, W., da Conceição, A. C., O'Sullivan, M., and Ciais, P.: Novel Representation of Leaf Phenology Improves Simulation of Amazonian Evergreen

Forest Photosynthesis in a Land Surface Model, Journal of Advances in Modeling Earth Systems, 12, https://doi.org/10.1029/2018ms001565, 2020.

Chen, X., Huang, Y., Nie, C., Zhang, S., Wang, G., Chen, S., and Chen, Z.: A long-term reconstructed TROPOMI solar-induced fluorescence dataset using machine learning algorithms, Scientific Data, 9, https://doi.org/10.1038/s41597-022-01520-1, 2022.

Cuartas, L. A., Tomasella, J., Nobre, A. D., Hodnett, M. G., Waterloo, M. J., and Múnera, J. C.: Interception water-partitioning dynamics for a pristine rainforest in Central Amazonia: Marked differences between normal and dry years, Agricultural and Forest Meteorology, 145, 69–83, https://doi.org/10.1016/j.agrformet.2007.04.008, 2007.

Cui, W. and Chui, T. F. M.: Temporal and spatial variations of energy balance closure across FLUXNET research sites, Agricultural and Forest Meteorology, 271, 12–21, https://doi.org/10.1016/j.agrformet.2019.02.026, 2019.

Cusack, D. F., Christoffersen, B., Smith-Martin, C. M., Andersen, K. M., Cordeiro, A. L., Fleischer, K., Wright, S. J., Guerrero-Ramírez, N. R., Lugli, L. F., McCulloch, L. A., Sanchez-Julia, M., Batterman, S. A., Dallstream, C., Fortunel, C., Toro, L., Fuchslueger, L., Wong, M. Y., Yaffar, D., Fisher, J. B., Arnaud, M., Dietterich, L. H., Addo-Danso, S. D., Valverde-Barrantes, O. J., Weemstra, M., Ng, J. C., and Norby, R. J.: Toward a coordinated understanding of hydro-biogeochemical root functions in tropical forests for application in vegetation models, New Phytologist, 242, 351–371, https://doi.org/10.1111/nph.19561, 2024.

De Frenne, P., Zellweger, F., Rodríguez-Sánchez, F., Scheffers, B. R., Hylander, K., Luoto, M., Vellend, M., Verheyen, K., and Lenoir, J.: Global buffering of temperatures under forest canopies, Nature Ecology & Evolution, 3, 744–749, https://doi.org/10.1038/s41559-019-0842-1, 2019.

De Kauwe, M. G., Medlyn, B. E., Knauer, J., and Williams, C. A.: Ideas and perspectives: how coupled is the vegetation to the boundary layer?, Biogeosciences, 14, 4435–4453, https://doi.org/10.5194/bg-14-4435-2017, 2017.

Diao, H., Cernusak, L. A., Saurer, M., Gessler, A., Siegwolf, R. T. W., and Lehmann, M. M.: Uncoupling of stomatal conductance and photosynthesis at high temperatures: mechanistic insights from online stable isotope techniques, New Phytologist, 241, 2366–2378, https://doi.org/10.1111/nph.19558, 2024.

Díaz-Yáñez, O., Käber, Y., Anders, T., Bohn, F., Braziunas, K. H., Brůna, J., Fischer, R., Fischer, S. M., Hetzer, J., Hickler, T., Hochauer, C., Lexer, M. J., Lischke, H., Mairota, P., Merganič, J., Merganičová, K., Mette, T., Mina, M., Morin, X., Nieberg, M., Rammer, W., Reyer, C. P. O., Scheiter, S., Scherrer, D., and Bugmann, H.: Tree regeneration in models of forest dynamics: A key priority for further research, Ecosphere, 15, https://doi.org/10.1002/ecs2.4807, 2024.

Dormann, C. F., Schymanski, S. J., Cabral, J., Chuine, I., Graham, C., Hartig, F., Kearney, M., Morin, X., Römermann, C., Schröder, B., and Singer, A.: Correlation and process in species distribution models: bridging a dichotomy, Journal of Biogeography, 39, 2119–2131, https://doi.org/10.1111/j.1365-2699.2011.02659.x, 2012.

dos-Santos, M. N., Keller, M. M., and Morton, D. C.: LiDAR Surveys over Selected Forest Research Sites, Brazilian Amazon, 2008-2018, https://doi.org/10.3334/ORNLDAAC/1644, 2019.

Doughty, C. E. and Goulden, M. L.: Seasonal patterns of tropical forest leaf area index and CO2 exchange, Journal of Geophysical Research: Biogeosciences, 113, https://doi.org/10.1029/2007jg000590, 2008.

877 Duursma, R. A., Blackman, C. J., Lopéz, R., Martin-StPaul, N. K., Cochard, H., and Medlyn, B. E.: On the minimum leaf
878 conductance: its role in models of plant water use, and ecological and environmental controls, New Phytologist, 221, 693–
879 705, https://doi.org/10.1111/nph.15395, 2018.

880 Estes, L., Elsen, P. R., Treuer, T., Ahmed, L., Caylor, K., Chang, J., Choi, J. J., and Ellis, E. C.: The spatial and temporal
881 domains of modern ecology, Nature Ecology & Evolution, 2, 819–826, https://doi.org/10.1038/s41559-018-0524-4, 2018.

882 Evans, M. R.: Modelling ecological systems in a changing world, Philosophical Transactions of the Royal Society B:
883 Biological Sciences, 367, 181–190, https://doi.org/10.1098/rstb.2011.0172, 2012.

884 Farquhar, G. D., Caemmerer, S. von, and Berry, J. A.: A biochemical model of photosynthetic CO_2 assimilation in leaves
885 of C3 species, Planta, 149, 78–90, https://doi.org/10.1007/bf00386231, 1980.

886 Fischer, F. J., Maréchaux, I., and Chave, J.: Improving plant allometry by fusing forest models and remote sensing, New
887 Phytologist, 223, 1159–1165, https://doi.org/10.1111/nph.15810, 2019.

888 Fischer, F. J., Jackson, T., Vincent, G., and Jucker, T.: Robust characterisation of forest structure from airborne laser
889 scanningA systematic assessment and sample workflow for ecologists, Methods in Ecology and Evolution,
890 https://doi.org/10.1111/2041-210x.14416, 2024.

891 Fischer, R., Bohn, F., Dantas de Paula, M., Dislich, C., Groeneveld, J., Gutiérrez, A. G., Kazmierczak, M., Knapp, N.,
892 Lehmann, S., Paulick, S., Pütz, S., Rödig, E., Taubert, F., Köhler, P., and Huth, A.: Lessons learned from applying a forest
893 gap model to understand ecosystem and carbon dynamics of complex tropical forests, Ecological Modelling, 326, 124–
894 133, https://doi.org/10.1016/j.ecolmodel.2015.11.018, 2016.

895 Fisher, J. B., Huntzinger, D. N., Schwalm, C. R., and Sitch, S.: Modeling the Terrestrial Biosphere, Annual Review of
896 Environment and Resources, 39, 91–123, https://doi.org/10.1146/annurev-environ-012913-093456, 2014.

897 Fisher, R. A., Muszala, S., Verteinstein, M., Lawrence, P., Xu, C., McDowell, N. G., Knox, R. G., Koven, C., Holm, J.,
898 Rogers, B. M., Spessa, A., Lawrence, D., and Bonan, G.: Taking off the training wheels: the properties of a dynamic
899 vegetation model without climate envelopes, CLM4.5(ED), Geoscientific Model Development, 8, 3593–3619,
900 https://doi.org/10.5194/gmd-8-3593-2015, 2015.

901 Fisher, R. A., Koven, C. D., Anderegg, W. R. L., Christoffersen, B. O., Dietze, M. C., Farrior, C. E., Holm, J. A., Hurtt, G.
902 C., Knox, R. G., Lawrence, P. J., Lichstein, J. W., Longo, M., Matheny, A. M., Medvigy, D., Muller-Landau, H. C., Powell,
903 T. L., Serbin, S. P., Sato, H., Shuman, J. K., Smith, B., Trugman, A. T., Viskari, T., Verbeeck, H., Weng, E., Xu, C., Xu,
904 X., Zhang, T., and Moorcroft, P. R.: Vegetation demographics in Earth System Models: A review of progress and priorities,
905 Global Change Biology, 24, 35–54, https://doi.org/10.1111/gcb.13910, 2017.

906 Fortunel, C., Stahl, C., Heuret, P., Nicolini, E., and Baraloto, C.: Disentangling the effects of environment and ontogeny
907 on tree functional dimensions for congeneric species in tropical forests, New Phytologist, 226, 385–395,
908 https://doi.org/10.1111/nph.16393, 2020.

909 Franklin, O., Harrison, S. P., Dewar, R., Farrior, C. E., Brännström, Å., Dieckmann, U., Pietsch, S., Falster, D., Cramer,
910 W., Loreau, M., Wang, H., Mäkelä, A., Rebel, K. T., Meron, E., Schymanski, S. J., Rovenskaya, E., Stocker, B. D., Zaehle,
911 S., Manzoni, S., Oijen, M. van, Wright, I. J., Ciais, P., Bodegom, P. M. van, Peñuelas, J., Hofhansl, F., Terrer, C.,

Soudzilovskaia, N. A., Midgley, G., and Prentice, I. C.: Organizing principles for vegetation dynamics, Nature Plants, 6, 444–453, https://doi.org/10.1038/s41477-020-0655-x, 2020.

Fu, R., Yin, L., Li, W., Arias, P. A., Dickinson, R. E., Huang, L., Chakraborty, S., Fernandes, K., Liebmann, B., Fisher, R., and Myneni, R. B.: Increased dry-season length over southern Amazonia in recent decades and its implication for future climate projection, Proceedings of the National Academy of Sciences, 110, 18110–18115, https://doi.org/10.1073/pnas.1302584110, 2013.

Funk, C., Peterson, P., Landsfeld, M., Pedreros, D., Verdin, J., Shukla, S., ... & Michaelsen, J. (2015). The climate hazards infrared precipitation with stations—a new environmental record for monitoring extremes. *Scientific data*, *2*(1), 1-21.https://doi.org/10.1038/sdata.2015.66

Gao, Z., Liu, H., Missik, J. E. C., Yao, J., Huang, M., Chen, X., Arntzen, E., and Mcfarland, D. P.: Mechanistic links between underestimated CO_2 fluxes and non-closure of the surface energy balance in a semi-arid sagebrush ecosystem, Environmental Research Letters, 14, 044016, https://doi.org/10.1088/1748-9326/ab082d, 2019.

GONCALVES, F. G., TREUHAFT, R. N., DOS SANTOS, J. R., GRACA, P., ALMEIDA, A., and LAW, B. E.: Tree Inventory and Biometry Measurements, Tapajos National Forest, Para, Brazil, 2010, https://doi.org/10.3334/ORNLDAAC/1552, 2018.

Gourlet-Fleury, S., Guehl, J. M. J. M., & Laroussinie, O. (2004). *Ecology and management of a neotropical rainforest. Lessons drawn from Paracou, a long-term experimental research site in French Guiana* (pp. 350-p). Elsevier.

Guan, K., Pan, M., Li, H., Wolf, A., Wu, J., Medvigy, D., Caylor, K. K., Sheffield, J., Wood, E. F., Malhi, Y., Liang, M., Kimball, J. S., Saleska, Scott R., Berry, J., Joiner, J., and Lyapustin, A. I.: Photosynthetic seasonality of global tropical forests constrained by hydroclimate, Nature Geoscience, 8, 284–289, https://doi.org/10.1038/ngeo2382, 2015.

Guillemot, J., Martin-StPaul, N. K., Bulascoschi, L., Poorter, L., Morin, X., Pinho, B. X., Maire, G. le, R. L. Bittencourt, P., Oliveira, R. S., Bongers, F., Brouwer, R., Pereira, L., Gonzalez Melo, G. A., Boonman, C. C. F., Brown, K. A., Cerabolini, B. E. L., Niinemets, Ü., Onoda, Y., Schneider, J. V., Sheremetiev, S., and Brancalion, P. H. S.: Small and slow is safe: On the drought tolerance of tropical tree species, Global Change Biology, 28, 2622–2638, https://doi.org/10.1111/gcb.16082, 2022.

Hanbury-Brown, A. R., Ward, R. E., and Kueppers, L. M.: Forest regeneration within Earth system models: current process representations and ways forward, New Phytologist, 235, 20–40, https://doi.org/10.1111/nph.18131, 2022.

Harper, A., Baker, I. T., Denning, A. S., Randall, D. A., Dazlich, D., and Branson, M.: Impact of Evapotranspiration on Dry Season Climate in the Amazon Forest*, Journal of Climate, 27, 574–591, https://doi.org/10.1175/jcli-d-13-00074.1, 2014.

Hérault, B., Bachelot, B., Poorter, L., Rossi, V., Bongers, F., Chave, J., ... & Baraloto, C. (2011). Functional traits shape ontogenetic growth trajectories of rain forest tree species. *Journal of ecology*, *99*(6), 1431-1440.

Holthuijzen, A. M. A. and Boerboom, J. H. A.: The cecropia seedbank in the surinam lowland rain forest, Biotropica, 14, 62, https://doi.org/10.2307/2387761, 1982.

Hubau, W., Lewis, S. L., Phillips, O. L., Affum-Baffoe, K., Beeckman, H., Cuní-Sanchez, A., Daniels, A. K., Ewango, C. E. N., Fauset, S., Mukinzi, J. M., Sheil, D., Sonké, B., Sullivan, M. J. P., Sunderland, T. C. H., Taedoumg, H., Thomas, S. C., White, L. J. T., Abernethy, K. A., Adu-Bredu, S., Amani, C. A., Baker, T. R., Banin, L. F., Baya, F., Begne, S. K., Bennett, A. C., Benedet, F., Bitariho, R., Bocko, Y. E., Boeckx, P., Boundja, P., Brienen, R. J. W., Brncic, T., Chezeaux, E., Chuyong, G. B., Clark, C. J., Collins, M., Comiskey, J. A., Coomes, D. A., Dargie, G. C., Haulleville, T. de, Kamdem, M. N. D., Doucet, J.-L., Esquivel-Muelbert, A., Feldpausch, T. R., Fofanah, A., Foli, E. G., Gilpin, M., Gloor, E., Gonmadje, C., Gourlet-Fleury, S., Hall, J. S., Hamilton, A. C., Harris, D. J., Hart, T. B., Hockemba, M. B. N., Hladik, A., Ifo, S. A., Jeffery, K. J., Jucker, T., Yakusu, E. K., Kearsley, E., Kenfack, D., Koch, A., Leal, M. E., Levesley, A., Lindsell, J. A., Lisingo, J., Lopez-Gonzalez, G., Lovett, J. C., Makana, J.-R., Malhi, Y., Marshall, A. R., Martin, J., Martin, E. H., Mbayu, F. M., Medjibe, V. P., Mihindou, V., Mitchard, E. T. A., Moore, S., Munishi, P. K. T., Bengone, N. N., Ojo, L., Ondo, F. E., Peh, K. S.-H., Pickavance, G. C., Poulsen, A. D., Poulsen, J. R., Qie, L., Reitsma, J., Rovero, F., Swaine, M. D., Talbot, J., Taplin, J., Taylor, D. M., Thomas, D. W., Toirambe, B., Mukendi, J. T., Tuagben, D., Umunay, P. M., et al.: Asynchronous carbon sink saturation in African and Amazonian tropical forests, Nature, 579, 80–87, https://doi.org/10.1038/s41586-020-2035-0, 2020.

Huntingford, C., Atkin, O. K., Martinez-de la Torre, A., Mercado, L. M., Heskel, M. A., Harper, A. B., Bloomfield, K. J., O'Sullivan, O. S., Reich, P. B., Wythers, K. R., Butler, E. E., Chen, M., Griffin, K. L., Meir, P., Tjoelker, M. G., Turnbull, M. H., Sitch, S., Wiltshire, A., and Malhi, Y.: Implications of improved representations of plant respiration in a changing climate, Nature Communications, 8, https://doi.org/10.1038/s41467-017-01774-z, 2017.

Jaouen, G.: Paracou forest permanent plots details, https://doi.org/10.18167/DVN1/8G8AHY, 2022.

Joetzjer, E., Maignan, F., Chave, J., Goll, D., Poulter, B., Barichivich, J., Maréchaux, I., Luyssaert, S., Guimberteau, M., Naudts, K., Bonal, D., and Ciais, P.: Effect of tree demography and flexible root water uptake for modeling the carbon and water cycles of Amazonia, Ecological Modelling, 469, 109969, https://doi.org/10.1016/j.ecolmodel.2022.109969, 2022.

Jucker, T., Fischer, F. J., Chave, J., Coomes, D. A., Caspersen, J., Ali, A., Loubota Panzou, G. J., Feldpausch, T. R., Falster, D., Usoltsev, V. A., Adu-Bredu, S., Alves, L. F., Aminpour, M., Angoboy, I. B., Anten, N. P. R., Antin, C., Askari, Y., Muñoz, R., Ayyappan, N., Balvanera, P., Banin, L., Barbier, N., Battles, J. J., Beeckman, H., Bocko, Y. E., Bond-Lamberty, B., Bongers, F., Bowers, S., Brade, T., Breugel, M. van, Chantrain, A., Chaudhary, R., Dai, J., Dalponte, M., Dimobe, K., Domec, J.-C., Doucet, J.-L., Duursma, R. A., Enríquez, M., Ewijk, K. Y. van, Farfán-Rios, W., Fayolle, A., Forni, E., Forrester, D. I., Gilani, H., Godlee, J. L., Gourlet-Fleury, S., Haeni, M., Hall, J. S., He, J.-K., Hemp, A., Hernández-Stefanoni, J. L., Higgins, S. I., Holdaway, R. J., Hussain, K., Hutley, L. B., Ichie, T., Iida, Y., Jiang, H., Joshi, P. R., Kaboli, H., Larsary, M. K., Kenzo, T., Kloeppel, B. D., Kohyama, T., Kunwar, S., Kuyah, S., Kvasnica, J., Lin, S., Lines, E. R., Liu, H., Lorimer, C., Loumeto, J.-J., Malhi, Y., Marshall, P. L., Mattsson, E., Matula, R., Meave, J. A., Mensah, S., Mi, X., Momo, S., Moncrieff, G. R., Mora, F., Nissanka, S. P., O'Hara, K. L., Pearce, S., Pelissier, R., Peri, P. L., Ploton, P., Poorter, L., Pour, M. J., Pourbabaei, H., Dupuy-Rada, J. M., Ribeiro, S. C., Ryan, C., Sanaei, A., Sanger, J., Schlund, M., Sellan, G., et al.: Tallo: A global tree allometry and crown architecture database, Global Change Biology, 28, 5254–5268, https://doi.org/10.1111/gcb.16302, 2022.

981   Kattge, J., Bönisch, G., and al., et: TRY plant trait database – enhanced coverage and open access, Global Change Biology,
982   26, 119–188, https://doi.org/10.1111/gcb.14904, 2020.

983   Kikuzawa, K.: A Cost-Benefit Analysis of Leaf Habit and Leaf Longevity of Trees and Their Geographical Pattern, The
984   American Naturalist, 138, 1250–1263, https://doi.org/10.1086/285281, 1991.

985   Knapp, N., Fischer, R., and Huth, A.: Linking lidar and forest modeling to assess biomass estimation across scales and
986   disturbance states, Remote Sensing of Environment, 205, 199–209, https://doi.org/10.1016/j.rse.2017.11.018, 2018.

987   Koch, A., Hubau, W., and Lewis, S. L.: Earth System Models Are Not Capturing Present-Day Tropical Forest Carbon
988   Dynamics, Earth's Future, 9, https://doi.org/10.1029/2020ef001874, 2021.

989   Köster, J. and Rahmann, S.: Snakemakea scalable bioinformatics workflow engine, Bioinformatics, 28, 2520–2522,
990   https://doi.org/10.1093/bioinformatics/bts480, 2012.

991   Kunert, N., Aparecido, L. M. T., Wolff, S., Higuchi, N., Santos, J. dos, Araujo, A. C. de, and Trumbore, S.: A revised
992   hydrological model for the Central Amazon: The importance of emergent canopy trees in the forest water budget,
993   Agricultural and Forest Meteorology, 239, 47–57, https://doi.org/10.1016/j.agrformet.2017.03.002, 2017.

994   Kurtzer, G. M., Sochat, V., and Bauer, M. W.: Singularity: Scientific containers for mobility of compute, PLOS ONE, 12,
995   e0177459, https://doi.org/10.1371/journal.pone.0177459, 2017.

996   Lamour, J., Davidson, K. J., Ely, K. S., Le Moguédec, G., Leakey, A. D. B., Li, Q., Serbin, S. P., and Rogers, A.: An
997   improved representation of the relationship between photosynthesis and stomatal conductance leads to more stable
998   estimation of conductance parameters and improves the goodness-of-fit across diverse data sets, Global Change Biology,
999   28, 3537–3556, https://doi.org/10.1111/gcb.16103, 2022.

1000   Lamour, J., Davidson, K.J., Ely, K.S., Le Moguédec, G., Anderson, J.A., Li, Q., Calderón, O., Koven, C.D., Wright, S.J.,
1001   Walker, A.P., Serbin, S.P. and Rogers, A.: The effect of the vertical gradients of photosynthetic parameters on the CO2
1002   assimilation and transpiration of a Panamanian tropical forest. New Phytol, 238: 2345-2362.
1003   https://doi.org/10.1111/nph.18901, 2023.

1004   Lapola, D. M., Pinho, P., Barlow, J., Aragão, L. E. O. C., Berenguer, E., Carmenta, R., Liddy, H. M., Seixas, H., Silva, C.
1005   V. J., Silva-Junior, C. H. L., Alencar, A. A. C., Anderson, L. O., Armenteras, D., Brovkin, V., Calders, K., Chambers, J.,
1006   Chini, L., Costa, M. H., Faria, B. L., Fearnside, P. M., Ferreira, J., Gatti, L., Gutierrez-Velez, V. H., Han, Z., Hibbard, K.,
1007   Koven, C., Lawrence, P., Pongratz, J., Portela, B. T. T., Rounsevell, M., Ruane, A. C., Schaldach, R., Silva, S. S. da,
1008   Randow, C. von, and Walker, W. S.: The drivers and impacts of Amazon forest degradation, Science, 379,
1009   https://doi.org/10.1126/science.abp8622, 2023.

1010   Lawrence, D. and Vandecar, K.: Effects of tropical deforestation on climate and agriculture, Nature Climate Change, 5,
1011   27–36, https://doi.org/10.1038/nclimate2430, 2014.

1012   Long, S. P., Postl, W. F., and Bolher-Nordenkampf, H. R.: Quantum yields for uptake of carbon dioxide in C3 vascular
1013   plants of contrasting habitats and taxonomic groupings, Planta, 189, https://doi.org/10.1007/bf00195081, 1993.

1014   Longo, M., Knox, R. G., Levine, N. M., Alves, L. F., Bonal, D., Camargo, P. B., Fitzjarrald, D. R., Hayek, M. N., Restrepo-
1015   Coupe, N., Saleska, S. R., Silva, R. da, Stark, S. C., Tapajós, R. P., Wiedemann, K. T., Zhang, K., Wofsy, S. C., and

Moorcroft, P. R.: Ecosystem heterogeneity and diversity mitigate Amazon forest resilience to frequent extreme droughts, New Phytologist, 219, 914–931, https://doi.org/10.1111/nph.15185, 2018.

Longo, M., Knox, R. G., Medvigy, D. M., Levine, N. M., Dietze, M. C., Kim, Y., Swann, A. L. S., Zhang, K., Rollinson, C. R., Bras, R. L., Wofsy, S. C., and Moorcroft, P. R.: The biophysics, ecology, and biogeochemistry of functionally diverse, vertically and horizontally heterogeneous ecosystems: the Ecosystem Demography model, version 2.2 Part 1: Model description, Geoscientific Model Development, 12, 4309–4346, https://doi.org/10.5194/gmd-12-4309-2019, 2019a.

Longo, M., Knox, R. G., Levine, N. M., Swann, A. L. S., Medvigy, D. M., Dietze, M. C., Kim, Y., Zhang, K., Bonal, D., Burban, B., Camargo, P. B., Hayek, M. N., Saleska, S. R., Silva, R. da, Bras, R. L., Wofsy, S. C., and Moorcroft, P. R.: The biophysics, ecology, and biogeochemistry of functionally diverse, vertically and horizontally heterogeneous ecosystems: the Ecosystem Demography model, version 2.2 Part 2: Model evaluation for tropical South America, Geoscientific Model Development, 12, 4347–4374, https://doi.org/10.5194/gmd-12-4347-2019, 2019b.

Malhi, Y., Doughty, C., and Galbraith, D.: The allocation of ecosystem net primary productivity in tropical forests, Philosophical Transactions of the Royal Society B: Biological Sciences, 366, 3225–3245, https://doi.org/10.1098/rstb.2011.0062, 2011.

Maréchaux, I., Bartlett, M. K., Sack, L., Baraloto, C., Engel, J., Joetzjer, E., and Chave, J.: Drought tolerance as predicted by leaf water potential at turgor loss point varies strongly across species within an Amazonian forest, Functional Ecology, 29, 1268–1277, https://doi.org/10.1111/1365-2435.12452, 2015.

Maréchaux, I., Saint-André, L., Bartlett, M. K., Sack, L., and Chave, J.: Leaf drought tolerance cannot be inferred from classic leaf traits in a tropical rainforest, Journal of Ecology, 108, 1030–1045, https://doi.org/10.1111/1365-2745.13321, 2019.

Maréchaux, I., Langerwisch, F., Huth, A., Bugmann, H., Morin, X., Reyer, C. P. O., Seidl, R., Collalti, A., Dantas de Paula, M., Fischer, R., Gutsch, M., Lexer, M. J., Lischke, H., Rammig, A., Rödig, E., Sakschewski, B., Taubert, F., Thonicke, K., Vacchiano, G., and Bohn, F. J.: Tackling unresolved questions in forest ecology: The past and future role of simulation models, Ecology and Evolution, 11, 3746–3770, https://doi.org/10.1002/ece3.7391, 2021.

Maréchaux, I., Fischer, F. J., Schmitt, S., & Chave, J.: TROLL-code/TROLL: GMD preprint (4.0.0-GMD), Zenodo, https://doi.org/10.5281/zenodo.14013147, 2024.

Marrs, J. K., Reblin, J. S., Logan, B. A., Allen, D. W., Reinmann, A. B., Bombard, D. M., Tabachnik, D., and Hutyra, L. R.: Solar-Induced Fluorescence Does Not Track Photosynthetic Carbon Assimilation Following Induced Stomatal Closure, Geophysical Research Letters, 47, https://doi.org/10.1029/2020gl087956, 2020.

McMahon, S. M., Harrison, S. P., Armbruster, W. S., Bartlein, P. J., Beale, C. M., Edwards, M. E., Kattge, J., Midgley, G., Morin, X., and Prentice, I. C.: Improving assessment and modelling of climate change impacts on global terrestrial biodiversity, Trends in Ecology & Evolution, 26, 249–259, https://doi.org/10.1016/j.tree.2011.02.012, 2011.

Medlyn, B. E., Robinson, A. P., Clement, R., and McMurtrie, R. E.: On the validation of models of forest CO_2 exchange using eddy covariance data: some perils and pitfalls, Tree Physiology, 25, 839–857, https://doi.org/10.1093/treephys/25.7.839, 2005.

1051 Medlyn, B. E., Duursma, R. A., De Kauwe, M. G., and Prentice, I. C.: The optimal stomatal response to atmospheric CO2
1052 concentration: Alternative solutions, alternative interpretations, Agricultural and Forest Meteorology, 182-183, 200–203,
1053 https://doi.org/10.1016/j.agrformet.2013.04.019, 2013.

1054 Meir, P., Grace, J., and Miranda, A. C.: Photographic method to measure the vertical distribution of leaf area density in
1055 forests, Agricultural and Forest Meteorology, 102, 105–111, https://doi.org/10.1016/s0168-1923(00)00122-2, 2000.

1056 Merganičová, K., Merganič, J., Lehtonen, A., Vacchiano, G., Sever, M. Z. O., Augustynczik, A. L. D., Grote, R., Kyselová,
1057 I., Mäkelä, A., Yousefpour, R., Krejza, J., Collalti, A., and Reyer, C. P. O.: Forest carbon allocation modelling under
1058 climate change, Tree Physiology, 39, 1937–1960, https://doi.org/10.1093/treephys/tpz105, 2019.

1059 Meunier, F., Verbruggen, W., Verbeeck, H., and Peaucelle, M.: Low sensitivity of three terrestrial biosphere models to soil
1060 texture over the South American tropics, Geoscientific Model Development, 15, 7573–7591, https://doi.org/10.5194/gmd-
1061 15-7573-2022, 2022.

1062 Mokany, K., Ferrier, S., Connolly, S. R., Dunstan, P. K., Fulton, E. A., Harfoot, M. B., Harwood, T. D., Richardson, A. J.,
1063 Roxburgh, S. H., Scharlemann, J. P. W., Tittensor, D. P., Westcott, D. A., and Wintle, B. A.: Integrating modelling of
1064 biodiversity composition and ecosystem function, Oikos, 125, 10–19, https://doi.org/10.1111/oik.02792, 2015.

1065 Molto, Q., Hérault, B., Boreux, J. J., Daullet, M., Rousteau, A., Rossi, V.: Predicting tree heights for biomass estimates in
1066 tropical forests–a test from French Guiana.,Biogeosciences, 11(12), 3121-3130, https://doi.org/10.5194/bg-11-3121-2014,
1067 2014.

1068 Montgomery, R. A. and Chazdon, R. L.: FOREST STRUCTURE, CANOPY ARCHITECTURE, AND LIGHT
1069 TRANSMITTANCE IN TROPICAL WET FORESTS, Ecology, 82, 2707–2718, https://doi.org/10.1890/0012-
1070 9658(2001)082[2707:fscaal]2.0.co;2, 2001.

1071 Moorcroft, P. R., Hurtt, G. C., and Pacala, S. W.: A METHOD FOR SCALING VEGETATION DYNAMICS: THE
1072 ECOSYSTEM DEMOGRAPHY MODEL (ED), Ecological Monographs, 71, 557–586, https://doi.org/10.1890/0012-
1073 9615(2001)071[0557:amfsvd]2.0.co;2, 2001.

1074 Muller-Landau, H. C.: The tolerancefecundity trade-off and the maintenance of diversity in seed size, Proceedings of the
1075 National Academy of Sciences, 107, 4242–4247, https://doi.org/10.1073/pnas.0911637107, 2010.

1076 Muñoz-Sabater, J., Dutra, E., Agustí-Panareda, A., Albergel, C., Arduini, G., Balsamo, G., Boussetta, S., Choulga, M.,
1077 Harrigan, S., Hersbach, H., Martens, B., Miralles, D. G., Piles, M., Rodríguez-Fernández, N. J., Zsoter, E., Buontempo, C.,
1078 and Thépaut, J.-N.: ERA5-Land: a state-of-the-art global reanalysis dataset for land applications, Earth System Science
1079 Data, 13, 4349–4383, https://doi.org/10.5194/essd-13-4349-2021, 2021.

1080 Nemetschek, D., Derroire, G., Marcon, E., Aubry-Kientz, M., Auer, J., Badouard, V., Baraloto, C., Bauman, D., Le Blaye,
1081 Q., Boisseaux, M., Bonal, D., Coste, S., Dardevet, E., Heuret, P., Hietz, P., Levionnois, S., Maréchaux, I., McMahon, S.
1082 M., Stahl, C., Vleminckx, J., Wanek, W., Ziegler, C., and Fortunel, C.: Climate anomalies and neighbourhood crowding
1083 interact in shaping tree growth in old-growth and selectively logged tropical forests, Journal of Ecology,
1084 https://doi.org/10.1111/1365-2745.14256, 2024.

1085   Nepstad, D. C., Moutinho, P., Dias-Filho, M. B., Davidson, E., Cardinot, G., Markewitz, D., Figueiredo, R., Vianna, N.,

1086   Chambers, J., Ray, D., Guerreiros, J. B., Lefebvre, P., Sternberg, L., Moreira, M., Barros, L., Ishida, F. Y., Tohlver, I.,

1087   Belk, E., Kalif, K., and Schwalbe, K.: The effects of partial throughfall exclusion on canopy processes, aboveground

1088   production, and biogeochemistry of an Amazon forest, Journal of Geophysical Research: Atmospheres, 107,

1089   https://doi.org/10.1029/2001jd000360, 2002.

1090   Nunes, M. H., Camargo, J. L. C., Vincent, G., Calders, K., Oliveira, R. S., Huete, A., Mendes de Moura, Y., Nelson, B.,

1091   Smith, M. N., Stark, S. C., and Maeda, E. E.: Forest fragmentation impacts the seasonality of Amazonian evergreen

1092   canopies, Nature Communications, 13, https://doi.org/10.1038/s41467-022-28490-7, 2022.

1093   Paschalis, A., De Kauwe, M. G., Sabot, M., and Fatichi, S.: When do plant hydraulics matter in terrestrial biosphere

1094   modelling?, Global Change Biology, 30, https://doi.org/10.1111/gcb.17022, 2023.

1095   Pastorello, Gilberto, Trotta, Carlo, Canfora, Eleonora, Chu, Housen, Christianson, Danielle, Cheah, You-Wei, Poindexter,

1096   Cristina, Chen, Jiquan, Elbashandy, Abdelrahman, Humphrey, Marty, Isaac, Peter, Polidori, Diego, Ribeca, Alessio, van

1097   Ingen, Catharine, Zhang, Leiming, Amiro, Brian, Ammann, Christof, Arain, M Altaf, Ardö, Jonas, Arkebauer, Timothy,

1098   Arndt, Stefan K, Arriga, Nicola, Aubinet, Marc, Aurela, Mika, Baldocchi, Dennis, Barr, Alan, Beamesderfer, Eric,

1099   Marchesini, Luca Belelli, Bergeron, Onil, Beringer, Jason, Paul-Limoges, Eugénie, and et al: The FLUXNET2015 dataset

1100   and the ONEFlux processing pipeline for eddy covariance data, Nature Publishing Group, https://doi.org/10.5167/UZH-

1101   190509, 2020.

1102   Poorter, L., Oberbauer, S. F., and Clark, D. B.: LEAF OPTICAL PROPERTIES ALONG A VERTICAL GRADIENT IN

1103   A TROPICAL RAIN FOREST CANOPY IN COSTA RICA, American Journal of Botany, 82, 1257–1263,

1104   https://doi.org/10.1002/j.1537-2197.1995.tb12659.x, 1995.

1105   Powell, T. L., Galbraith, D. R., Christoffersen, B. O., Harper, A., Imbuzeiro, H. M. A., Rowland, L., Almeida, S., Brando,

1106   P. M., Costa, A. C. L. da, Costa, M. H., Levine, N. M., Malhi, Y., Saleska, S. R., Sotta, E., Williams, M., Meir, P., and

1107   Moorcroft, P. R.: Confronting model predictions of carbon fluxes with measurements of Amazon forests subjected to

1108   experimental drought, New Phytologist, 200, 350–365, https://doi.org/10.1111/nph.12390, 2013.

1109   Prentice, I. C., Liang, X., Medlyn, B. E., and Wang, Y.-P.: Reliable, robust and realistic: the three R's of next-generation

1110   land-surface modelling, Atmospheric Chemistry and Physics, 15, 5987–6005, https://doi.org/10.5194/acp-15-5987-2015,

1111   2015.

1112   Purves, D. and Pacala, S.: Predictive Models of Forest Dynamics, Science, 320, 1452–1453,

1113   https://doi.org/10.1126/science.1155359, 2008.

1114   Qie, L., Lewis, S. L., Sullivan, M. J. P., Lopez-Gonzalez, G., Pickavance, G. C., Sunderland, T., Ashton, P., Hubau, W.,

1115   Abu Salim, K., Aiba, S.-I., Banin, L. F., Berry, N., Brearley, F. Q., Burslem, D. F. R. P., Dančák, M., Davies, S. J.,

1116   Fredriksson, G., Hamer, K. C., Hédl, R., Kho, L. K., Kitayama, K., Krisnawati, H., Lhota, S., Malhi, Y., Maycock, C.,

1117   Metali, F., Mirmanto, E., Nagy, L., Nilus, R., Ong, R., Pendry, C. A., Poulsen, A. D., Primack, R. B., Rutishauser, E.,

1118   Samsoedin, I., Saragih, B., Sist, P., Slik, J. W. F., Sukri, R. S., Svátek, M., Tan, S., Tjoa, A., Nieuwstadt, M. van,

1119   Vernimmen, R. R. E., Yassir, I., Kidd, P. S., Fitriadi, M., Ideris, N. K. H., Serudin, R. M., Abdullah Lim, L. S., Saparudin,

M. S., and Phillips, O. L.: Long-term carbon sink in Borneo's forests halted by drought and vulnerable to edge effects, Nature Communications, 8, https://doi.org/10.1038/s41467-017-01997-0, 2017.

Quesada, C. A., Lloyd, J., Schwarz, M., Patiño, S., Baker, T. R., Czimczik, C., Fyllas, N. M., Martinelli, L., Nardoto, G. B., Schmerler, J., Santos, A. J. B., Hodnett, M. G., Herrera, R., Luizão, F. J., Arneth, A., Lloyd, G., Dezzeo, N., Hilke, I., Kuhlmann, I., Raessler, M., Brand, W. A., Geilmann, H., Moraes Filho, J. O., Carvalho, F. P., Araujo Filho, R. N., Chaves, J. E., Cruz Junior, O. F., Pimentel, T. P., and Paiva, R.: Variations in chemical and physical properties of Amazon forest soils in relation to their genesis, Biogeosciences, 7, 1515–1541, https://doi.org/10.5194/bg-7-1515-2010, 2010.

Rau, E. P., Fischer, F., Joetzjer, É., Maréchaux, I., Sun, I. F., & Chave, J. (2022). Transferability of an individual-and trait-based forest dynamics model: A test case across the tropics. Ecological Modelling, 463, 109801. https://doi.org/10.1016/j.ecolmodel.2021.109801

Reichstein, M., Falge, E., Baldocchi, D., Papale, D., Aubinet, M., Berbigier, P., Bernhofer, C., Buchmann, N., Gilmanov, T., Granier, A., Grünwald, T., Havránková, K., Ilvesniemi, H., Janous, D., Knohl, A., Laurila, T., Lohila, A., Loustau, D., Matteucci, G., Meyers, T., Miglietta, F., Ourcival, J.-M., Pumpanen, J., Rambal, S., Rotenberg, E., Sanz, M., Tenhunen, J., Seufert, G., Vaccari, F., Vesala, T., Yakir, D., and Valentini, R.: On the separation of net ecosystem exchange into assimilation and ecosystem respiration: review and improved algorithm, Global Change Biology, 11, 1424–1439, https://doi.org/10.1111/j.1365-2486.2005.001002.x, 2005.

Restrepo-Coupe, N., Levine, N. M., Christoffersen, B. O., Albert, L. P., Wu, J., Costa, M. H., Galbraith, D., Imbuzeiro, H., Martins, G., Araujo, A. C. da, Malhi, Y. S., Zeng, X., Moorcroft, P., and Saleska, S. R.: Do dynamic global vegetation models capture the seasonality of carbon fluxes in the Amazon basin? A data-model intercomparison, Global Change Biology, 23, 191–208, https://doi.org/10.1111/gcb.13442, 2016.

Restrepo-Coupe, N., Campos, K. S., Alves, L. F., Longo, M., Wiedemann, K. T., Oliveira, R. C. de, Aragao, L. E. O. C., Christoffersen, B. O., Camargo, P. B., Figueira, A. M. e. S., Ferreira, M. L., Oliveira, R. S., Penha, D., Prohaska, N., Araujo, A. C. da, Daube, B. C., Wofsy, S. C., and Saleska, S. R.: Contrasting carbon cycle responses to dry (2015 El Niño) and wet (2008 La Niña) extreme events at an Amazon tropical forest, Agricultural and Forest Meteorology, 353, 110037, https://doi.org/10.1016/j.agrformet.2024.110037, 2024.

RICE, A. H., HAMMOND, E. P., SALESKA, S. R., HUTYRA, L. R., PALACE, M. W., KELLER, M. M., DE CAMARGO, P. B., PORTILHO, K., MARQUES, D., and WOFSY, S. C.: LBA-ECO CD-10 Forest Litter Data for km 67 Tower Site, Tapajos National Forest, https://doi.org/10.3334/ORNLDAAC/862, 2008.

Ross, J.: Net radiation in plant stands, Springer Netherlands, 344–353, https://doi.org/10.1007/978-94-009-8647-3_19, 1981.

Rutishauser, E., Wagner, F., Herault, B., Nicolini, E.-A., and Blanc, L.: Contrasting above-ground biomass balance in a Neotropical rain forest, Journal of Vegetation Science, https://doi.org/10.1111/j.1654-1103.2010.01175.x, 2010.

Sabatier, D., Grimaldi, M., Prévost, M.-F., Guillaume, J., Godron, M., Dosso, M., and Sabatier, D.: The influence of soil cover organization on the floristic and structural heterogeneity of a Guianan rain forest, Plant Ecology formerly "Vegetatio," 131, 81–108, https://doi.org/10.1023/a:1009775025850, 1997.

Sabot, M., De Kauwe, M., Medlyn, B., and Pitman, A.: One stomatal model to rule them all? Evaluating competing hypotheses to regulate the exchange of carbon and water against experimental data, 2020.

Sakschewski, B., Bloh, W. von, Boit, A., Rammig, A., Kattge, J., Poorter, L., Peñuelas, J., and Thonicke, K.: Leaf and stem economics spectra drive diversity of functional plant traits in a dynamic global vegetation model, Global Change Biology, 21, 2711–2725, https://doi.org/10.1111/gcb.12870, 2015.

Saleska, S. R., Miller, S. D., Matross, D. M., Goulden, M. L., Wofsy, S. C., Rocha, H. R. da, Camargo, P. B. de, Crill, P., Daube, B. C., Freitas, H. C. de, Hutyra, L., Keller, M., Kirchhoff, V., Menton, M., Munger, J. W., Pyle, E. H., Rice, A. H., and Silva, H.: Carbon in Amazon Forests: Unexpected Seasonal Fluxes and Disturbance-Induced Losses, Science, 302, 1554–1557, https://doi.org/10.1126/science.1091165, 2003.

Scheiter, S., Langan, L., and Higgins, S. I.: Next-generation dynamic global vegetation models: learning from community ecology, New Phytologist, 198, 957–969, https://doi.org/10.1111/nph.12210, 2013.

Schmitt, S. and Boisseaux, M.: Higher local intra- than interspecific variability in water- and carbon-related leaf traits among Neotropical tree species, Annals of Botany, 131, 801–811, https://doi.org/10.1093/aob/mcad042, 2023.

Schmitt, S., Salzet, G., Fischer, F. J., Maréchaux, I., and Chave, J.: rcontroll: An R interface for the individual-based forest dynamics simulator TROLL, Methods in Ecology and Evolution, 14, 2749–2757, https://doi.org/10.1111/2041-210x.14215, 2023.

Schmitt, S., Hérault, B., & Derroire, G.: High intraspecific growth variability despite strong evolutionary legacy in an Amazonian forest. *Ecology Letters*, *26*(12), 2135-2146, 2023

Schmitt, S., Salzet, G., Fischer, F. J., Maréchaux, I., & Chave, J.: sylvainschmitt/rcontroll: GMD preprint (v0.2.0), Zenodo, https://doi.org/10.5281/zenodo.14012116, 2024.

Schmitt, S.: sylvainschmitt/troll_eval: GMD preprint (0.1.0), Zenodo, https://doi.org/10.5281/zenodo.14012085, 2024.

Silver, W. L., Neff, J., McGroddy, M., Veldkamp, E., Keller, M., and Cosme, R.: Effects of soil texture on belowground carbon and nutrient storage in a lowland amazonian forest ecosystem, Ecosystems, 3, 193–209, https://doi.org/10.1007/s100210000019, 2000.

Slot, M., Rifai, S. W., Eze, C. E., and Winter, K.: The stomatal response to vapor pressure deficit drives the apparent temperature response of photosynthesis in tropical forests, New Phytologist, https://doi.org/10.1111/nph.19806, 2024.

Smith, B., Prentice, I. C., and Sykes, M. T.: Representation of vegetation dynamics in the modelling of terrestrial ecosystems: comparing two contrasting approaches within European climate space, Global Ecology and Biogeography, 10, 621–637, https://doi.org/10.1046/j.1466-822x.2001.t01-1-00256.x, 2001.

Smith, M. N., Stark, S. C., Taylor, T. C., Ferreira, M. L., Oliveira, E. de, Restrepo-Coupe, N., Chen, S., Woodcock, T., Santos, D. B. dos, Alves, L. F., Figueira, M., Camargo, P. B. de, Oliveira, R. C. de, Aragão, L. E. O. C., Falk, D. A., McMahon, S. M., Huxman, T. E., and Saleska, S. R.: Seasonal and drought-related changes in leaf area profiles depend on height and light environment in an Amazon forest, New Phytologist, 222, 1284–1297, https://doi.org/10.1111/nph.15726, 2019.

Thuiller, W., Albert, C., Araújo, M. B., Berry, P. M., Cabeza, M., Guisan, A., Hickler, T., Midgley, G. F., Paterson, J., Schurr, F. M., Sykes, M. T., and Zimmermann, N. E.: Predicting global change impacts on plant species' distributions: Future challenges, Perspectives in Plant Ecology, Evolution and Systematics, 9, 137–152, https://doi.org/10.1016/j.ppees.2007.09.004, 2008.

Trugman, A. T., Medvigy, D., Mankin, J. S., and Anderegg, W. R. L.: Soil Moisture Stress as a Major Driver of Carbon Cycle Uncertainty, Geophysical Research Letters, 45, 6495–6503, https://doi.org/10.1029/2018gl078131, 2018.

Ukkola, A.: PLUMBER2: forcing and evaluation datasets for a model intercomparison project for land surface models v1.0, https://doi.org/10.25914/5FDB0902607E1, 2020.

Van Langenhove, L., Verryckt, L. T., Bréchet, L., Courtois, E. A., Stahl, C., Hofhansl, F., Bauters, M., Sardans, J., Boeckx, P., Fransen, E., Peñuelas, J., and Janssens, I. A.: Atmospheric deposition of elements and its relevance for nutrient budgets of tropical forests, Biogeochemistry, 149, 175–193, https://doi.org/10.1007/s10533-020-00673-8, 2020.

Van Langenhove, L., Depaepe, T., Verryckt, L. T., Vallicrosa, H., Fuchslueger, L., Lugli, L. F., Bréchet, L., Ogaya, R., Llusia, J., Urbina, I., Gargallo-Garriga, A., Grau, O., Richter, A., Penuelas, J., Van Der Straeten, D., and Janssens, I. A.: Impact of Nutrient Additions on Free-Living Nitrogen Fixation in Litter and Soil of Two French-Guianese Lowland Tropical Forests, Journal of Geophysical Research: Biogeosciences, 126, https://doi.org/10.1029/2020jg006023, 2021.

Villarreal, S. and Vargas, R.: Representativeness of FLUXNET Sites Across Latin America, Journal of Geophysical Research: Biogeosciences, 126, https://doi.org/10.1029/2020jg006090, 2021.

Vincent, G., Antin, C., Laurans, M., Heurtebize, J., Durrieu, S., Lavalley, C., and Dauzat, J.: Mapping plant area index of tropical evergreen forest by airborne laser scanning. A cross-validation study using LAI2200 optical sensor, Remote Sensing of Environment, 198, 254–266, https://doi.org/10.1016/j.rse.2017.05.034, 2017.

VINCENT, G., PIMONT, F., and VERLEY, P.: Various PAD/LAD estimators implemented in AMAPVox 1.8, https://doi.org/10.23708/1AJNMP, 2021.

Vincent, G., Verley, P., Brede, B., Delaitre, G., Maurent, E., Ball, J., Clocher, I., and Barbier, N.: Multi-sensor airborne lidar requires intercalibration for consistent estimation of light attenuation and plant area density, Remote Sensing of Environment, 286, 113442, https://doi.org/10.1016/j.rse.2022.113442, 2023.

Vleminckx, J., Fortunel, C., Valverde-Barrantes, O., Timothy Paine, C. E., Engel, J., Petronelli, P., Dourdain, A. K., Guevara, J., Béroujon, S., and Baraloto, C.: Resolving whole-plant economics from leaf, stem and root traits of 1467 Amazonian tree species, Oikos, 130, 1193–1208, https://doi.org/10.1111/oik.08284, 2021.

Wagner, F. H., Hérault, B., Bonal, D., Stahl, C., Anderson, L. O., Baker, T. R., Becker, G. S., Beeckman, H., Boanerges Souza, D., Botosso, P. C., Bowman, D. M. J. S., Bräuning, A., Brede, B., Brown, F. I., Camarero, J. J., Camargo, P. B., Cardoso, F. C. G., Carvalho, F. A., Castro, W., Chagas, R. K., Chave, J., Chidumayo, E. N., Clark, D. A., Costa, F. R. C., Couralet, C., Silva Mauricio, P. H. da, Dalitz, H., Castro, V. R. de, Freitas Milani, J. E. de, Oliveira, E. C. de, Souza Arruda, L. de, Devineau, J.-L., Drew, D. M., Dünisch, O., Durigan, G., Elifuraha, E., Fedele, M., Ferreira Fedele, L., Figueiredo Filho, A., Finger, C. A. G., Franco, A. C., Freitas Júnior, J. L., Galvão, F., Gebrekirstos, A., Gliniars, R., Graça, P. M. L. de A., Griffiths, A. D., Grogan, J., Guan, K., Homeier, J., Kanieski, M. R., Kho, L. K., Koenig, J., Kohler, S. V.,

Krepkowski, J., Lemos-Filho, J. P., Lieberman, D., Lieberman, M. E., Lisi, C. S., Longhi Santos, T., López Ayala, J. L., Maeda, E. E., Malhi, Y., Maria, V. R. B., Marques, M. C. M., Marques, R., Maza Chamba, H., Mbwambo, L., Melgaço, K. L. L., Mendivelso, H. A., Murphy, B. P., O'Brien, J. J., Oberbauer, S. F., Okada, N., Pélissier, R., Prior, L. D., Roig, F. A., Ross, M., Rossatto, D. R., Rossi, V., Rowland, L., Rutishauser, E., Santana, H., Schulze, M., Selhorst, D., Silva, W. R., Silveira, M., Spannl, S., Swaine, M. D., Toledo, J. J., Toledo, M. M., Toledo, M., Toma, T., Tomazello Filho, M., Valdez Hernández, J. I., Verbesselt, J., Vieira, S. A., Vincent, G., Volkmer de Castilho, C., et al.: Climate seasonality limits leaf carbon assimilation and wood productivity in tropical forests, Biogeosciences, 13, 2537–2562, https://doi.org/10.5194/bg-13-2537-2016, 2016.

Wu, J., Albert, L. P., Lopes, A. P., Restrepo-Coupe, N., Hayek, M., Wiedemann, K. T., Guan, K., Stark, S. C., Christoffersen, B., Prohaska, N., Tavares, J. V., Marostica, S., Kobayashi, H., Ferreira, M. L., Campos, K. S., Silva, R. da, Brando, P. M., Dye, D. G., Huxman, T. E., Huete, A. R., Nelson, B. W., and Saleska, S. R.: Leaf development and demography explain photosynthetic seasonality in Amazon evergreen forests, Science, 351, 972–976, https://doi.org/10.1126/science.aad5068, 2016.

Wu, J., Serbin, S. P., Xu, X., Albert, L. P., Chen, M., Meng, R., Saleska, S. R., and Rogers, A.: The phenology of leaf quality and its within-canopy variation is essential for accurate modeling of photosynthesis in tropical evergreen forests, Global Change Biology, 23, 4814–4827, https://doi.org/10.1111/gcb.13725, 2017.

Wu, W., Sun, Y., Xiao, K., and Xin, Q.: Development of a global annual land surface phenology dataset for 19822018 from the AVHRR data by implementing multiple phenology retrieving methods, International Journal of Applied Earth Observation and Geoinformation, 103, 102487, https://doi.org/10.1016/j.jag.2021.102487, 2021.

Xu, X., Medvigy, D., Joseph Wright, S., Kitajima, K., Wu, J., Albert, L. P., Martins, G. A., Saleska, S. R., & Pacala, S. W.: Variations of leaf longevity in tropical moist forests predicted by a trait-driven carbon optimality model. Ecology Letters, 20(9), 1097–1106. https://doi.org/10.1111/ele.12804, 2017.

Yang, X., Wu, J., Chen, X., Ciais, P., Maignan, F., Yuan, W., Piao, S., Yang, S., Gong, F., Su, Y., Dai, Y., Liu, L., Zhang, H., Bonal, D., Liu, H., Chen, G., Lu, H., Wu, S., Fan, L., Gentine, P., and Wright, S. J.: A comprehensive framework for seasonal controls of leaf abscission and productivity in evergreen broadleaved tropical and subtropical forests, The Innovation, 2, 100154, https://doi.org/10.1016/j.xinn.2021.100154, 2021.

Yang, X., Chen, X., Ren, J., Yuan, W., Liu, L., Liu, J., Chen, D., Xiao, Y., Wu, S., Fan, L., Dai, X., and Su, Y.: A grid dataset of leaf age-dependent LAI seasonality product (lad-LAI) over tropical and subtropical evergreen broadleaved forests, 2023.

Yao, Y., Ciais, P., Viovy, N., Joetzjer, E., and Chave, J.: How drought events during the last century have impacted biomass carbon in Amazonian rainforests, Global Change Biology, 29, 747–762, https://doi.org/10.1111/gcb.16504, 2022.

Yuan, Q.: Semantic-based clustering for 3D instance segmentation in sparse radar point clouds, 2023 International Conference on Algorithms, Computing and Data Processing (ACDP), 9370, 209–216, https://doi.org/10.1109/acdp59959.2023.00041, 2023.

1258 Ziegler, C., Coste, S., Stahl, C., Delzon, S., Levionnois, S., Cazal, J., Cochard, H., Esquivel-Muelbert, A., Goret, J.-Y.,
1259 Heuret, P., Jaouen, G., Santiago, L. S., and Bonal, D.: Large hydraulic safety margins protect Neotropical canopy rainforest
1260 tree species against hydraulic failure during drought, Annals of Forest Science, 76, https://doi.org/10.1007/s13595-019-
1261 0905-0, 2019.

1262 **Appendix**

1263 **Table A1: TROLL 4.0 global parameters.**

Abbreviation	Definition	Units	Value	Nature*	Reference
c_a	Carbon free air concentration	µmol mol^{-1}	375	Constant	
P_{ress}	Atmospheric pressure	kPa	101	Constant	
k_{geom}	Light extinction coefficient, reflecting leaf geometric arrangement	unitless	0.5	Constant	Ross 1981
absorptance$_{leaves}$	leaves absorptance	unitless	0.83	Literature	Long et al., 1993; Poorter et al., 1995
θ	Curvature factor (Farquhar model parameter)	unitless	0.7	Literature	Farquhar et al., 1980
g_0	leaf minimum conductance for water vapor	mmol H$_2$0 m^{-2} s^{-1}	5	Literature	Duursma et al., 2019
$a_{T,o}$	Phenological parameter that modulates old leaf drought tolerance	unitless		Calibrated	
$b_{T,o}$	Phenological parameter that modulates the height dependence of leaf susceptibility to drought	MPa		Calibrated	
δ_o	Phenological parameter that controls the pace of old leaf shedding acceleration	unitless		Calibrated	

f_{wood}	Fraction of carbon allocated to wood	unitless	0.35	Literature	Aragão et al., 2019; Malhi et al., 2011
f_{canopy}	Fraction of carbon allocated to canopy		0.25	Literature	Aragão et al., 2019; Malhi et al., 2011
f_{gap}	Fraction of gaps in the tree crown		0.15	Literature	Fischer et al., 2019
a_{CR}	Crown radius intercept	unitless		Calibrated	
b_{CR}	Crown radius slope	unitless		Calibrated	
a_{CD}	Crown depth intercept	m	0	Literature	Chave et al., 2005
b_{CD}	Crown depth slope	unitless	0.2	Literature	Chave et al., 2005
$shape_{crown}$	Crown shape parameter		0.72	Calibrated	
N_{tot}	Intensity of the external seed rain	seeds ha^{-1}	50,000	Assumed	
n_s	Number of reproduction opportunities per mature tree	seeds tree^{-1}	10	Assumed	
m	Reference background mortality	death year^{-1}		Calibrated	
v_T	Variance of the flexion moment for treefall		0.021	Calibrated	
σ_h	Intraspecific variation in height (log scale)	m	0.19	Inferred	Baraloto et al., 2010
σ_{cr}	Intraspecific variation in crown radius (log scale)	m	0.29	Calibrated	Fischer et al., 2019
σ_{cd}	Intraspecific variation in crown depth (log scale)	m	0		
$\sigma_{dbhthres}$	Intraspecific variation in maximum diameters (log scale)	m	0.05	Inferred	Baraloto et al., 2010
$corr_{cr-h}$	Intraspecific correlation between crown radius and height		0		

σ_P	Intraspecific variation in phosphorus (log scale)	mg g^{-1}	0.24	Inferred	Baraloto et al., 2010
σ_N	Intraspecific variation in nitrogen (log scale)	mg g^{-1}	0.12	Inferred	Baraloto et al., 2010
σ_{LMA}	Intraspecific variation in leaf mass per area (log scale)	g m^{-2}	0.24	Inferred	Baraloto et al., 2010
σ_{wsg}	Intraspecific variation in wood specific gravity	g cm^{-3}	0.06	Inferred	Baraloto et al., 2010
σ_{LA}	Intraspecific variation in leaf area (log scale)	cm^2	0.48	Inferred	Schmitt and Boisseaux 2023
σ_{tlp}	Intraspecific variation in turgor loss point (log scale)	MPa	0.10	Inferred	Schmitt and Boisseaux 2023
$corr_{N-P}$	Intraspecific correlation between nitrogen and phosphorous		0.65	Inferred	Baraloto et al., 2010
$corr_{N-LMA}$	Intraspecific correlation between nitrogen and leaf mass per area		-0.43	Inferred	Baraloto et al., 2010
$corr_{P-LMA}$	Intraspecific correlation between phosphorus and leaf mass per area		-0.39	Inferred	Baraloto et al., 2010

*Assumed is a value that is supposed; Calibrated is a value that was previously calibrated; Constant is a physical constant; Inferred is a value that has been derived from an existing dataset; Literature is a value prescribed from the literature.

1267 **Table A2: Evaluation of forest structure, composition and fluxes explored at Paracou and Tapajos. Evaluations include the goodness-**
1268 **of-fit R^2 from the linear regression with a null intercept, the Pearson's r correlation coefficient CC, the root mean square error of**
1269 **prediction RMSEP, the standard deviation of the error of prediction SD.**

Site	Variable	Unit	Observations	Temporal resolution	R^2	CC	RMSEP	SD
Paracou	height	%	Plane	single	0.93	0.95	0.76	0.76
Tapajos	height	%	Plane	single	0.94	0.94	0.56	0.55
Paracou	height	%	Satellite	single	0.95	0.96	0.55	0.55
Tapajos	height	%	Satellite	single	0.92	0.91	0.69	0.62
Paracou	BA understory	$m^2\ ha^{-1}$	Inventory	single	0.94	0.90	0.12	0.08
Paracou	Number of stems in understory	ha^{-1}	Inventory	single	0.99	1.00	342.15	309.81
Paracou	Rank-abundance	ha^{-1}	Inventory	single	0.89	0.88	0.59	0.44
Tapajos	Rank-abundance	ha^{-1}	Inventory	single	0.47	0.96	1.10	0.68
Paracou	GPP	$kgC\ m^{-2}\ year^{-1}$	eddy flux	day	0.97	0.60	0.75	0.67
Tapajos	GPP	$kgC\ m^{-2}\ year^{-1}$	eddy flux	day	0.97	0.45	1.12	0.67
Paracou	GPP	$kgC\ m^{-2}\ year^{-1}$	Satellite	day	0.95	0.45	1.18	0.80
Tapajos	GPP	$kgC\ m^{-2}\ year^{-1}$	Satellite	day	0.96	0.22	1.54	0.28
Paracou	LAI	$m^2\ m^{-2}$	Satellite	15 days	1.00	0.69	0.29	0.13
Tapajos	LAI	$m^2\ m^{-2}$	Satellite	15 days	1.00	0.55	0.26	0.17
Paracou	LAI	$m^2\ m^{-2}$	Drone	15 days	1.00	0.84	0.11	0.11
Tapajos	LAI	$m^2\ m^{-2}$	Terrestrial	15 days	1.00	0.25	0.32	0.20
Tapajos	LAI	$m^2\ m^{-2}$	Phenocam	15 days	1.00	0.91	0.11	0.08
Paracou	ET	$mm\ day^{-1}$	eddy flux	day	0.96	0.69	0.60	0.60
Tapajos	ET	$mm\ day^{-1}$	eddy flux	day	0.96	0.75	0.75	0.63
Paracou	RSWC	%	eddy flux	day	0.97	0.77	0.24	0.13
Tapajos	RSWC	%	eddy flux	day	0.99	0.39	0.20	0.11

1270

1271 **Table A3: Comparisons of forest structure and phenology parameter values from the five best fits, including minimum, maximum**
1272 **and median values, as well as the one of the best fit. Note that the median of the parameter values of the five best fits always equal**
1273 **the value of the best fit, except for m at Paracou with a small difference of 0.0025 and δ_0 in both sites.**

Site	Parameter	minimum	median	best	maximum
Paracou	a_{CR}	1.80	1.80	1.80	1.90
Paracou	b_{CR}	0.386	0.386	0.386	0.443
Paracou	m	0.0325	0.0325	0.0350	0.0375
Paracou	$a_{T,0}$	0.2	0.2	0.2	0.2
Paracou	$b_{T,0}$	0.015	0.02	0.015	0.02
Paracou	δ_0	0.1	0.4	0.1	0.5
Tapajos	a_{CR}	2.35	2.45	2.45	2.50
Tapajos	b_{CR}	0.6994	0.7565	0.7565	0.7850
Tapajos	m	0.0300	0.0400	0.0400	0.0500
Tapajos	$a_{T,0}$	0.2	0.2	0.2	0.3
Tapajos	$b_{T,0}$	0.015	0.015	0.015	0.015
Tapajos	δ_0	0.2	0.3	0.2	0.5

1274

1275 **Table A4: Calibrated parameters intervals for the 5 best simulations for each of stem distribution, number of stems, basal area and**
1276 **aboveground biomass, as well as the one with equal weighing among them. Values show median first followed by minimum and**
1277 **maximum values in brackets.**

Site	Metric	RMSEP	a_{CR}	b_{CR}	m
Paracou	Number of stems	5.75 [2-7.75]	1.75 [1.75-1.8]	0.3575 [0.3575-0.386]	0.0475 [0.0375-0.05]
Paracou	Basal Area	0.04 [0.03-0.07]	1.85 [1.65-2]	0.4715 [0.3505-0.5075]	0.0325 [0.03-0.05]
Paracou	Stem distribution	2.4 [1.38-2.7]	1.85 [1.8-1.9]	0.4145 [0.386-0.443]	0.0425 [0.0325-0.05]
Paracou	All equally weighted	0.16 [0.13-0.17]	1.8 [1.8-1.9]	0.386 [0.386-0.443]	0.0325 [0.0325-0.0375]
Tapajos	Number of stems	3 [0-3.5]	2.5 [2.4-2.65]	0.785 [0.728-0.9205]	0.035 [0.03-0.04]
Tapajos	Aboveground Biomass	0.13 [0.04-0.19]	2.45 [2.35-2.5]	0.835 [0.6495-0.885]	0.045 [0.03-0.05]
Tapajos	Stem distribution	2.54 [2.38-2.74]	2.35 [2.3-2.35]	0.6995 [0.671-0.6995]	0.045 [0.0375-0.05]
Tapajos	All equally weighted	0.25 [0.18-0.25]	2.45 [2.35-2.5]	0.7565 [0.6995-0.785]	0.04 [0.03-0.05]

1278

1279
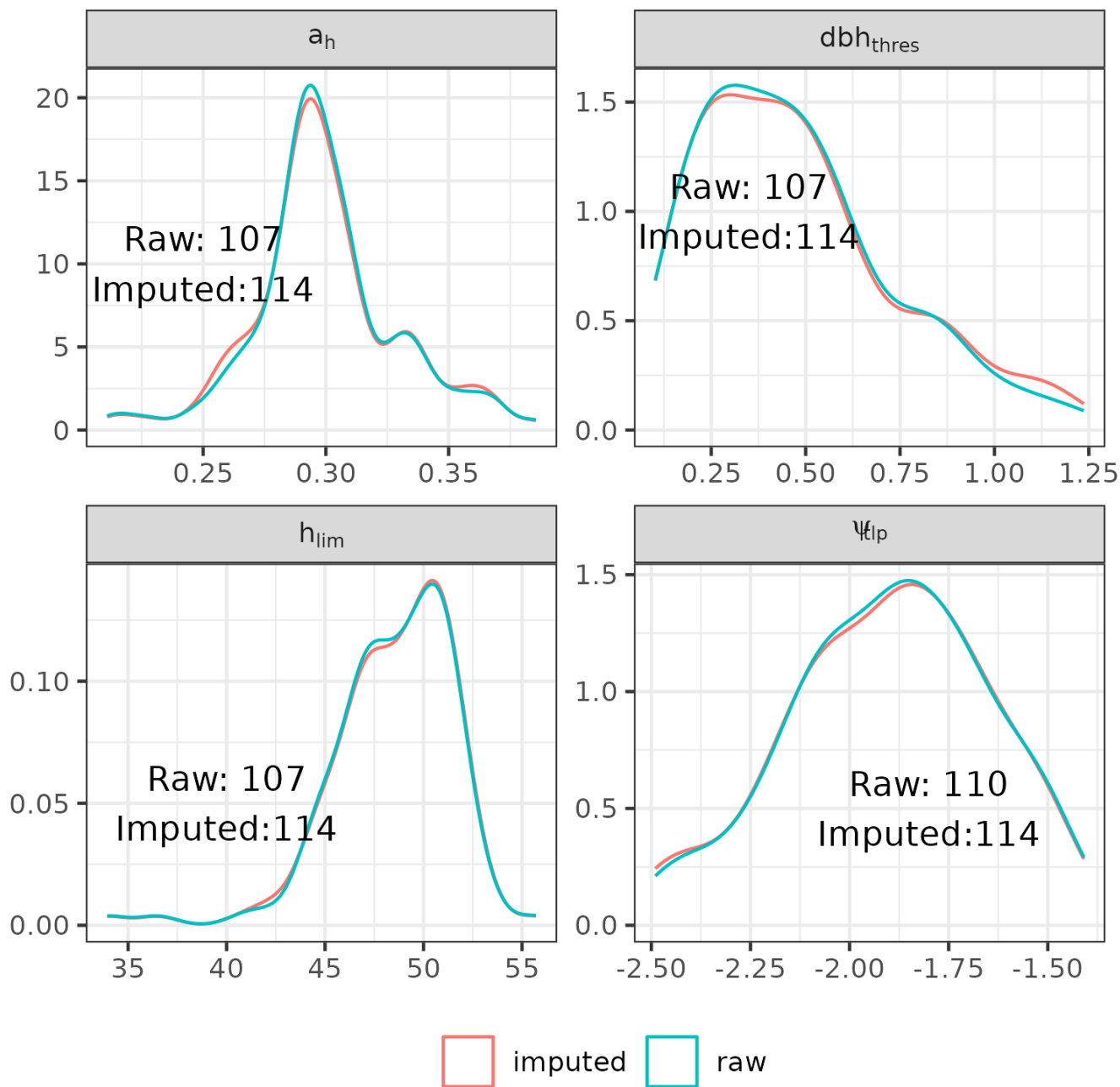
Figure A1: Representativity of imputed functional traits values (red) against raw functional trait values (blue) from various datasets (see methods). Traits were imputed using predictive means matching for a_h, dbh_{thres}, hlim, and π_{tlp} only. The number in each subplots represents the number of species with a trait value in the raw data and after imputation composing respectively the blue and red curves.

1284
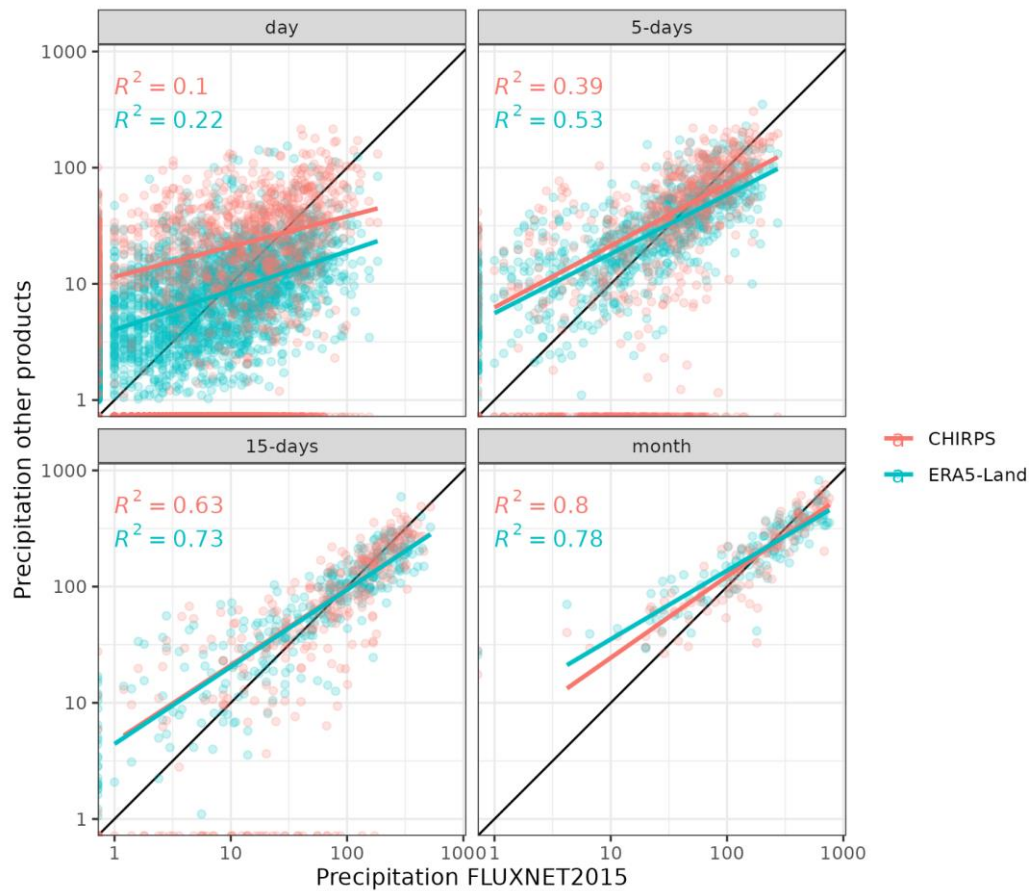
Figure A2: Comparisons of CHIRPS (red) and ERA5-Land (blue) precipitation products against local eddy-flux tower measurements retrieved from FLUXNET 2015 in Paracou at daily, 5-day, 15-day, and monthly resolutions. CHIRPS and ERA5-Land had similar agreement to locally measured precipitations, with even higher correlations for ERA5-Land than CHIRPS. However, they both overestimated low precipitation events and underestimated high precipitation events, resulting in low agreement for daily variations (R2 of 0.10 and 0.22), which quickly increases for 5-day (R2 of 0.39 and 0.53) and 15-day variations (R2 of 0.63 and 0.73). Although a similar assessment was not possible in Tapajos due to a lack of local reliable rainfall data, we therefore decided to keep ERA5-Land for filling the precipitation data gaps in Tapajos.

1292
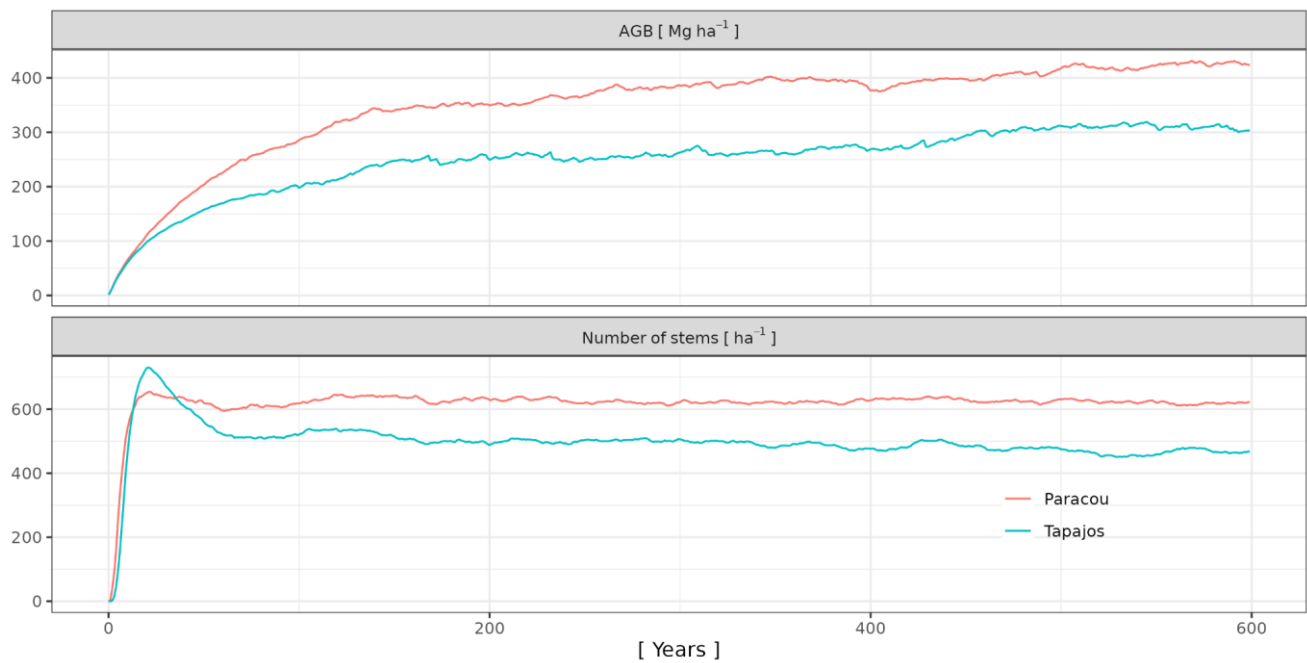
Figure A3: 600-year spin-up simulations from bareground with calibrated parameters showing equilibrium reached by number of stems (bottom) aboveground biomass (AGB, top) at Paracou (red) and Tapajos (blue).

1295
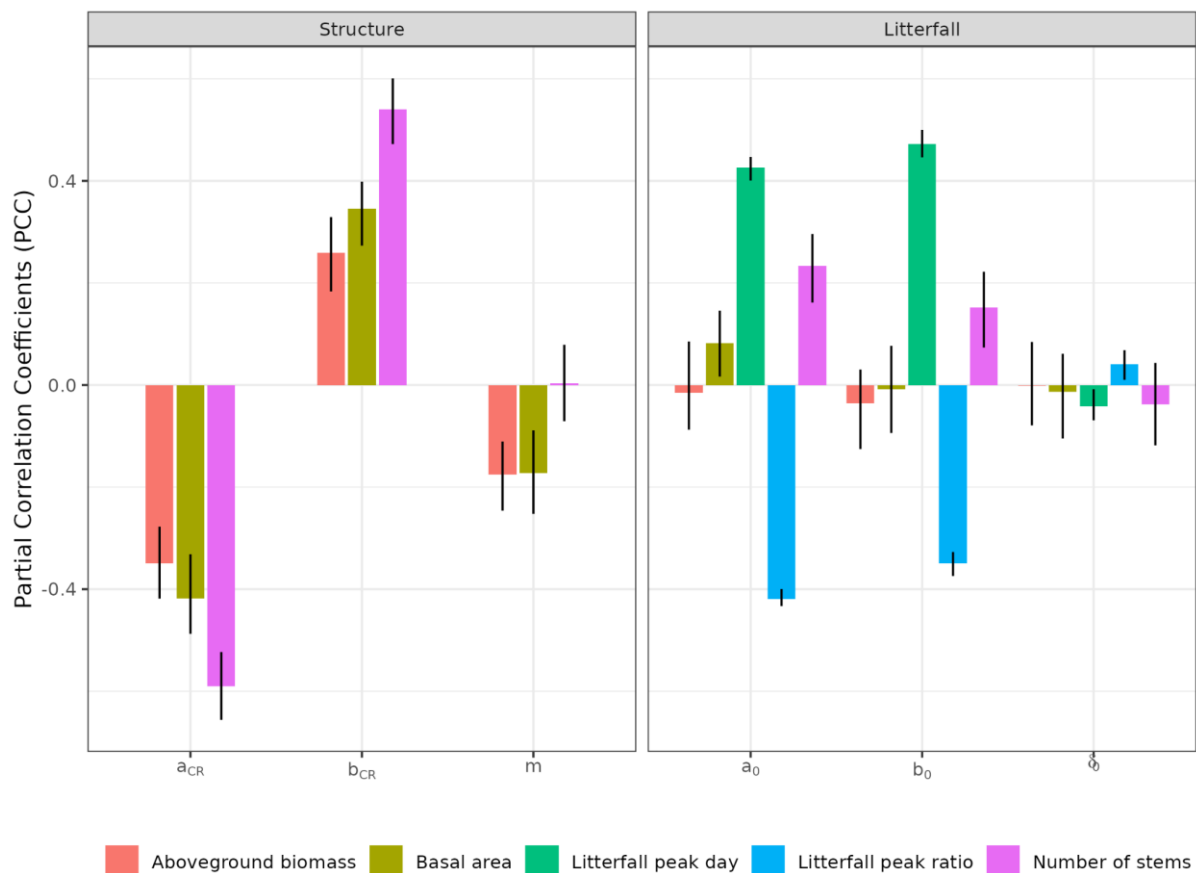
Figure A4: Sensitivity of forest structure (left panel) and forest litterfall (right panel) to calibrated parameters. Forest structure and forest litterfall sensitivity to each parameter was assessed with partial correlation coefficients (PCC) using the function *pcc* of the R package *sensitivity* with a thousand bootstrap draws to assess confidence intervals. The intercept and slope of the crown radius allometry a_{CR} and b_{CR} had a strong effect on forest structure , i.e., number of stems (red), aboveground biomass (AGB, light green), and basal area (BA, green). Basal mortality m also had a strong effect on aboveground biomass (AGB) and basal area (BA) but little to no effect on the number of stems. $a_{T,0}$ and $b_{T,0}$ had a strong positive effect on the peak day of litterfall (blue) and negative effect on the ratio of the peak of litterfall (purple), but $delta_0$ had only a weak effect on the peak of litterfall. The forest structure variables, namely number of stems, aboveground biomass (AGB), and basal area (BA) showed little to no partial correlations to $a_{T,0}$, $b_{T,0}$ and $delta_0$.

1305
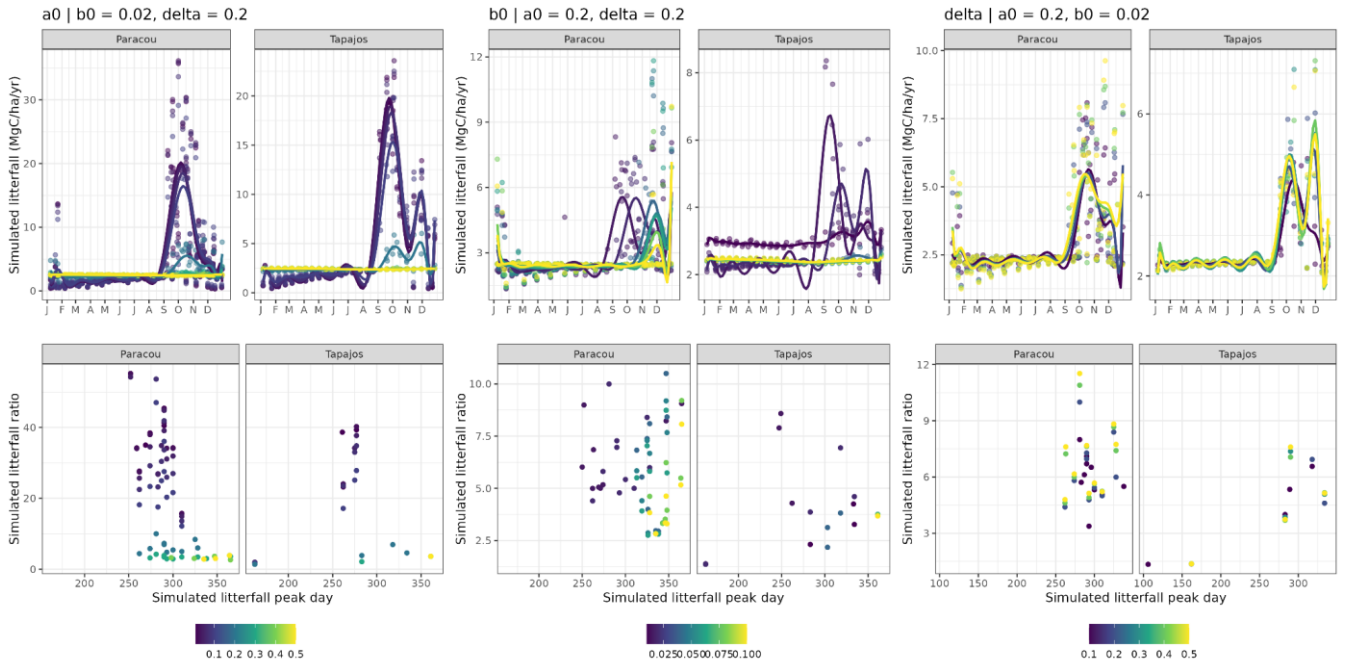
Figure A5. Effect of each parameter of the new leaf shedding module on the simulated timing and intensity of the litterfall peak during the dry season. Top panels illustrate simulated variations of litterfall at both sites for varying $a_{T,0}$, $b_{T,0}$, and δ_0 with the other parameters fixed to a calibrated value. Bottom panels illustrate the corresponding timing and intensity of the dry season litterfall peak: (i) the day of the litterfall peak as the julian day of the maximum annual value (day), and (ii) the ratio between the peak value (computed as the average of litterfall flux over the two consecutive time intervals before and after the peak day) divided by the basal flux (computed as the average between January and April) (ratio). $a_{T,0}$ mainly limited the intensity of the peak with a peak up to 60 times the wet season base litter flux with small parameter values close to 0.01 and no peak with values greater than 0.3, when $b_{T,0}$=0.02 and δ_0 =0.2. Values of $a_{T,0}$ greater than 0.1 also resulted in a later peak during the dry season. $b_{T,0}$ mainly influenced the date of the simulated peak during the dry season, as well as the intensity of the simulated peak for values greater than 0.1. Indeed, low values of $b_{T,0}$, close to 0.01, resulted in a peak starting in September, while high values showed a peak starting in December, when $a_{T,0}$=0.2 and δ_0=0.2. Finally, δ_0 appeared to have a smaller influence on the intensity and timing of the simulated litter peaks. Higher values of δ_0 increased the duration of the simulated peaks or the litter flux between two peaks during the same dry season.
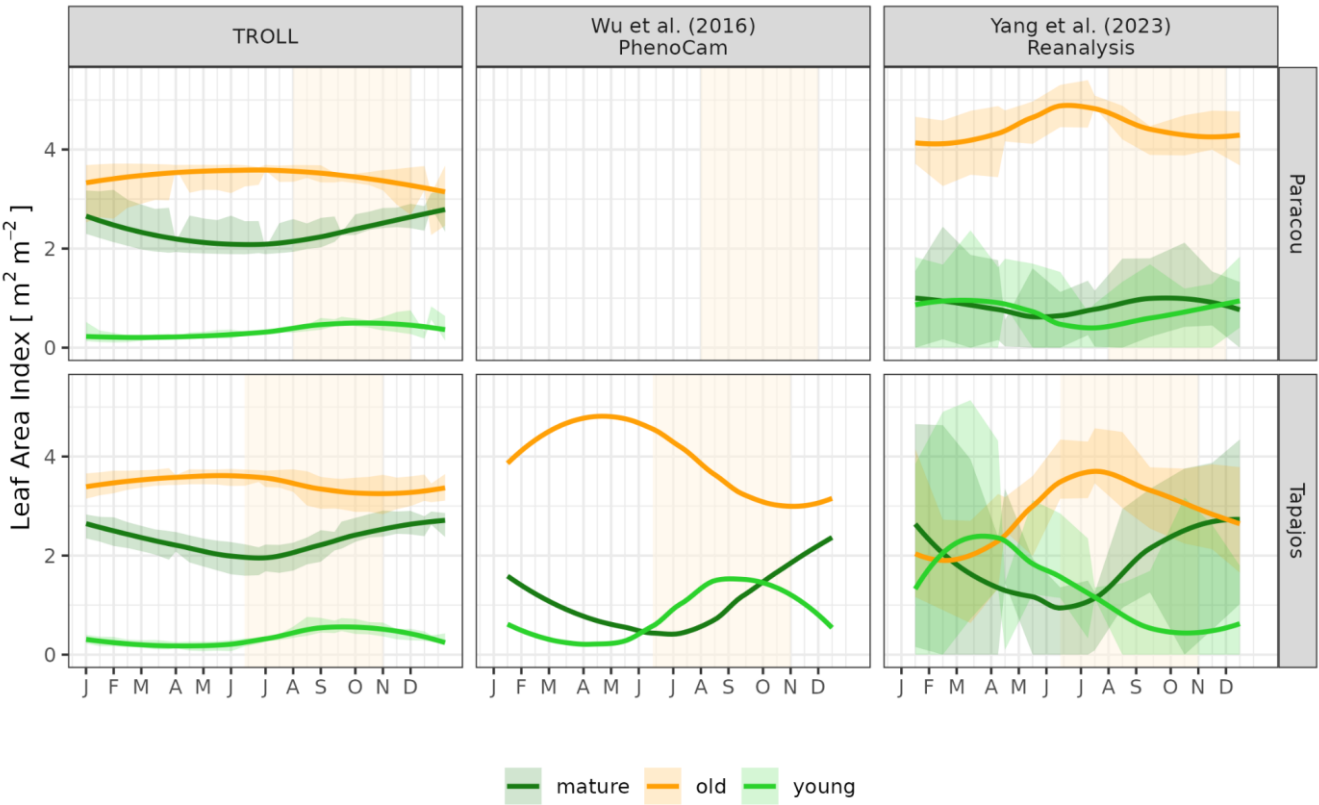
Figure A6: Mean annual cycle of leaf area index per leaf age cohorts, derived from fortnightly means, at Paracou and Tapajos. Note that the three leaf age cohorts (young, mature and old leaves) are not defined the same way in the three sources. Leaf age per cohort depends on the individual leaf lifespan in TROLL 4.0 (see Maréchaux et al., submitted companion paper), while the transition from young to mature and mature to old are respectively fixed to 1.71 and 5.14 months in Yang et al. (2023) and fitted to 1 and 3 months in Wu et al. (2016). Bands are the intervals of means across years, and the vertical yellow bands in the background correspond to the site's climatological dry season.

1326

1327
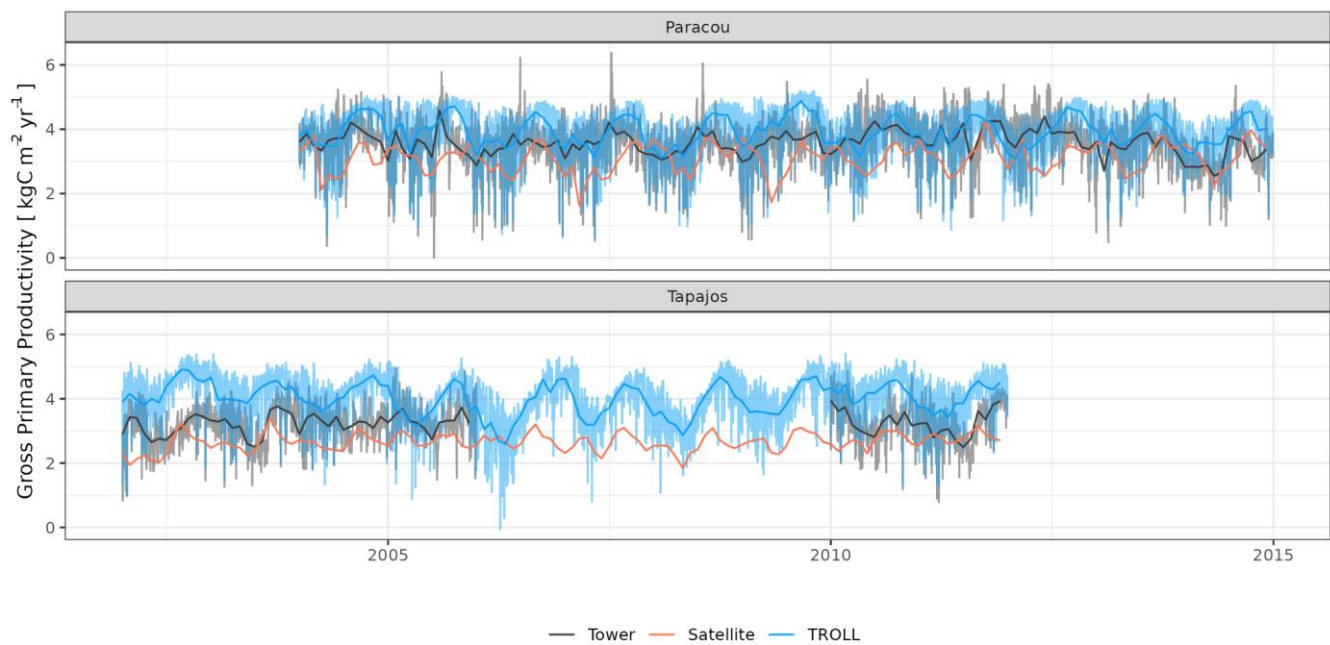
1328

Figure A7: Daily and monthly means of gross primary productivity for Paracou and Tapajos. Dark lines are the monthly means,
semi-transparent lines are the daily means variations with the exception of satellite data for which data are available only every 8
days.

1332
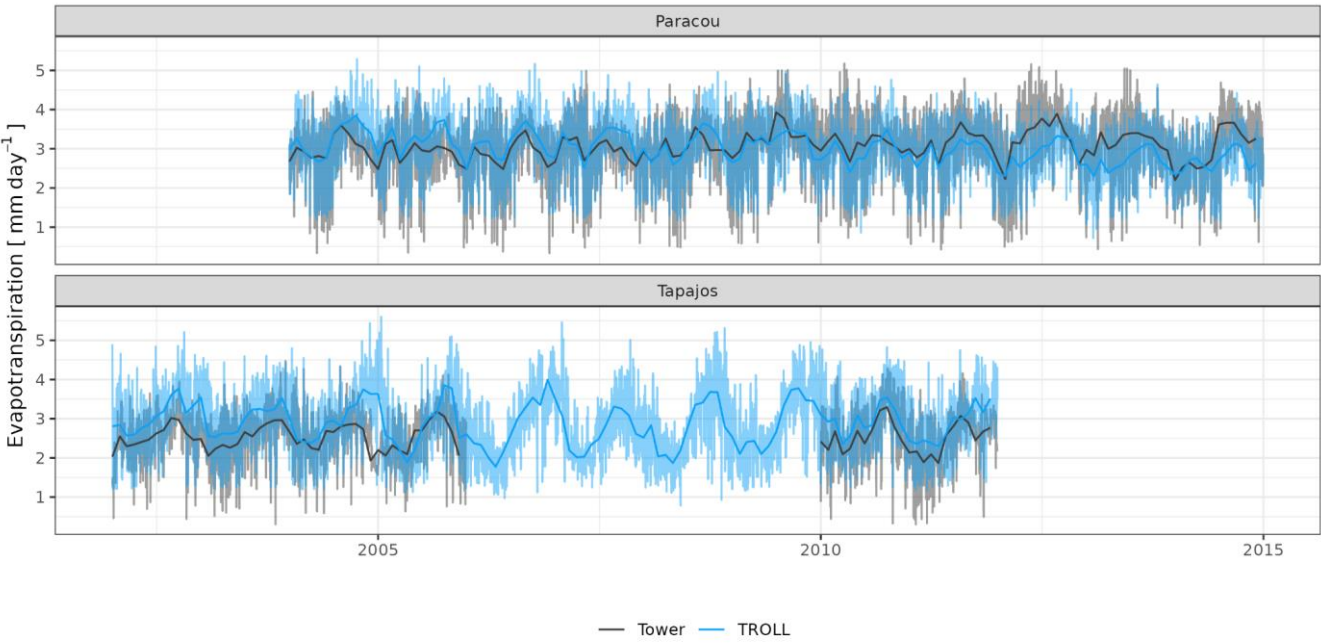
1333

Figure A8: Daily and monthly total of evapotranspiration for Paracou and Tapajos. Dark lines are the monthly means, semi-transparent lines are the daily means variations.
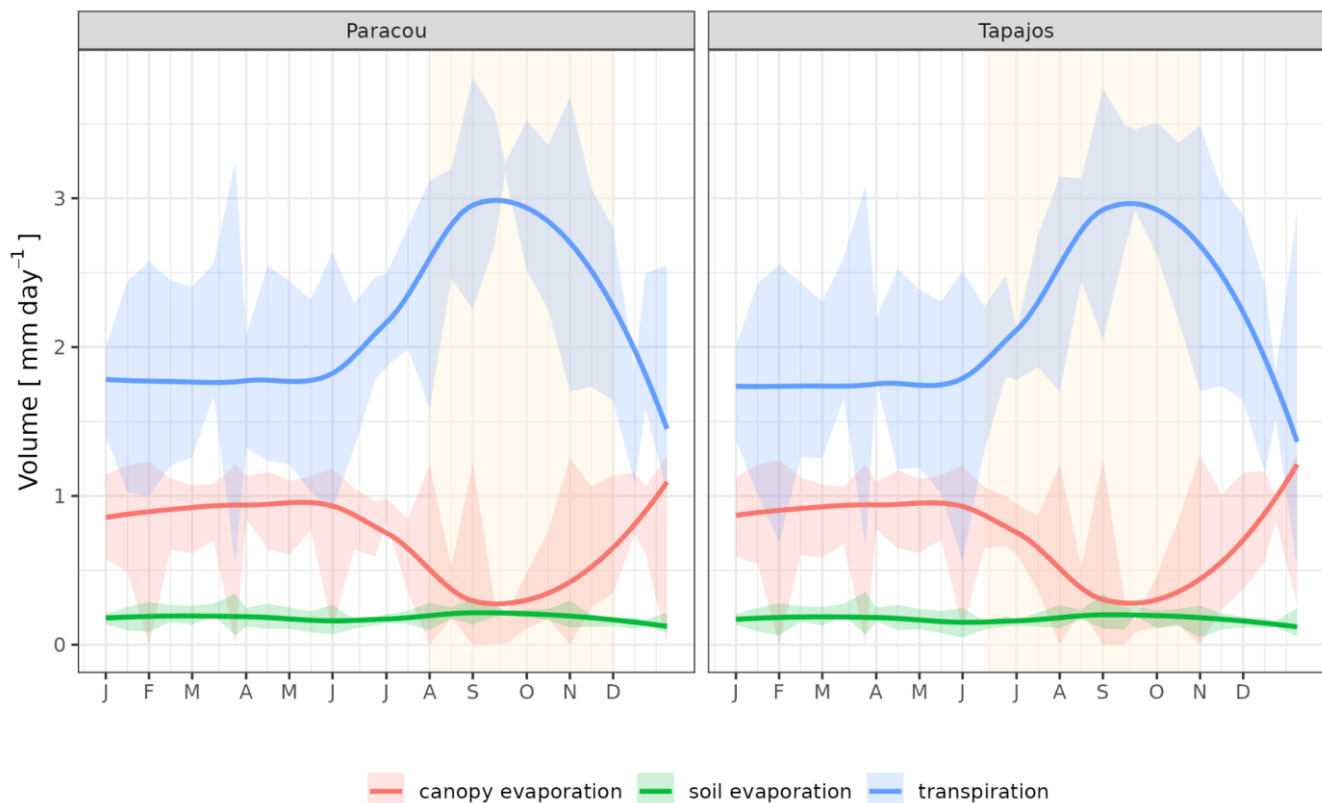
1336

Figure A09: Mean annual cycle of evapotranspiration partitioning between canopy evaporation (red), soil evaporation (green), and tree transpiration (blue) for Paracou (left) and Tapajos (right), derived from fortnightly means simulated with TROLL 4.0. Bands are the intervals of means across years, and the yellow vertical bands in the background correspond to the site's climatological dry season. Simulated values correspond to 10 years of simulations starting from the end-state of 600-year regeneration from bare ground with calibrated parameters at each site.

1342
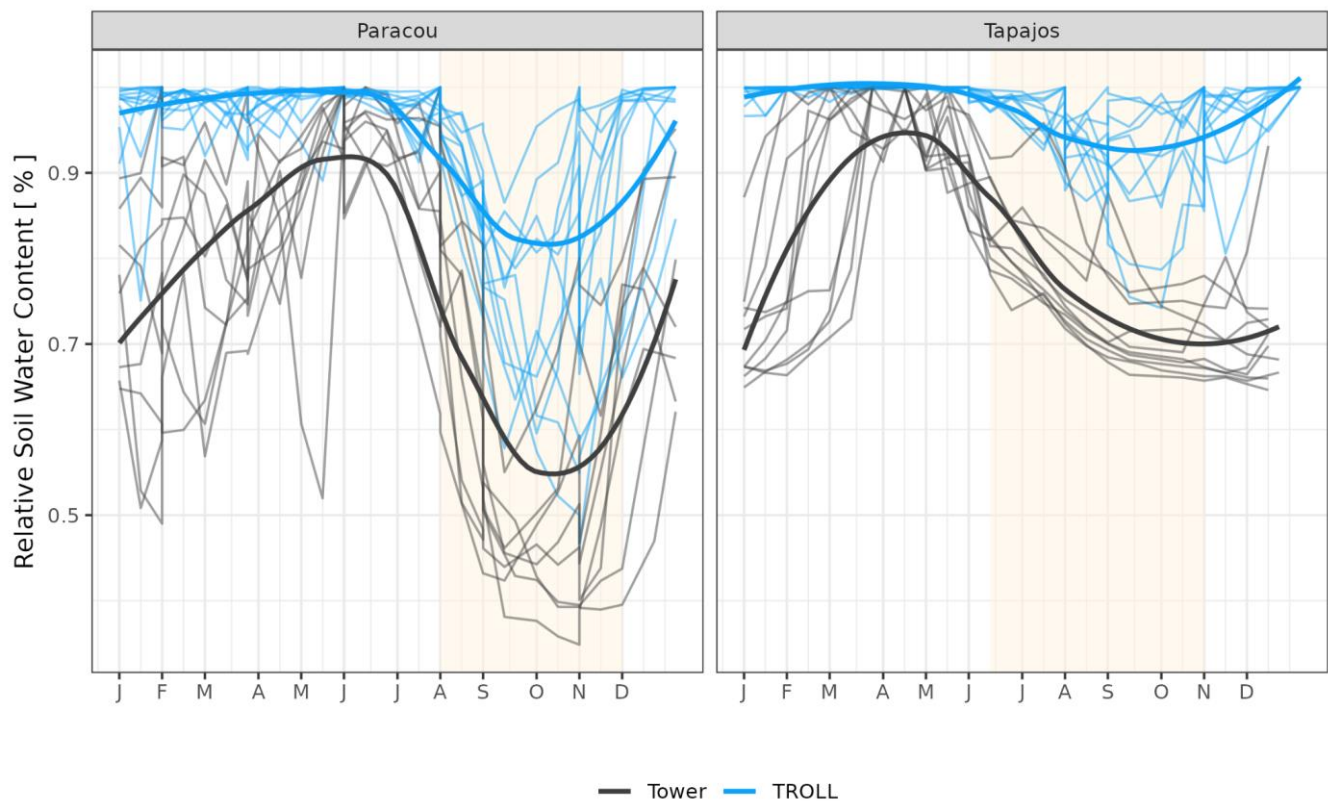
1343 **Figure A10: Mean annual cycle from daily means of relative soil water content for Paracou and Tapajos for the topsoil layer up to**
1344 **10 cm. Dark lines are the daily mean across years, semi-transparent lines are the daily means per year. The vertical yellow bands in**
1345 **the background correspond to the site's climatological dry season.**

1346

1347
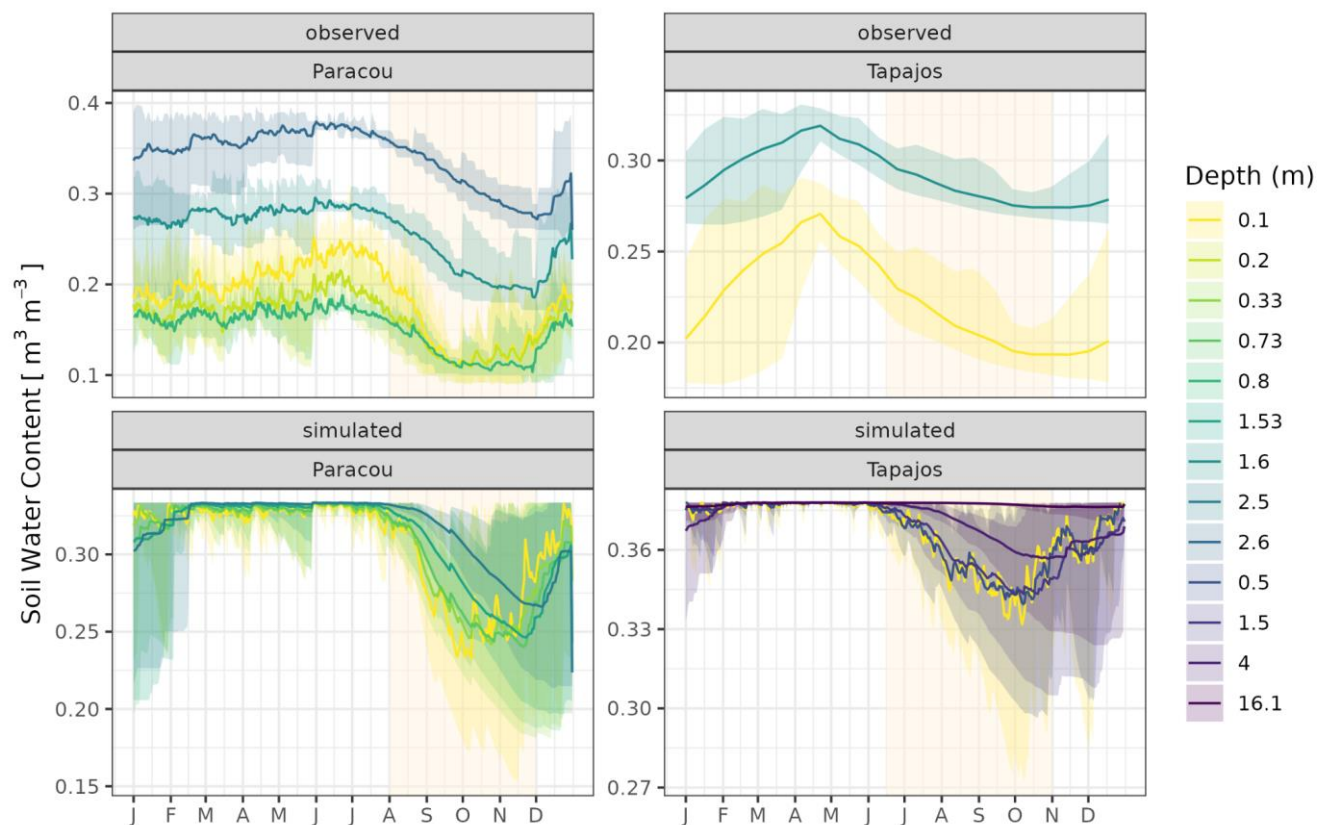
1348 **Figure A11: Mean annual cycle from daily means of soil water content for Paracou and Tapajos at different depths. The depth value**
1349 **indicates the maximum depth of the layer. Dark lines are the daily means across years, and bands are the intervals of means across**
1350 **ten years The vertical yellow bands in the background correspond to the site's climatological dry season.**

1351
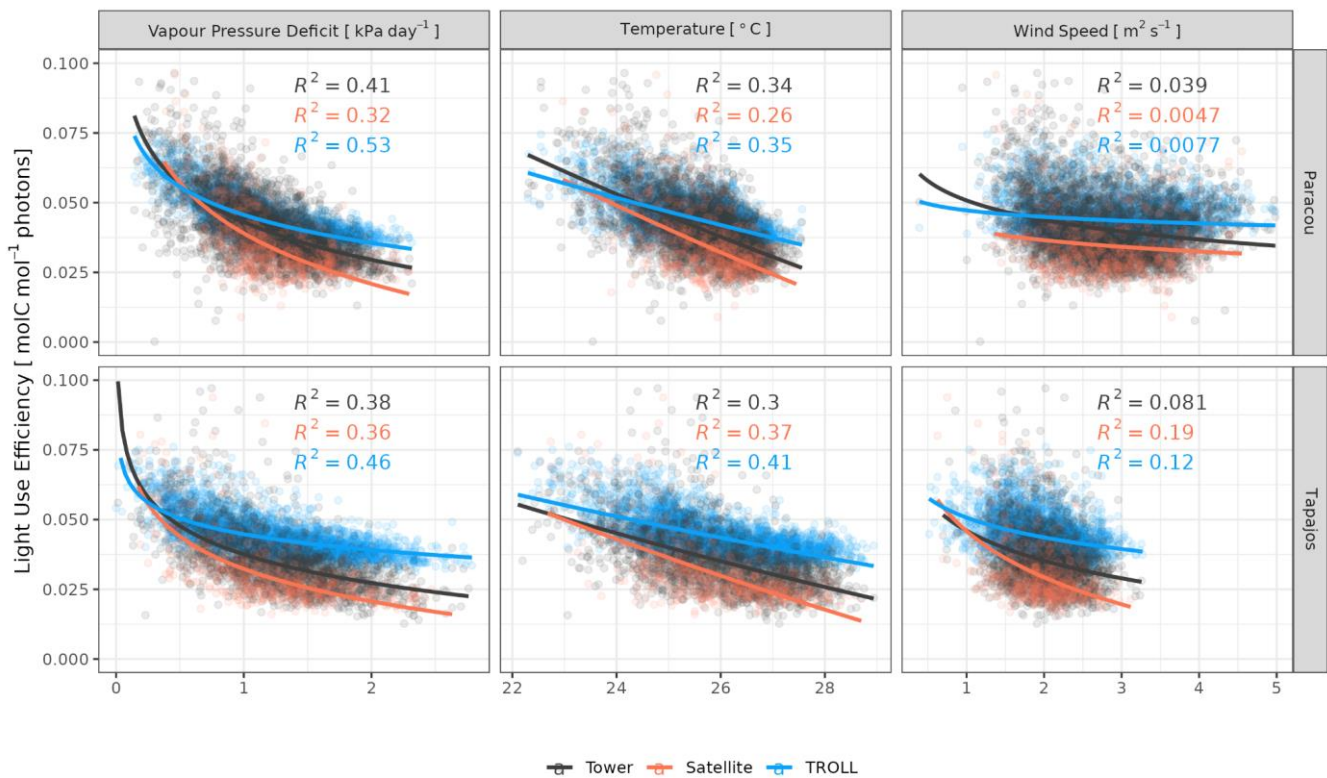
Figure A12: Daily averages of light use efficiency as a function of daily maximum vapour pressure deficit, average temperature, and average wind speed for model-, satellite- and eddy flux-based estimates at Paracou (top) and Tapajos (bottom). Lines illustrate the linear regression of form y ~ log(x), and text the squared Pearson's R correlation coefficient. The light use efficiency (LUE) was obtained by normalizing gross primary productivity (GPP) by photosynthetic photon flux density (PPFD) and the fraction of absorbed photosynthetically active radiation (fAPAR) itself derived from leaf area index (LAI).